FINNISH ROAD ADMINISTRATION

Leena Korkiala-Tanttu, Pekka Jauhiainen, Pekka Halonen, Rainer Laaksonen,
Markku Juvankoski, Heikki Kangas, Janne Sikiö

Effect of steepness of sideslope on rutting

Research of low-volume roads
HVS-test structures

Finnra Reports 19/2003

Leena Korkiala-Tanttu, Pekka Jauhiainen, Pekka Halonen, Rainer Laaksonen,
Markku Juvankoski, Heikki Kangas, Janne Sikiö

Effect of steepness of sideslope on rutting

Research of low-volume roads
HVS-test structures

Finnra Reports 19/2003

FINNRA
Helsinki 2003

ISSN 1457-9871
ISBN 951-803-042-1
TIEH 3200765E

Internet: www.tiehallinto.fi/julkaisut
ISSN 1459-1553
ISBN 951-803-042-1
TIEH 3200765E-v

Edita Prima Oy
Helsinki 2003

This publication is available at:
Finnra Publications Sales
fax int. +358 204 22 2652
e-mail julkaisumyynti@tiehallinto.fi

Finnish Road Administration
Opastinsilta 12 A
PB 33
FIN-00521 HELSINKI
Phone int. +358 204 22 11

Leena KORKIALA-TANTTU, Pekka JAUHIAINEN, Pekka HALONEN, Rainer LAAKSONEN, Markku JUVANKOSKI, Heikki KANGAS, Janne SIKIÖ: Effect of steepness of sideslope on rutting. Helsinki 2003. Finnish Road Administration. Finnra Reports 19/2003, 40 p. + 17 app. ISSN 1457-9871, ISBN 951-803-042-1, TIEH 3200765E

Keywords: low-volume road, accelerated pavement test, rutting, permanent deformation
Classification: 32

SUMMARY

The objective of the Heavy Vehicle Simulator tests (HVS) was to study the influence of the road cross section and edge effects on the structural strength and permanent deformations of low-volume roads. The purpose of the test results was to verify design methods and calculation models. The second purpose was to verify laboratory tests in a full-scale model test. The tests were financed by the Finnish Road Administration, Finnra.

The test consisted of three test sections: one without a slope, one with 1:3 slope and one with 1:1.5 slope. The test sections were constructed and instrumented in autumn 2000. The area was insulated during the winter and the test was performed one year later. The structures were designed to be equivalent to the structure of a low-volume road. All test sections consisted of a thin asphalt layer of 40 mm, a 400 mm base layer of crushed rock and a 200 mm subbase layer of gravel. The gravel included fine-grained particles, so the capillary rise of the water is evident.

Instrumentation and measurements were mainly focused on the dynamic and permanent deformations in pavement layers and slope in both vertical and horizontal direction during test loading. The water content, pore water and earth pressures were also measured. The deformation characteristics were determined with triaxial tests from test samples of each layer. The instrumentation was similar in all sections. Most test instruments seemed to work well during the test and give reliable results.

The tested structures were designed to withstand only about 15000 passes. The structures were constructed carefully according to the quality requirements of Finnra. The quality of the construction was monitored using level control, density and bearing capacity measurements. The layers were of even thickness and clearly fulfilled the quality requirements. The densities of the layers did not completely fulfil the quality requirements. The bearing capacities were only about 20 - 35 % of the Finnra's requirements.

Test parameters and environmental conditions, including the water table regulation, were controlled during the HVS test. All sections were tested identically. At the beginning of the test, the water table was 50 mm below the surface of the clay subgrade. At the end of the test, the water table was elevated to the top of the gravel layer and to the centre of the crushed rock. Static and cumulative pore pressures were monitored using transducers. A super single wheel was used as a loading wheel and the load was raised with a step of 10 kN from 30 to 50 kN.

The wheel loaded the structure in three different positions: 400 mm, 700 mm and 1000 mm from the edge of the slope. One test step consisted of 600 passes in each position. The pavement response to the moving wheel load with several offsets was measured and, finally, the pavement performance was evaluated with accelerated testing.

The permanent and dynamic deformations were followed up with Emu-Coil sensors from the lowest part of the crushed rock and gravel and from the two topmost parts of the clay (each 200 mm thick). The permanent horizontal deformations were also followed from the side slopes. HVS-profilometer measurements were used to monitor the deformations on the asphalt layer. Deformations were measured after each 600 passes.

It was assumed that the asphalt layer (40 mm) did not deform during the test and all deformations happened in unbound layers. The distributions of permanent deformations were calculated for each 200 mm layer. 63 to 80 % of the permanent deformations occurred in the base layer of crushed rock (400 mm) and were distributed evenly between the top and lowest 200 mm. The gravel layer underneath deformed about 8 to 13 % and the upper part of the clay layer (400 mm) deformed by 4 to 6 %.

There were significant deformations in the sloped structures and it can be assumed that the loading situation in the steepest structure with a high water table was quite close to failure. The damage of the sloped structures was easy to notice and the ruts were over 40 mm deep.

A significant part of the relative vertical deformations of the structure with 1:1.5 slope was concentrated in the upper 400 mm part of the structure. It is obvious that the failure surface develops in this part of the structure with the highest deformations and continues towards the slope. The measurements of the horizontal displacements from the side slopes confirm this. The horizontal displacements of the gentle slope (1:3) were concentrated near the surface, while no clear signs of the failure surface were detected.

The development of the permanent deformations both in vertical and horizontal directions was compared with the dynamic deformations. The dynamic deformations were measured during one loading pulse. The permanent deformations remain quite moderate up to a certain threshold value, but beyond that they grow relatively fast. In the gravel layer, the threshold value of dynamic deformation was about 100 micrometers/pass. This threshold value can be compared to the yield strength of soil. Once the yield strength is exceeded the permanent deformations begin to grow. The structures should be designed in such a way that the yield strength is not exceeded.

To be able to estimate the effect of the cross section on rutting in low-volume roads, a factor of geometry is introduced. With the help of this factor, the effect of the steepness of the slope and also the road width on the rutting can be estimated. The basic assumption was that the factor is 1, when the width of the road is 6.5 m and the steepness of the slope is 1:3.

Besides the above observations, other significant results were:

- The backward calculated resilient moduli of the gravel were a little lower than those defined by the laboratory tests. Therefore, the deformations of the layer exceeded the anticipated deformations.
- The backward calculated resilient moduli of the clay layer were a little higher than those defined by the laboratory tests. Therefore, the deformations of this layer were below the anticipated deformations.
- The speed of the rutting inside each loading step decelerated while the test proceeded except when the water table was raised near the asphalt. When this happened the speed of the rutting accelerated and it can be assumed that the loading situation was near failure.

FOREWORD

The research project on low-volume roads formed part of the Road Structures Research Project, TPPT, financed by the Finnish Road Administration Finnra. The low-volume road structure project was realised through co-operation between University of Oulu, and VTT Building and transport under a steering body consisting also of Finnish Road Authority (Finnra) and Finnish Road Enterprise representatives.

The project steering body consisted of:

Aarno Valkeisenmäki	Finnish Road Enterprise, Chair
Panu Tolla	Finnish Road Enterprise
Pertti Virtala	Finnra
Ismo Iso-Heiniemi	Finnra
Tuomas Toivonen	Finnra
Tuomo Kallionpää	Finnra
Kari Lehtonen	Finnra
Esko Ehrola	University of Oulu, co-ordinator
Jouko Belt	University of Oulu
Laura Apilo	VTT
Jouko Törnqvist	VTT
Harri Spoof	VTT
Sami Petäjä	VTT, secretary

The purpose of this research sub-project was to study the behaviour, bearing capacity, deforming and deterioration of various pavement structures with a slope under a Heavy Vehicle Simulator (HVS) load simulating the passing of a lorry.

The research was carried out by VTT Building and transport. Heikki Kangas was responsible for preparing the study, building the test structures and instrumentation. Loading of structures was carried out by Pekka Halonen and Janne Sikiö. Laboratory tests were conducted by Rainer Laaksonen and structure modelling by Markku Juvankoski. Pekka Jauhiainen and Leena Korkiala-Tanttu processed the test data. The sub-tasks were compiled, analysed and the report written by Leena Korkiala-Tanttu.

Espoo, February 2003

VTT Building and transport

Tiehallinto
Konsultointi

Sisältö

1 GENERAL DESCRIPTION OF THE TEST BASIN AND LOAD

1.1 Test basin

VTT has test basins in Otaniemi, Espoo, for conducting load tests with the Heavy Vehicle Simulator (HVS). A concrete basin was used for the low-volume structures (Figure 1.1).

The test basin walls are reinforced concrete and the walls and base are insulated on the outside with 100 mm thermal insulation. The water level in the test basin can be regulated with water from the municipal water distribution system.

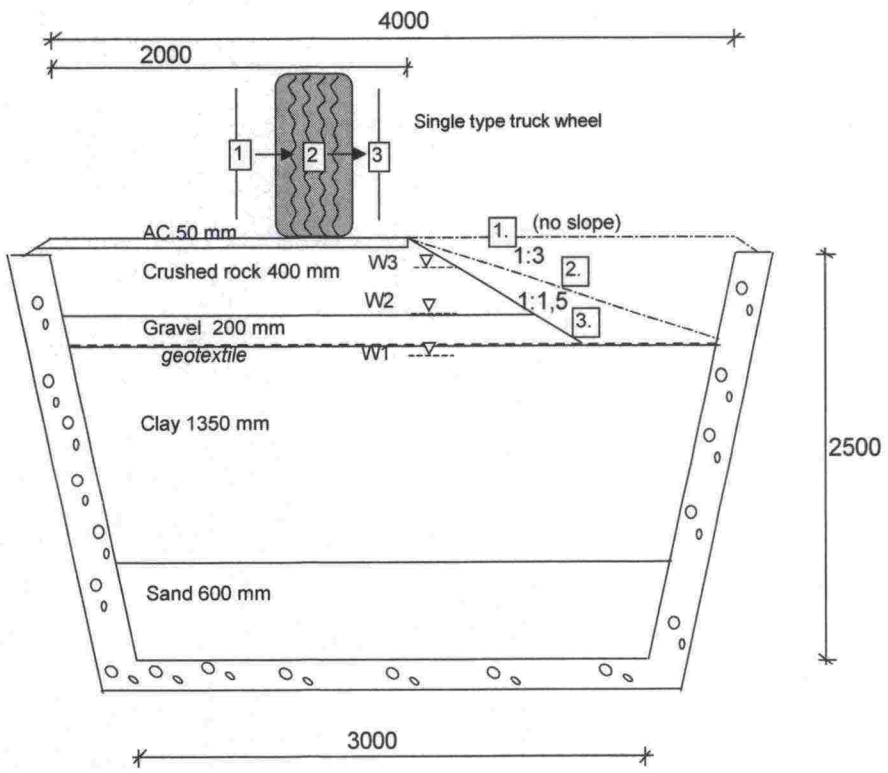

Figure 1.1 Cross section of low-volume structure (no slope, 1:3 and 1:1.5 slopes).

1.2 Load with Heavy Vehicle Simulator (HVS)

The Heavy Vehicle Simulator (HVS) is 23 m long, 3.7 m wide, 4.2 m high and its total mass is 46 metric tons. The maximum width of HVS's loading area is 1.5 m. The total length of the loading area is eight metres, of which six metres can be used with even wheel load and speed. At either end of the

loading area, a distance of one metre is necessary for accelerating and braking the wheel, and, in one-way application of load, for lowering and lifting the wheel to and from the surface. The speed of the wheel can be adjusted between 1 to 15 km/h. However, in long-term load, the maximum speed is 12 km/h. Any distribution with 50 millimetre lateral adjustments can be selected as the lateral movement of the test wheel. The load can be applied either one-way or in both directions.

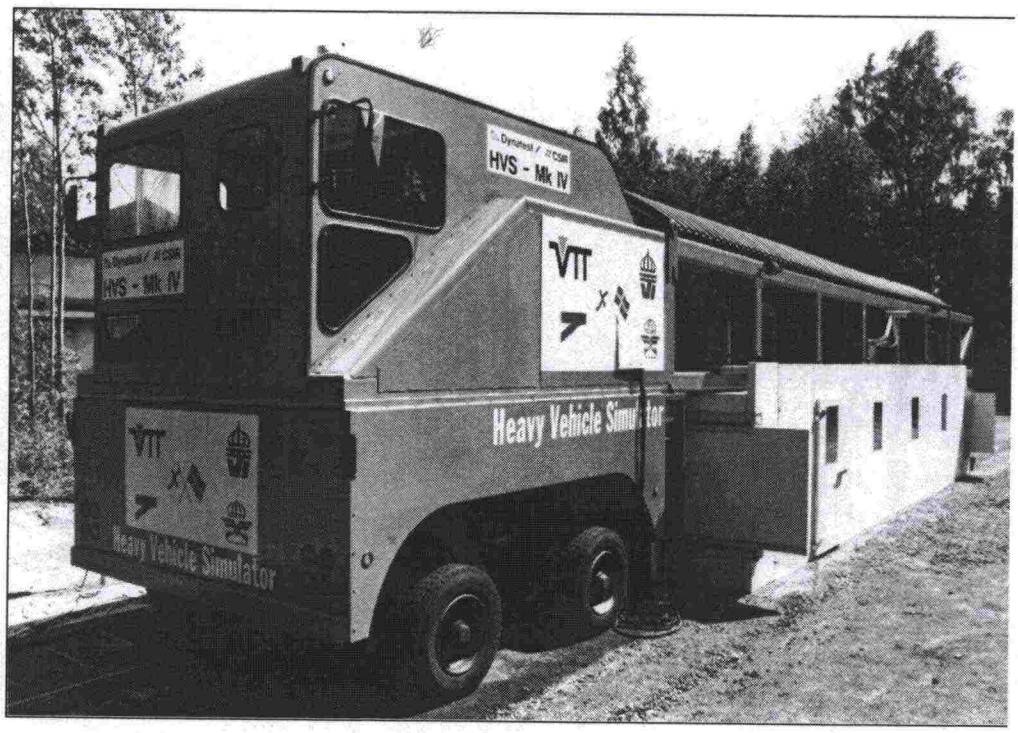

Figure 1.2 The Heavy Vehicle Simulator (HVS).

The maximum load achieved with the simulator is 110 kN and the minimum 25 to 30 kN. The load can be applied on the structure via either a lorry single tyre or twin tyre. The simulator includes a heating/cooling unit for keeping the road structure to be tested at a desired temperature. In this test, the temperature was +10 □C.

2 CONSTRUCTION

2.1 Tested structures

Three different structures were constructed in the test basin: one with no slope, one with gentle slope (1:3) and one with steep slope (1:1.5). Before moving the HVS to the test site, the slopes were covered with filter cloth and filled with gravel to facilitate the move, after which the slopes were dug open again.

The materials of the structure and the thickness of layers were identical on all load sections. The length of each section was 8 m, with the load parameters and conditions remaining constant on 6 m (Figure 2.1).

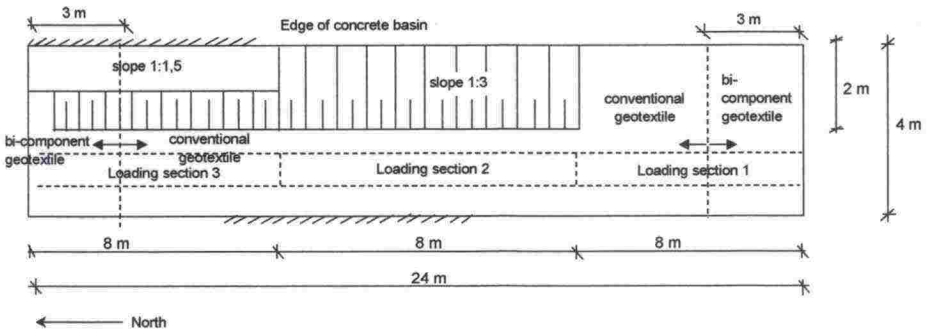

Figure 2.1. Map of the structure.

The subgrade of the structure consisted of the existing subsoil drainage and a clay layer which had been constructed for studying frost test structures in 1997. The thickness of the pavement was increased from the previous test by removing approximately 150 mm of clay and replacing it with gravel, thus, creating a pavement with a total thickness of approximately 640 mm (Figure 1.1)

2.2 Construction work

The surface of the subgrade clay was carefully levelled. An application class 3 filter cloth was fitted over it and a 3-metre wide bi-component geotextile, the functioning of which has been the subject of a separate report /Korkiala-Tanttu *et al.* 2002/, was fitted to the ends of the basin.

The lowest layer of the unbound pavement (subbase) consisted of a 200 mm layer of compacted gravel (sandy gravel) and an upper layer (base course) of 400 mm of crushed rock. A more detailed description of the materials can be found in Section 4. The subbase was applied so that it could also be compacted in the slope structures for the whole width of the loading area. The gravel was compacted by a smooth roller (approx. 10 tons) with three passes without vibration. The layer of crushed rock was spread and compacted as one layer. It could not be spread as thinner layers because the bearing capacity of the gravel layer underneath was low at the time of construction. Compacting was carried out using a 400 kg vibrating plate and three passes. The bound pavement consisted of 40 mm asphalt (AB16/100) with grain size of 0 to 16 mm, and bitumen B70/100. The layer was compacted in the normal way with a smooth vibratory roller.

The construction work was carried out in autumn 2000 and the test structure was then protected for the winter by insulating it. The actual testing began in June 2001. The quality control results of the construction phase are presented in Appendices 1 to 3.

2.3 Regulating the water table level

The basic water table level was +15.70. In the final phases of loading each section, the ground water table was elevated to the level of the top of the gravel layer (W2) at the minimum, and on sections with gentle or steep slope, also to the layer of crushed rock (W3 +16.15). The variation in the ground water level and the loads on each section are presented in Figure 2.2.

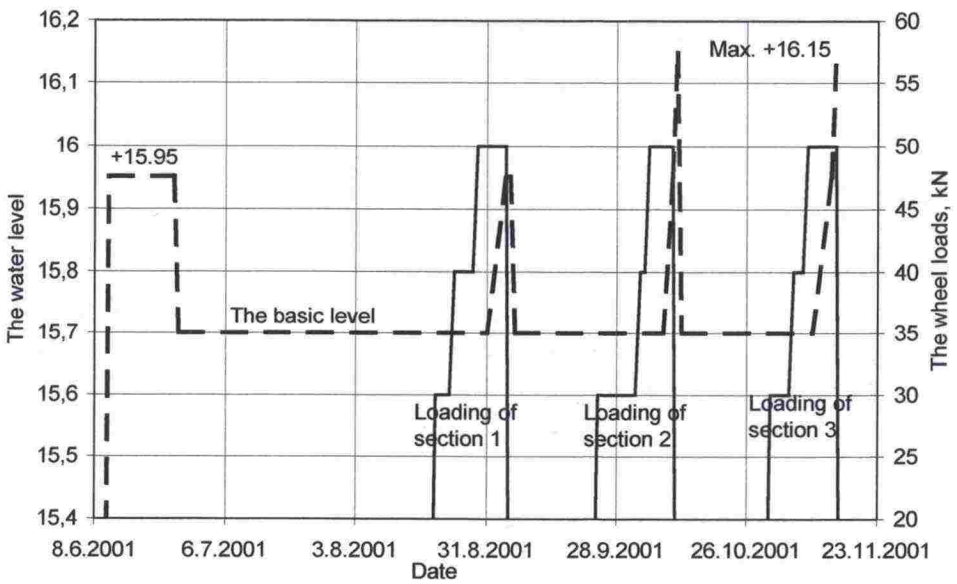

Figure 2.2 The ground water level and the loading times of the different sections.

3 INSTRUMENTATION

All sensors were carefully installed according to a separate instrumentation plan. The sensors were calibrated before installation and their functioning was double-checked immediately prior to installation. Sensors for volumetric water content, earth pressure, pore pressure and displacements (Emu-Coil sensors and settlement profile tubes) were installed during the construction. Detail drawings of the instrumentation of various structures are given in Appendix 4.

Post-construction instrumentation consisted of instruments including installation tubes for measuring temperature, water content in the structures and variations in the pore pressure, as well as asphalt deflection and slope displacement. Surface layer deflection was measured in the asphalt with an accelerometer, which was installed in each structure immediately prior to beginning the test. After being dug open, LVDT displacement gauges were installed in the slopes to measure horizontal displacement in the slope. The static water table level was monitored in a pilot well.

4 TESTING

4.1 Structural measurements before testing

The purpose of the tests and measurements conducted during construction and before actual HVS testing was to study those properties of test structures the changes in which were to be monitored during and after the testing. The tests also formed part of the quality control of the test structure.

Falling weight deflectometer measurements

Falling weight deflectometer (FWD) measurements were conducted on the surface of the structure on three instances: 23 May 2001 when the structure was 'dry'; 21 June 2001 when the water level was elevated to level W2; and finally, 9 July 2001 after it was lowered to the basic level before the testing. The results are presented in Appendix 5.

Radiometric measurements

Radiometric measurements were conducted when the ground water table was at level W2 +15.95 (25 June 2001) and after it had been lowered to level W1 +15.75 (29 June 2001). The results for different sections are presented in Appendix 6.

4.2 Laboratory tests of unbound materials

In addition to grain size distribution and compactibility tests, only tests to determine the resilient moduli and permanent deformations were conducted. The strength properties of the materials were not determined.

The materials and their grain size distribution

The unbound materials used in the tests were lean clay, sandy gravel and crushed rock. The lean clay came from Lahti, sandy gravel (#0–50 mm) from Hyvinkää and the crushed rock (#0–32 mm) from Teisko. Grains of over 32 mm were removed from the crushed rock and gravel before the tests. The grading curves of the materials are presented in Figure 4.1.

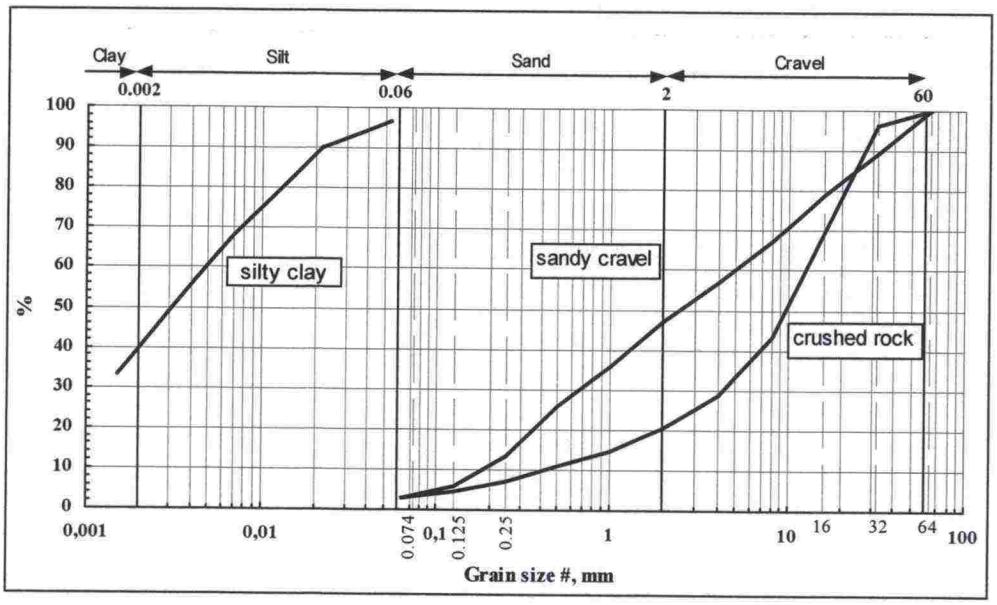

Figure 4.1. Grading curves of the materials studied.

Compactibility

Improved Proctor tests were conducted on the sandy gravel and crushed rock to determine the maximum dry bulk density and optimum water content. The results are presented in Table 4.1. The table also records the dry density and water content of the clay sample studied.

Table 4.1. Results of the Proctor tests on the materials and the density and water content values for clay.

Material	Maximum dry bulk density / dry density (g/cm^3 / kN/m^3)	Optimum water content (%)
Crushed rock	2.23 / 21.9	5.0
Sandy gravel	2.17 / 21.3	6.5
Lean clay (*in situ* values)	1.46 / 14.4	32

The state of the samples in the deformation tests

The laboratory tests were conducted, as far as possible, in stress states that would be realised in the structures during loading. The stress states were estimated with Plaxis element program using resilient modulus values typical of the soil layers and loads that would be realised in the HVS tests. The density and water content of the materials were selected on the basis of the results of volumeter tests and radiometric measurements on the gravel and crushed rock. The clay was tested for the *in situ* bulk density and water content (Table 4.2).

Table 4.2. The target stress states, bulk densities and moisture content at the beginning of resilient modulus tests and deformation tests

Material	Confining pressure (kPa)	Deviatoric stress (kPa)	Bulk density (kN/m^3)	Water content (%)
Crushed rock, upper layer	60	17 – 350	20.15	4.0
Crushed rock, middle layer	25	7 – 140	20.15	4.0
Crushed rock, lowest layer	15	4 – 85	20.15	4.0
Sandy gravel	10	2 – 40	19.56	6.0
Lean clay	18	1 – 21		

Loading and measurements

The tests were conducted with the selected confining pressures and axial loads. During the tests, confining pressure was kept constant, while the axial stress varied cyclically within pre-set limits. The target duration for the tests was 400,000 cycles, but the maximum permissible value for axial deformation was set at approximately 2%. During the test, vertical deformation of the sample was measured so that the resilient modulus and both dynamic and permanent deformation could be calculated at cycles 10, 100, 10,000, 100,000 (400,000), unless the test was suspended earlier due to reaching the deformation limits.

The load used was a sinusoidal force pulse, the corresponding stress amplitudes of which are given in Table 5. The loading frequency was 5 Hz.

The average densities, water contents and confining pressures realised in the samples during testing are presented in Table 4.3.

Resilient moduli

A resilient modulus was calculated for each material on the basis of the test results. Three moduli were defined for crushed rock, one for gravel and two for clay. From one test, two values were calculated for clay, because the amplitude of the loading pulse was increased during the test. The results are collected in Table 4.4. The values presented in the table were calculated at 100 load cycles. The other values are presented in Figure 4.2. The target deviatoric stress value was not quite achieved for clay.

Table 4.3. State variables and stress states realised in the tests.

Material	Confining pressure (kPa)	Deviatoric stress (kPa)	Density / Bulk density (g/cm^3 / kN/m^3)	Water content (%)
Crushed rock, upper layer	60.0	19 – 350	2.09/20.5	3.7
Crushed rock, middle layer	25.4	8.5 – 140	2.09/20.5	3.6
Crushed rock, lowest layer	15.6	6.0 – 80	2.11/20.7	3.6
Sandy gravel	10.7	4.2– 40	2.03/19.9	6.0
Lean clay	18.3	9.0 – 14	1.46/14.4	32
Lean clay	18.3	4.0 – 20	1.46/14.4	32

Table 4.4. The resilient moduli, and stress and deformation values realised at 100 load cycles.

Material	Resilient modulus (MPa)	Deviatoric stress (kPa)	Dynamic relative deformation (-)	Permanent relative deformation (-)
Crushed rock, upper layer	349	18.9 – 350	0.00095	0.00384
Crushed rock, middle layer	213	8.2 – 140	0.00062	0.00098
Crushed rock, lowest layer	179	5.6 – 85	0.00044	0.00053
Sandy gravel	80	4.3 – 40	0.00044	0.01670
Lean clay	11.7	9.0 – 14	0.00041	0.00839
Lean clay (10,000 cycles)	7.0	4.2 - 19	0.00213	0.0155

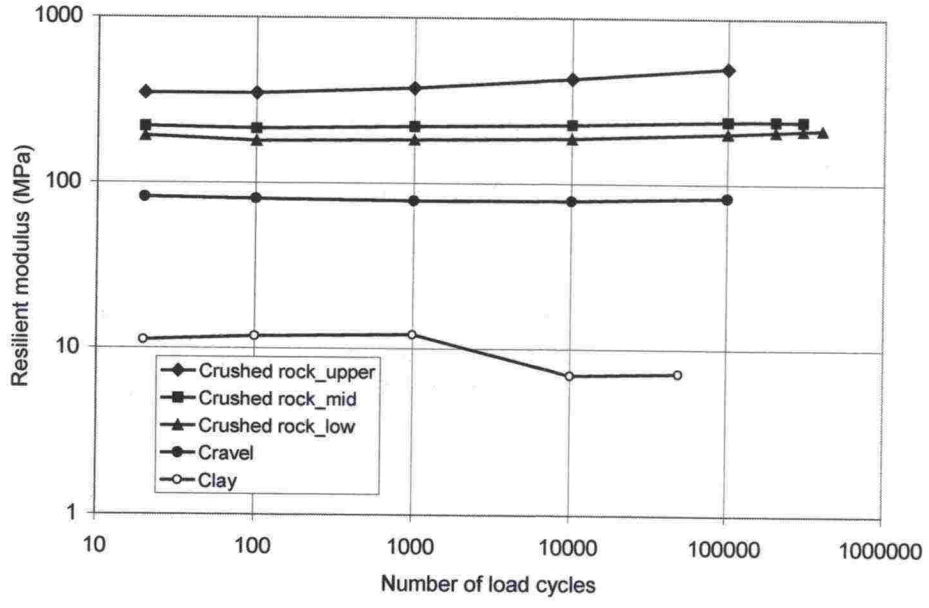

Figure 4.2. Resilient modulus values as a function of a cumulative number of load repetitions (cycles).

Permanent deformation

A value for permanent deformation was defined for each test as a function of the number of cycles. Permanent deformation for all tests is presented in Figure 4.3. Figure 4.4 compares the relationship between the dynamic and permanent deformation in crushed rock on different load levels and load cycles. The results clearly reveal that after a certain dynamic deformation (stress state), the proportion of permanent deformations significantly increases. In this test, the threshold value is approximately 0.055% to 0.06%.

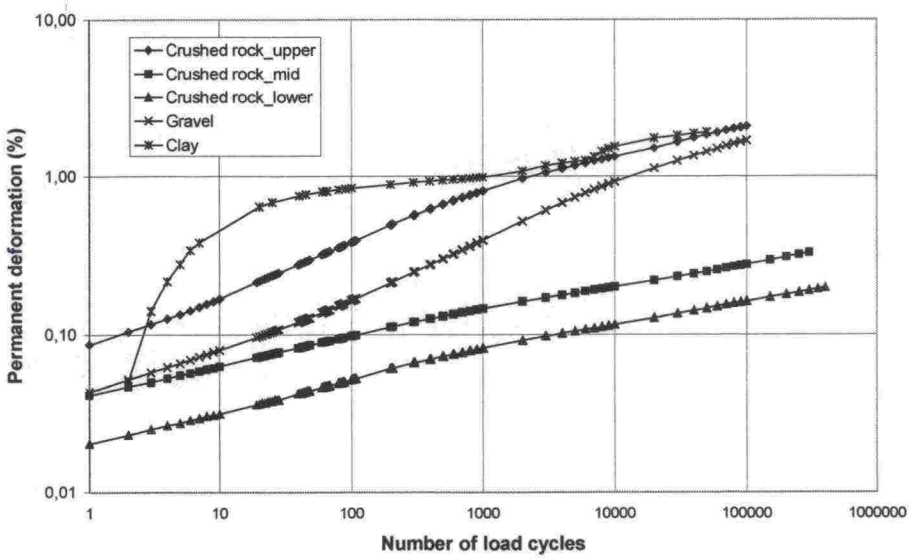

Figure 4.3. Development of permanent deformation in the tests due to the number of load repetitions.

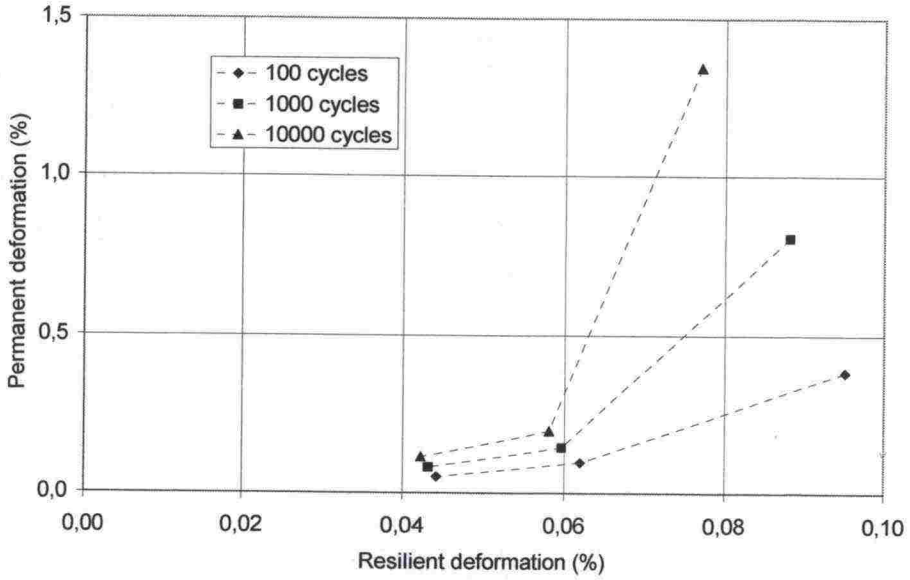

Figure 4.4. Crushed rock: the relationship between resilient and permanent deformation.

4.3 Loading programme

All the structures in the low volume test were loaded according to the same loading programme (Table 4.5). In addition, the sloped structures were finally loaded with a load of 50 kN, after the water table level had been elevated to half-way through the crushed rock. The tyre pressure on all wheel loads was 700 kPa. The centre lines of loading and instrumentation were located 700 mm from the edge of the surface layer. In interpreting the results, the position 400 mm from the edge corresponds to 300 mm to the right of the centre line and the position 1000 mm corresponds to 300 mm to the left of the centre line (-300 mm).

Table 4.5. Loading programme

All structures			
Number of load repetitions	**Wheel load (kN)**	**Water table level from the surface layer (mm)**	**Lateral position of wheel from the edge of the surface layer (mm).**
0 – 250	20	700	300 – 1100 (at 50 mm intervals)
250 – 340	30	700	400, 700 and 1000
340 – 430	40	700	400, 700 and 1000
430 – 520	50	700	400, 700 and 1000
520 – 5900	30	700	400, 700 and 1000
5900 – 11300	40	700	400, 700 and 1000
11300 – 14900	50	700	400, 700 and 1000
14900 – 16700	50	450	400, 700 and 1000
Sloped structures also:			
16700 – 18500	50	250	400, 700 and 1000

5 MEASUREMENT RESULTS

5.1 Pore pressure measurements

The development of pore pressure in each load section was monitored with pore pressure sensors. The sensor tips were located in the clay subgrade at least 60 mm below the basic water level. The measurement results are presented in Appendix 7. The changes in load levels, which are clearly visible in the results, have been indicated with arrows.

5.2 Earth pressure measurements

Earth pressure measurements were conducted to monitor earth pressure in the upper surface of the gravel and clay layers. Each measuring point had 3 earth pressure cells. The measurements are the average results from these three cells. The measurement results by section are presented in Appendix 8. The results of earth pressure measurements seem reliable and correspond quite well to the changes in loading. The cells measure total pressure, that is, the sum of the contact pressure and pore pressure. The elevation of the water table level towards the end of the testing is evident in the results, particularly for the clay layer.

5.3 Asphalt deformation

Accelerometers

The deflection of the load section centre line in the surface of the asphalt was measured with accelerometers in each structure. Appendix 9 presents the accelerometer results from the various loading sections.

The vertical displacements measured at different sections for wheel loads 30 and 40 kN increase as the slope steepness increases. With the maximum wheel load, 50 kN, there is a great difference between the slopeless structure and the structures with slope. The difference in the maximum value for transient vertical displacement in the structure with no slope and structures with slope is more than double (from 1.9 mm to over 4 mm). The steepness of the slope is not significant as regards the maximum value, as the transient vertical displacements were nearly equal for 1:3 and 1:1.5 slopes.

Profilometer measurements

The development of ruts as a function of load was measured with a laser profilometer. The profilometer measurements were conducted on three levelling lines on each loading section. The average development of a rut on different loading sections is presented in Appendix 10. A clear increase in the speed of rutting could be detected in the slopeless section after 9,600 load repetitions. At that time, the water content of the structure increased due to heavy rain. The greatest increases in the speed of rutting could be detected in all structures in connection with elevating the water table level.

Loadman measurements

Appendix 11 presents the results of Loadman measurements from the top surface of the structure for different sections during testing. The results of the Loadman measurements only reflect the bearing capacity of the top layers. For the structure with no slope, there is a measurement from 29 August 2001, in which the bearing capacity has dropped due to increased water content (heavy rains).

5.4 Deformation in unbound layers

The permanent and resilient deformations in the lowest part of crushed rock, subbase and top part of the clay layer were monitored with Emu-Coil sensors in each section. The sensors were at approximately 200 mm intervals at the beginning of the test. The permanent and resilient deformation measurement results for the sensors are presented in Appendices 12 to 14.

5.5 Lateral displacement

Permanent lateral displacements of the surface layer on all loading sections were monitored in relation to a reference tack on the side of the basin. Lateral displacement gauges monitored both permanent and resilient horizontal displacements in the middle of the crushed rock and gravel layers on both sections with slopes. (Appendix 15).

5.6 Distress survey

Distress surveys were made on the top of the surface layer immediately after the first cracks appeared. Subsequently, the damage was surveyed after each loading phase. The damage was recorded on maps, which indicated when they appeared and the corresponding loading figure. Only some minor damage (short, narrow cracks) was observed in structures with no slope or gentle slope. The structure with steep slope, however, showed significant

cracks, with the largest appearing behind the rut. Appendix 17 presents images of the damage in the structure with steep slope.

6 MODELLING

6.1 Defining the task

The purpose of studying the structures of the Heavy Vehicle Simulator (HVS) by calculations was to find out how well the calculated results correspond to the results measured in the structures. The calculated results were compared to loading results from HVS structure measurements corresponding to "one pass of the load".

HVS loads were simulated in the calculations according to the loading programme in a total of nine calculations: for all three slope steepnesses and three different load positions. Each calculation also included all three loading levels used in the test programme (wheel loads 30 kN, 40 kN, 50 kN). Figure 6.1 presents the monitoring points used in the element grid corresponding to the sensor locations in the structure.

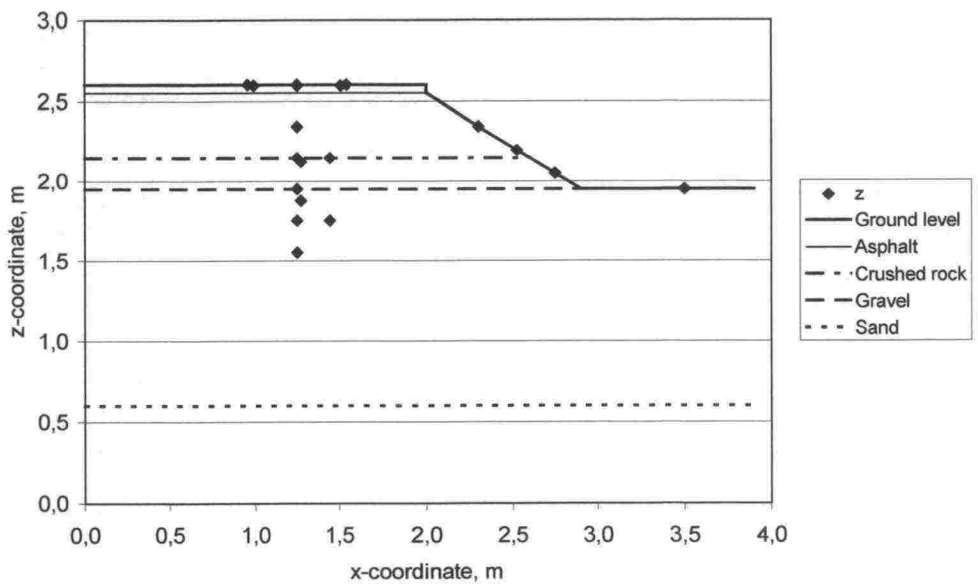

Figure 6.1. The positions of the element grid monitoring points, structure with deep slope (correspond mainly to sensor positions in the test structure).

Modelling the structures was carried out with 3D-FLAC v. 2.00 software. It is a numerical modelling tool based on an explicit finite difference formulation for analysing soil and rock structures developed by the U.S. company Itasca Consulting Group.

The element grids used in the study for the 1:1.5 slope are given in Appendix 18. The figures in the appendices also show the pavements in the structures and their division into elements.

6.2 Material parameters and material models

The material parameter values used in studying the various materials are given in Table 6.1. In the study, the asphalt layer is described as an elastic material and the soil materials as based on Mohr-Coulomb's elastic-plastic model.

Table 6.1. The material properties used in studying the various materials.

Material	Bulk density γ	Modulus E	Poisson's ratio ν	Angle of friction / dilatation ϕ / (ψ)	Cohesion c	Bulk modulus K	Shear modulus G
	kg/m^3	kPa	-	°	kPa	Pa	Pa
Asphalt, AB	2400	2000	0.35	-	-	2.22*10^9	7.41*10^8
Base course 1, KaM	2000	349	0.30	38 (8)	5	2.91*10^8	1.34*10^8
Base course 2, KaM	2000	194	0.30	38 (8)	5	1.78*10^8	8.19*10^7
Base course 3, KaM	2000	125	0.30	38 (8)	5	1.49*10^8	6.88*10^7
Subbase, Sr	1900	80	0.35	33 (1)	5	8.89*10^7	2.96*10^7
Subgrade, Sa	1800	7	0.45	5 (0)	30	2.33*10^7	2.41*10^6
Sand	1900	60	0.35	34 (4)	5	6.67*10^7	2.22*10^7

6.3 Results from the calculations and comparison with observed responses

Appendix 18 (load nearest to the slope, slope 1:1.5) presents the level curves for the displacement of the surface of the whole structure, and the graphs of the state of the structure's elements on the load line.

The calculated results were compared to results measured in the structure. The results observed in the actual structure are calculated as an average of 1 to 3 individual results. The results for displacements and deformations observed and calculated for different slope steepnesses are compared in Figure 6.2.

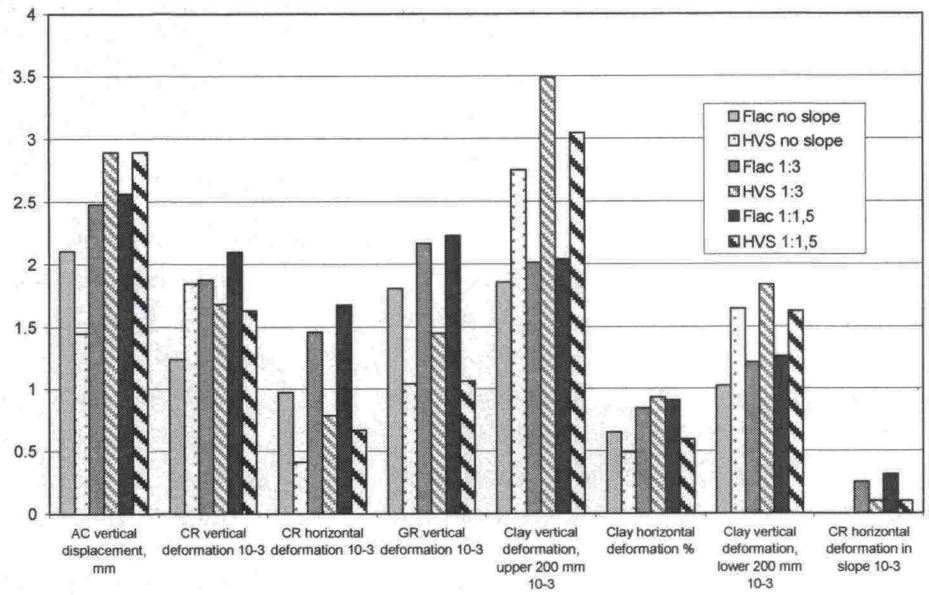

Figure 6.2. Main results measured in the structures for different slope gradients. Displacements and deformations.

In general, when comparing the results observed and calculated for different slope steepnesses, it can be noted that:

- the calculated displacements in the top surface of the asphalt (transient settlement) corresponded reasonably well to the measured displacements (variation from –15% to +45%).
- the calculated relative deformations in the lowest part of the crushed rock corresponded reasonably well to the measured deformations (variation from –29% to +32%).
- the calculated relative horizontal tensile strain in the lowest part of the crushed rock were greater than the measured ones (variation from +85% to +149%).
- the calculated relative deformations in the gravel were greater than the observed ones (variation from +50% to +112%).
- the calculated relative deformations in the top part of the clay were smaller than the observed ones (variation from –33% to –42%).
- the calculated relative horizontal tensile strains in the top part of the clay corresponded reasonably well to the measured tensile strains (variation from –9% to +53%).
- the calculated relative deformations in the "middle part" of the clay were smaller than the measured ones (variation from –22% to –38%).
- the calculated horizontal displacements in the slope corresponded poorly to the measured displacements (variation from +103% to +120% in crushed rock and +723% in gravel).

On the basis of this comparison, it can be said that the deformations and stresses appearing in the test structures during loading can be estimated reasonably well with quite rough initial values and models. The greatest differences seem to be related to horizontal tensile strains and deformations in the gravel and clay layers. In general, it can be said that the calculated

failure mechanisms of a deforming structure do not correspond to those in a real, tested structure.

6.4 The effect of the test basin on deformations in the structures

Before the testing began, a pilot study was carried out with Plaxis element program on the effect of the test basin on the scale of deformations /Kangas & Törnqvist 2001/. The effect of the basin was studied with two different calculations: the first with the actual test basin and a second which modelled a wider cross section. On the basis of the calculations, both displacements and failure loads in the basin structure were smaller than in the corresponding wider cross section. For failure load, the differences were in the order of –12 to –33%, for horizontal displacements –4 to –7% and for vertical displacements –12 to –15%. For failure load, the range was quite wide, for displacements it was smaller.

7 DISCUSSION

7.1 Quality of construction

The basis for test structure design was to construct a structure that corresponds to the structure of a low-volume road. In actual practice, the structure was designed with a multilayer programme to have such a load capacity that the structure rutted sufficiently under a reasonable number of load repetitions (approximately 15,000 passes). That is, the structure was not designed to correspond to any actual road class.

According to the compaction measurements and laboratory tests, the average degree of compaction achieved was 93.6% and the individual minimum value was 91.5% (Appendix 2). The average E_{300} bearing capacity defined on the basis of Loadman measurements was 22.5 MPa and the lowest value 20 MPa, which is clearly below the general minimum bearing capacity for subbase, 105 kPa.

According to the compaction measurements of base course crushed rock, the average degree of compaction was 93.9% and the lowest value 89%. The average value from falling weight deflectometer measurements was 46 MPa and lowest individual value 37 MPa. The average E_{300} defined on the basis of Loadman measurements was 44 MPa and the lowest value 38 MPa (Figure 7.1). The general minimum bearing capacities for the base course (215 kPa) were also not met.

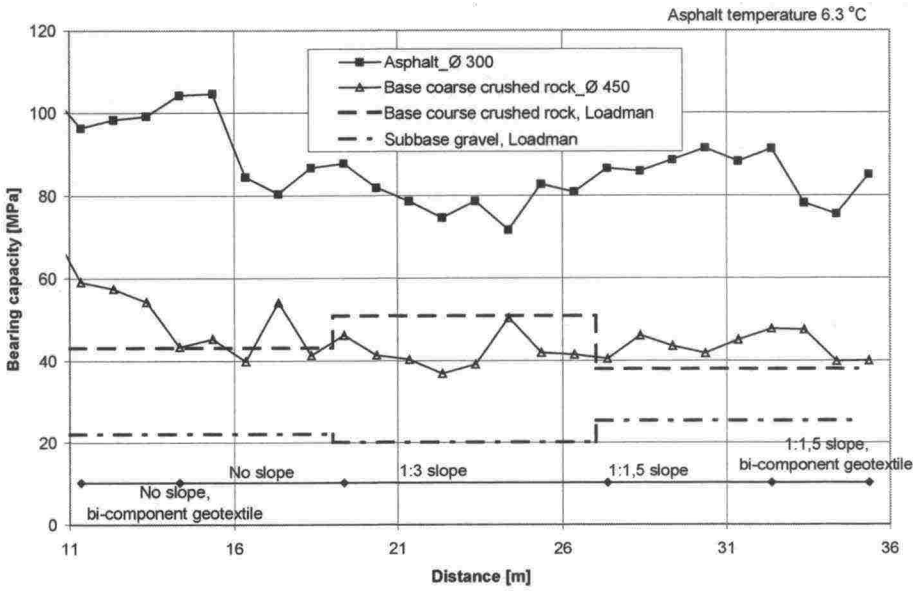

Figure 7.1. Bearing capacity measurements from the top of each layer before testing.

The thickness of the surface layer was calculated from the levelling results. According to them, the average thickness of the surface layer in the structure with no slope was 47 mm, that of the structure with gentle slope 37 mm and that of the structure with steep slope 41 mm. On the basis of APAS calculations, it can be estimated that the 10 mm difference in the thickness of the surface layer increases stress in the base course by 11 to 29% and in the subbase by 5 to 11%. The thinness of the surface layer in the structure with gentle slope is clearly evident in the bearing capacity measurements conducted on the top of the surface layer (Figure 7.1).

7.2 The distribution of permanent deformations in the structure

The amount of permanent deformations in the structures was monitored with Emu-Coil measurements. The top sides of the upper Emu-Coil sensors were levelled after the tests and the deformation of the base course and the surface layer was calculated from the results. It was assumed that the asphalt layer was incompressible. Figure 7.2 shows the proportion of deformation in each layer in the total rutting defined in this way. Changes in the water table level had a crucial effect on the results, so the comparisons were based on cases in which the water table level was identical, +15.95.

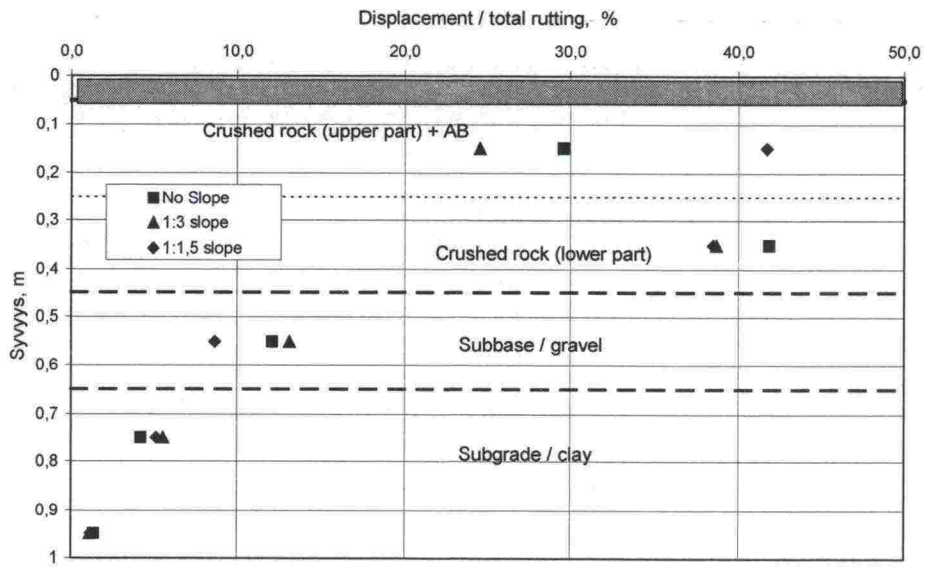

Figure 7.2. The proportion of the deformation of total rutting in 200 mm layers, with the water table level in all structures at +15.95.

The results indicate that in structures with no slope or gentle slope, the greatest deformations occur in the lowest part of the base course, while in the structure with steep slope, the deformations were equally large in both parts. 63 to 80% of permanent deformations occur in the 400 mm thick base course and the surface layer. The share of the subbase (200 mm) of the settlements is approximately 9 to 13%, and that of the upper parts of the subgrade (400 mm) 4 to 6%. The permanent deformations for the different 200 mm layers are presented in Figure 7.3.

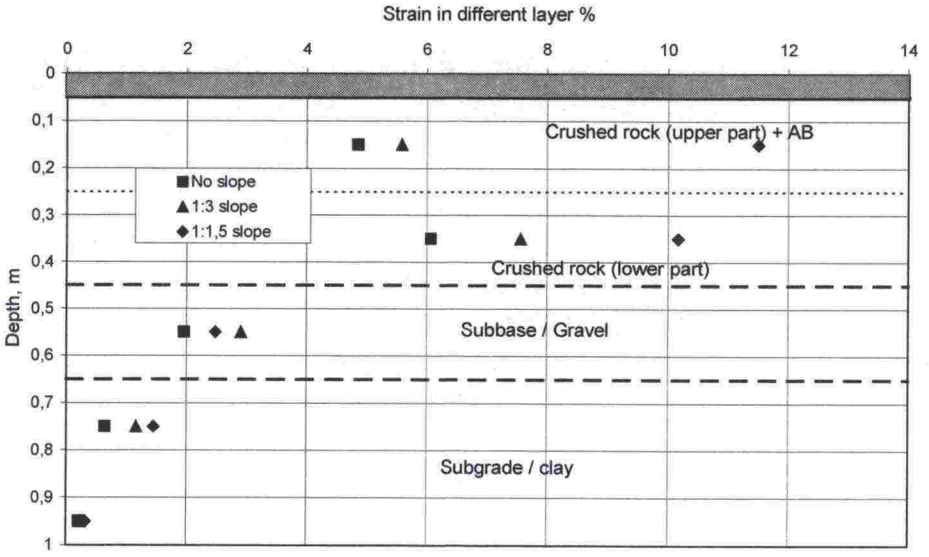

Figure 7.3. The deformations (calculated from maximum settlement) for the different 200 mm layers.

The development of permanent deformations in different structures under different loads is presented in Figures 7.4 to 7.6. The deformation for the upper part of crushed rock is calculated, the others are based on Emu-Coil measurements. In the structure with no slope, the maximum of permanent deformations develops in the lowest part of the crushed rock layer approximately 0.24 to 0.44 m from the surface when the load increases to 40 kN or greater. In both structures with slopes, however, the deformations concentrate the more strongly on the upper part of the crushed rock the greater the load and the higher the water table level. According to calculations, the thinner surface layer of the structure with gentle slope increases the stress in the upper layers and, thus, deformations in relation to corresponding layers in other structures should also be greater. Yet, the measurements did not reveal any significant increase in deformations.

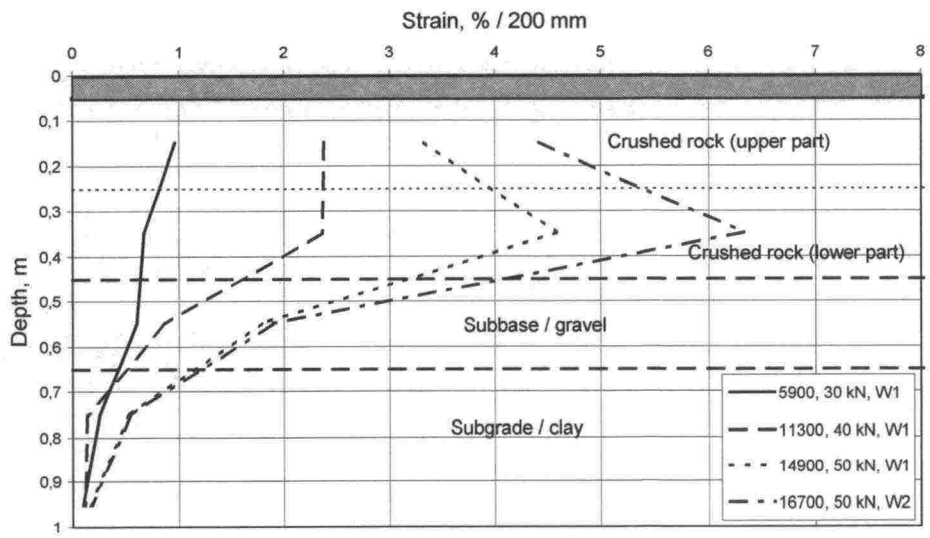

Figure 7.4. The development of deformations under different loads in the structure with no slope.

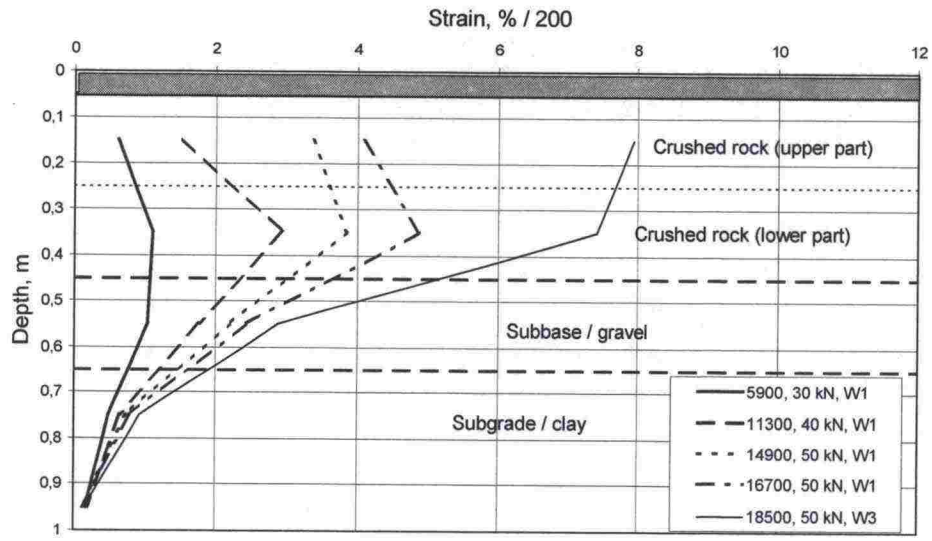

Figure 7.5. The development of deformations under different loads in the structure with 1:3 slope.

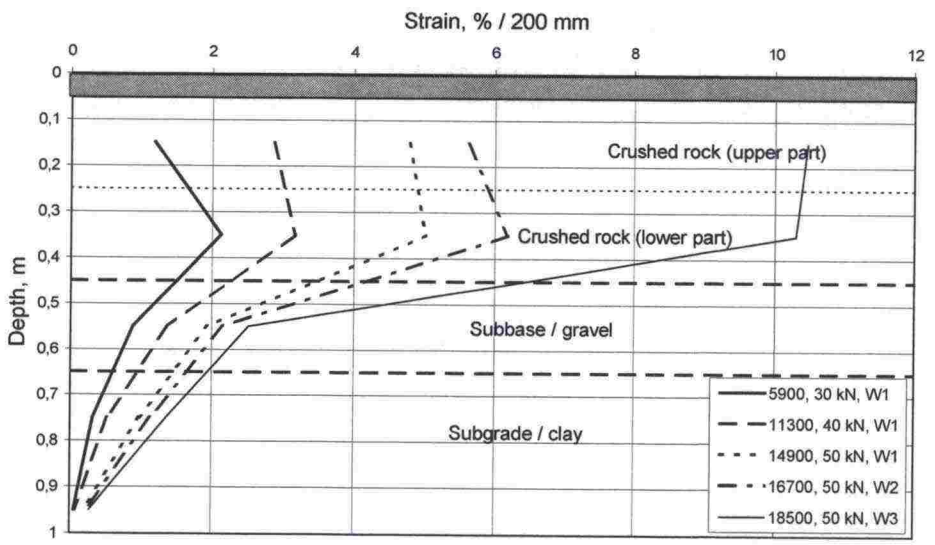

Figure 7.6. The development of deformations under different loads in the structure with 1:1.5 slope.

The distribution of permanent horizontal displacements in the sloped sections is presented in Figures 7.7 (1:3 slope) and 7.8 (1:1.5 slope) as a function of the load. The uppermost measurement is based on the displacements of reference tacks in the surface of the structure and the lower ones on lateral displacement gauges in the slopes. According to the measurements, on gentle slopes, the displacements are at their greatest near the surface, and on steep slopes, the displacements concentrate in the crushed rock layer. The structure with steep slope is very near to failure and

the deformations generated are great. The concentration of permanent deformations in the crushed rock layer indicates that the failure surface is located in this layer. Whereas, in the structure with gentle slope, the deformations concentrate in the upper parts of the structure, in which case the failure surface is probably located higher and reaches the soil surface.

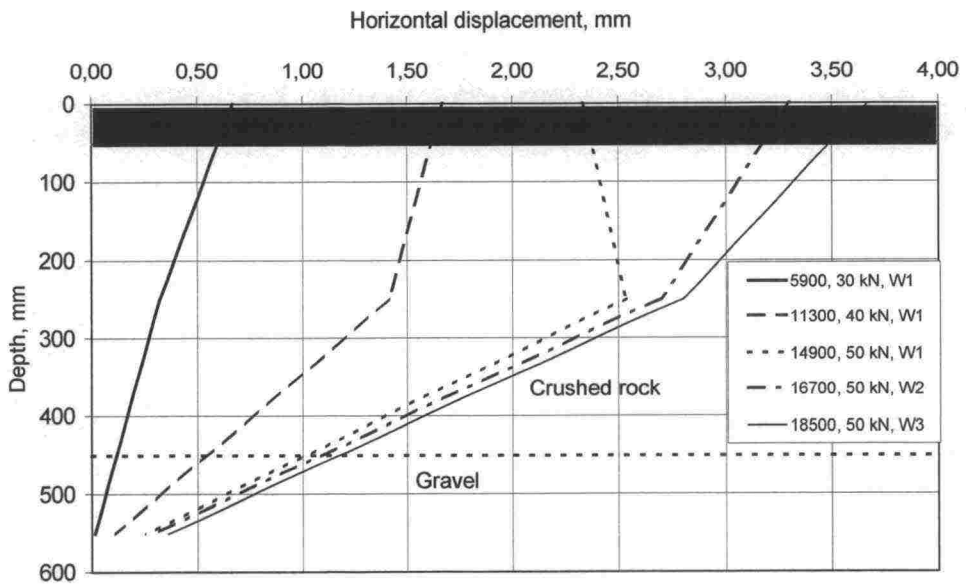

Figure 7.7 *The development of horizontal displacement under different loads in the structure with 1:3 slope.*

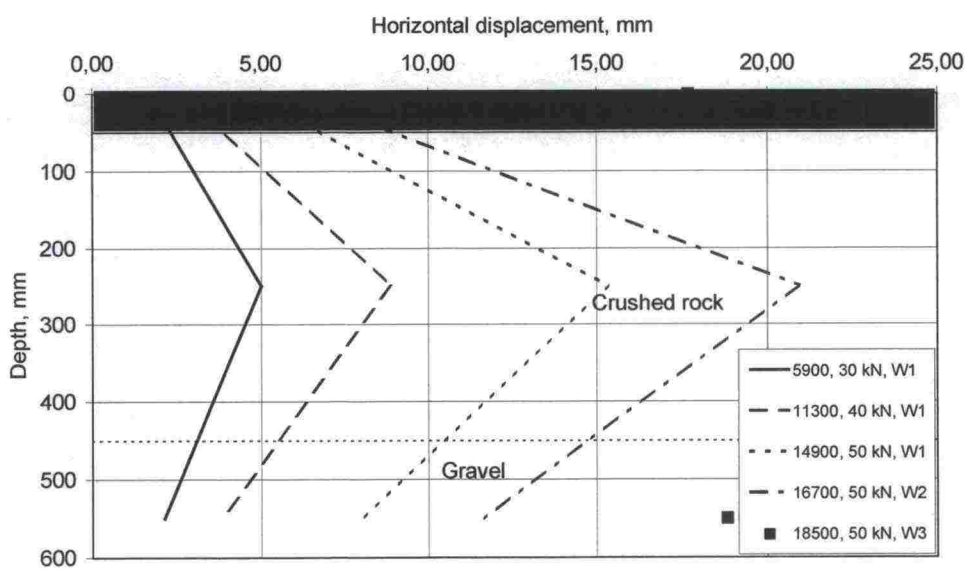

Figure 7.8. *The development of horizontal displacement under different loads in the structure with 1:1.5 slope.*

7.3 The ratio of resilient and permanent deformations

7.3.1 The ratio of horizontal deformations

The ratio of resilient and permanent (plastic) horizontal deformations adhere to the principle that permanent deformations increase as resilient deformations increase. Figure 7.9 shows the ratio of horizontal deformations in the lowest part of crushed rock under a load of 50 kN. Both resilient and permanent deformations were measured with lateral displacement gauges that were in the slopes. The positions of the lateral displacement gauges are shown in the cross section in Appendix 4.

The figure 7.9 shows a clear increase in permanent deformations per pass once a certain threshold value in resilient deformations is exceeded. This threshold value for crushed rock and gravel is approximately 100 μm. The extent of resilient deformations depends on the stress state prevalent in the structure at the time. The increase in permanent deformations is also significantly influenced by changes in water content and the steepness of the slope.

The great differences in resilient horizontal deformations, while the steepness of the slope and the water content remained the same, are due to the way the structure was loaded. The structure was loaded in cycles of 600 passes so that the loading wheel was first positioned on the left side of the rut, approximately 300 mm from the centre, then in the centre and finally 300 mm to the right of the rut (positions 1, 2 and 3 in Figure 1.1). The greatest displacements were naturally observed in load position 3 when the wheel was nearest to the slope, and the smallest when the load was the farthest from the slope.

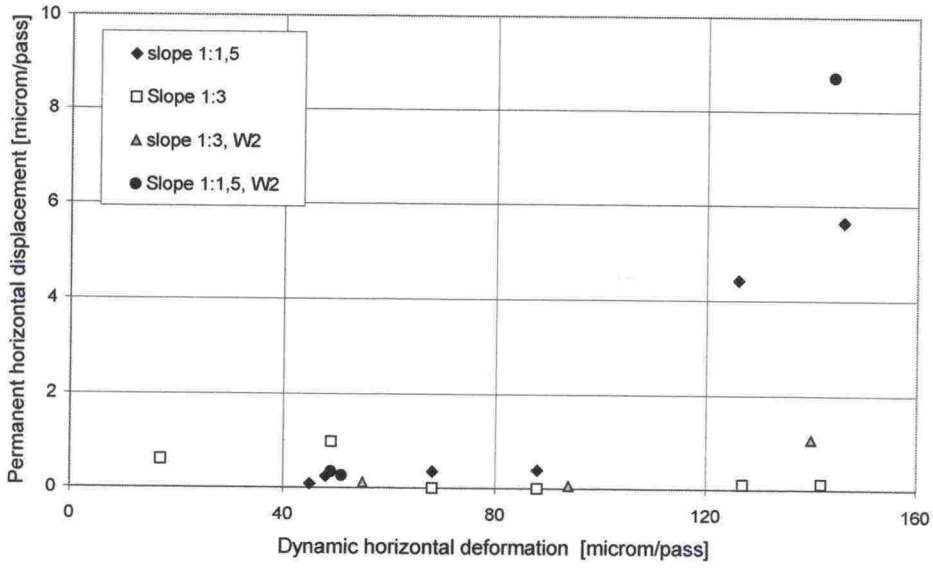

Figure 7.9 Ratios of horizontal deformations in the lowest part of crushed rock under a load of 50 kN.

7.3.2 The ratio of vertical deformations

Vertical deformations were compared on the basis of Emu-Coil measurements. The comparison follows the same principles as for horizontal deformations. However, the position of the sensors differed significantly, as the lateral displacement gauges were located in the slope whereas deformation sensors were directly underneath the centre line of loading. Vertical deformations have only been compared for measurements from directly under the load.

Figure 7.10 presents the ratios of resilient and permanent vertical deformations in the lowest part of crushed rock under a load of 50 kN. In this study, resilient deformation is the total deformation, that is, it is the sum of dynamic and plastic resilient deformation. Such a clear turning point or threshold value as for horizontal deformations cannot be detected for vertical ones.

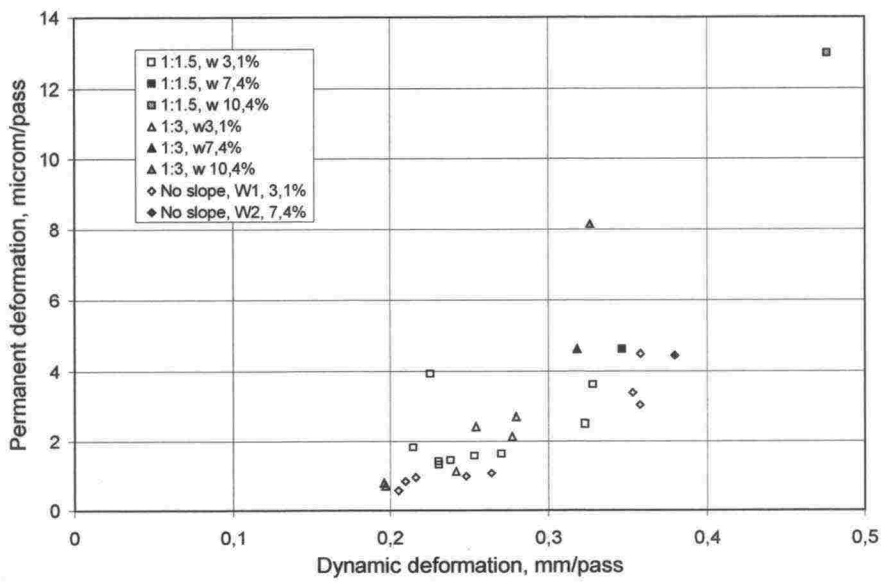

Figure 7.10 Ratios of vertical deformations in the lowest part of the crushed rock.

7.3.3 Resilient moduli back-calculated from the structure

When the transient stress state of the structure (earth pressure σ_{zmax}) and resilient deformation ε_{zmax} (Emu-Coil) are known, the corresponding dynamic resilient moduli can be determined with the Formula 7.1:

$$E = \frac{\Delta\sigma_{z\max}}{\Delta\varepsilon_{z\max}}. \qquad (7.1)$$

in which
- E — dynamic resilient modulus (MPa)
- $\Delta\varepsilon_{zmax}$ — incremental resilient vertical deformation
- $\Delta\sigma_{zmax}$ — incremental transient vertical earth pressure

Earth pressure was monitored in both the gravel and clay layers. The dynamic resilient modulus of gravel is presented in Figure 7.11 and that of clay in Figure 7.12. The figures furthermore show the change in wheel load during the testing and the results from Loadman bearing capacity measurements of the gravel layer. The values of the moduli, for gravel, in particular, show significant variation. The average values for the moduli are given in Table 7.2.

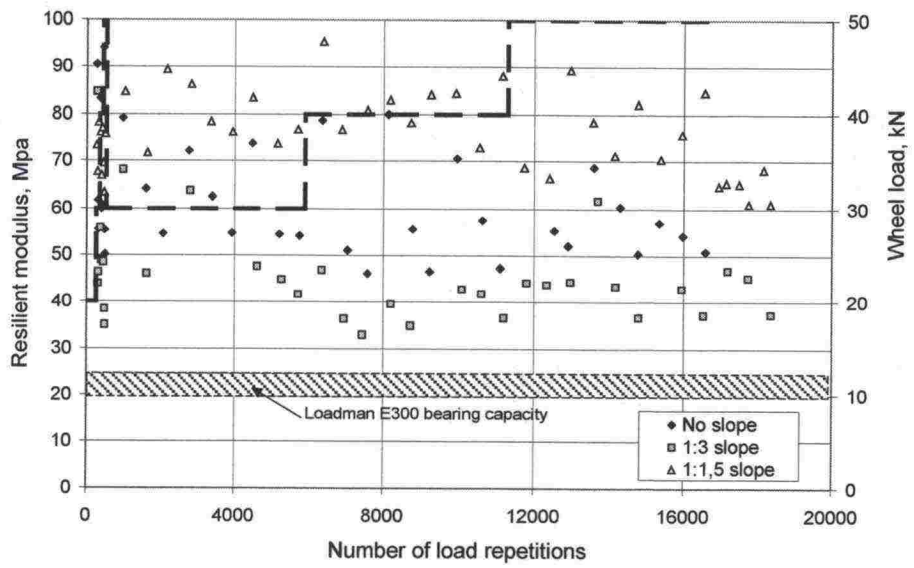

Figure 7.11 The dynamic resilient modulus of the gravel layer.

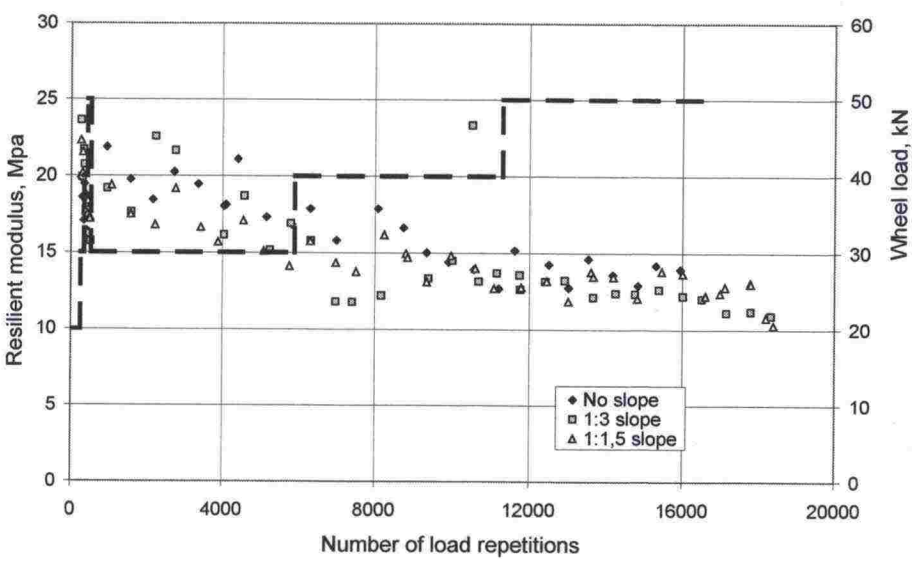

Figure 7.12 The dynamic resilient modulus of the clay layer (determined from the top part of the layer).

On the basis of the results, it cannot be said that the steepness of the slope influenced the values of the modulus in an unambiguous way. The structure with steep slope received higher modulus values than structures with no slope or gentle slope, particularly in the gravel layer. The greater variation in measurement results in the gravel layer can be due to defective functioning of earth pressure cells and/or Emu-Coil measurements in granular materials. The modulus defined for clay in laboratory tests after 10,000 load cycles is approximately 7.0 MPa and for gravel after 100 cycles 80 MPa in the corresponding range of stress. The E_{300} resilient modulus values (Loadman) measured from the surface of the gravel varied between 20 and 25 MPa.

Table 7.1. Average resilient moduli in clay and gravel layers for different structures.

Structure	Resilient modulus, gravel, MPa	Resilient modulus, clay, MPa
laboratory result	80	7
no slope	62	17
1:3	46	16
1:1,5	76	15

7.4 Separate interesting phenomena

According to profilometer measurements, the speed of rutting within each load step decreased (Figures 7.13 and 7.14) in all structures. The results show some variation, but, on average, the trend is clear. However, if the material's water content increased (heavy rains, elevating the water table level to W2 and W3), rutting speed also increased. In the structure with steep slope, the elevation of the water table level to the crushed rock (W3) significantly accelerated rutting speed. It is even possible that continuing the loading might have caused a local failure.

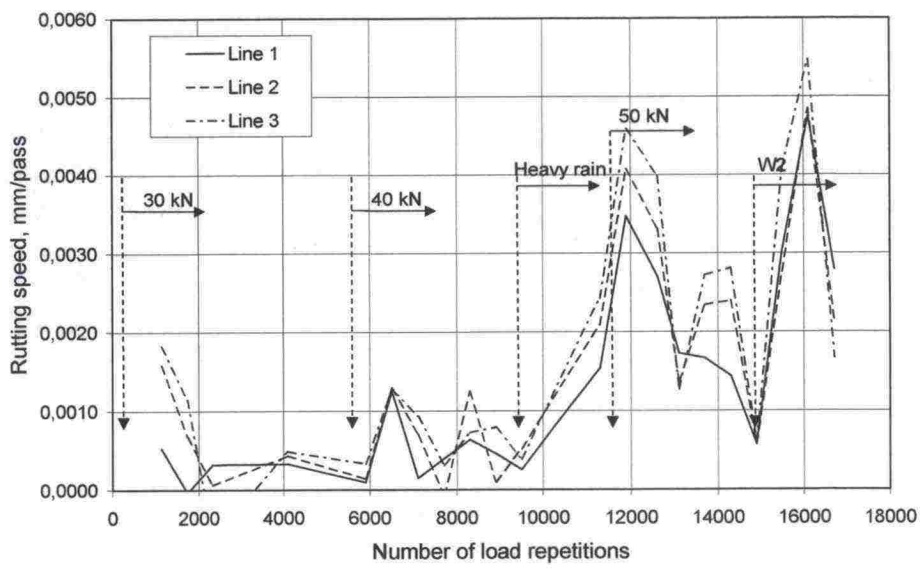

Figure 7.13 Rutting speed, no slope.

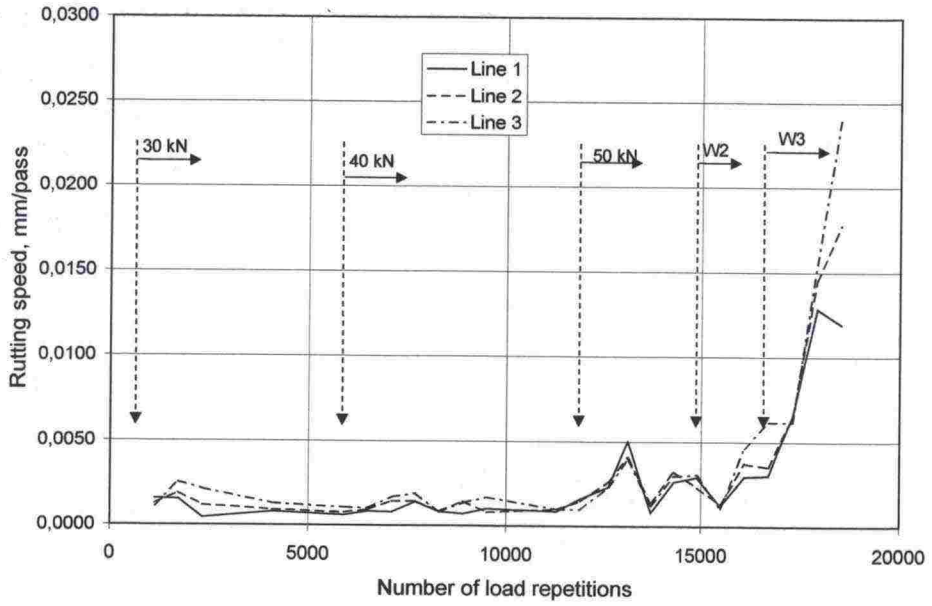

Figure 7.14 Rutting speed, slope 1:1.5

8 GEOM FACTOR

8.1 GEOM factor on the basis of HVS tests

A structural deformation design method developed in the low-volume road project represents the width of the road and the steepness of the slope with the GEOM factor. The GEOM factor was determined in the HVS test on the basis of the development of rut deepness measured by a profilometer. Figure 8.1 shows the development of rut deepness for all three structures.

Thus, in order to determine the GEOM factor, there was data on the development of rut deepness inflicted on the structure on different structures, different distances from the edge of the slope and different loads. As for the road width that affects the factor, it was decided on the basis of the results that loading 450 mm from the edge corresponded to road width 5.5 m, loading at 750 mm to 6.5 m and loading at 1050 mm to 7.5 m. The solution was arrived at on the basis of average rut positions measured on roads. That is, the GEOM factor cannot be directly applied for roads with wider pavements.

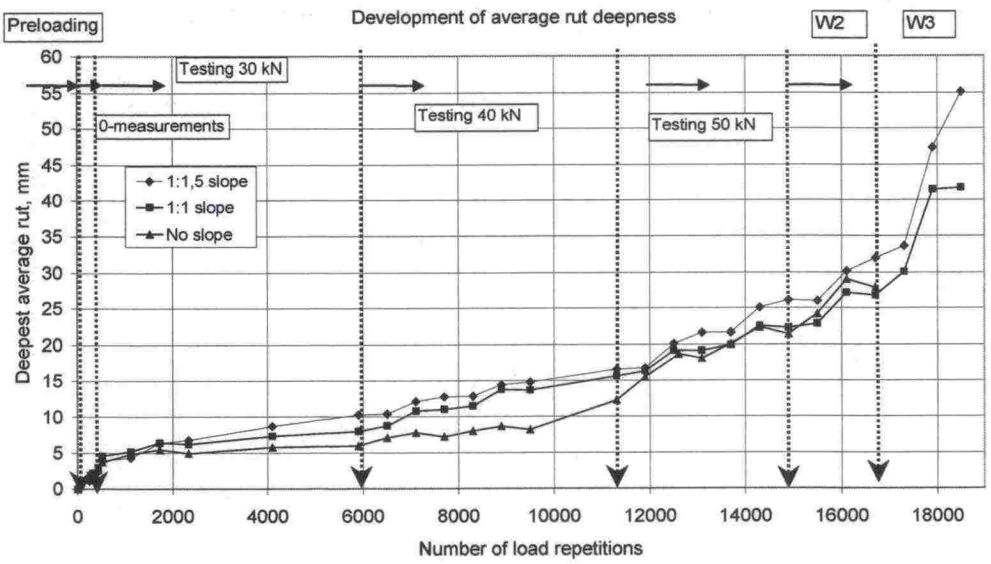

Figure 8.1 Development of rut deepness as a function of load.

The results for rutting speed are comparable, except for the results on the structure with no slope after 9,500 load repetitions. After this number of load repetitions, the development of rut deepness shows a strong increase as compared with the corresponding results for other structures. This was due to the structure getting wet because of heavy rains, thus increasing rutting.

Because of the limitations caused by the increase in water content, it was decided to use development of rut deepness for 500 to 9,500 passes as basic data for all structures (load 30/40 kN) and, for sloped structures, development of rut deepness that occurred at 11,300 to 14,900 passes (load 50 kN). A suitable fitted curve was sought on the basis of these rutting speeds.

In the last phase of determining the GEOM factor, the value of rutting speed for 6.5 m road width and 1:3 slope was set as a reference value. The value of this rutting speed was defined as 1 and other figures were converted to correspond to the reference value. This gives the equation in Formula 8.1 for the GEOM factor. Figure 8.2 presents the value of the GEOM factor in a graphic format.

$$GEOM = 0.407 + \frac{-0.273 \cdot B^2 + 2.785 \cdot B - 4.971}{2.7^{\left(kalt/3\right)}} \qquad (8.1)$$

in which

B	road width, metres
kalt	steepness of the slope, 1: kalt

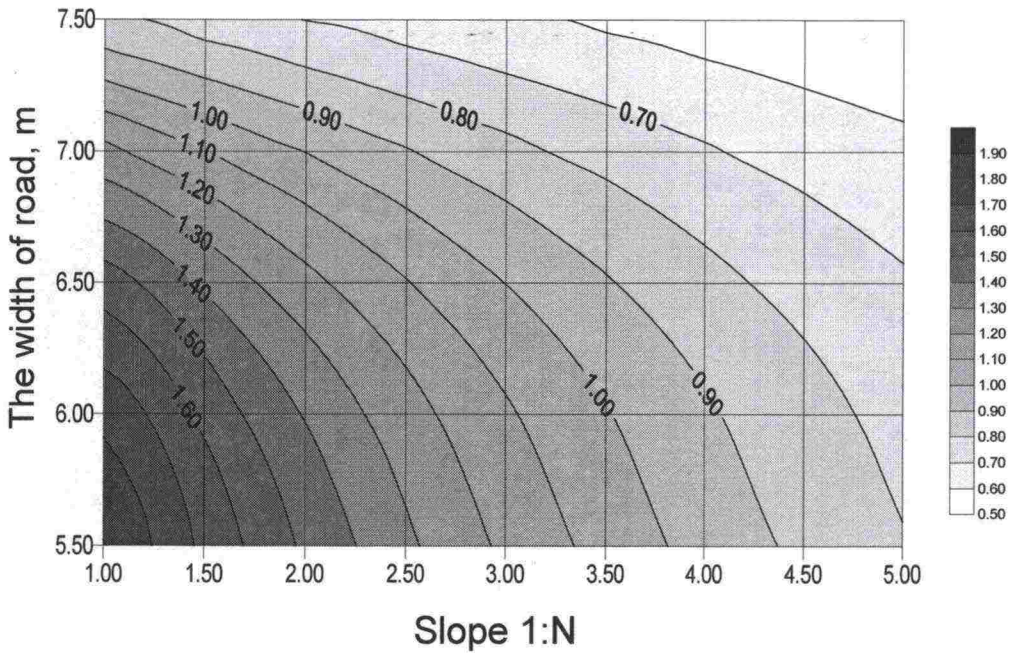

Figure 8.2 The GEOM factor as a function of slope steepness and road width.

9 CONCLUSIONS AND SUGGESTIONS FOR FURTHER RESEARCH

A great deal of measurement data was generated in different phases of the HVS tests. In this report, the data has been analysed in view of the aims of the study. The results will be analysed further in the future. Further research will look more deeply into the ways permanent deformations are created and the effect changes in water content have on them.

On the basis of research already carried out, it can be concluded that:

- Most of the deformation in the test structures occurred in the lowest part of the base course, 240 to 440 mm from the surface of the road. 63 to 80% of total rutting occurred in the uppermost 400 mm of the unbound layers. The share of the gravel layer deeper down was 9 to 13%. In the structure with no slope, the deformation maximum was located deeper (250 to 450 mm) than in structures with slope – 1:3 slope in particular – in which the maximum was located the highest (50 to 250 mm).
- Deformations in the structure with gentle slope were not much greater compared to other structures even though its surface layer was, on average, the thinnest.
- Changes in the structure's water content had a significant effect on permanent deformations.
- Permanent deformations begin to increase significantly after exceeding a threshold value for stress (dynamic deformation) that depends on the material and its state of compaction. This phenomenon was observed in

both laboratory tests and the test structures. It was particularly clear for horizontal displacements. The threshold value for resilient horizontal deformation for both gravel and crushed rock was approximately 100 μm.

- It was possible to design the test structure in advance quite well.
- Although the test structure was constructed carefully, there were significant variations in the thickness of the surface layer, bearing capacities and densities of the layers. Preloading the structures before testing adjusted these differences slightly.
- Apart from the settlement profile measurements, the results of deformation measurements were reliable.
- On the basis of studying the modelling, it can be said that the deformations and stresses appearing in the test structures during loading can be estimated reasonably well with quite rough initial values and models.
- The location of the failure surface in different structures can be deduced on the basis of the results of deformation measurements.
  - The structure with steep slope was very near failure limit state, and the deformations generated were great. The greatest horizontal displacements in the slope were located in the gravel layer, which suggests that the whole slope moved horizontally to a significant extent and that the failure surface was located deeper in the gravel layer.
  - The greatest horizontal displacements in the structure with gentle slope occurred in the upper parts of the slope. The majority of displacements, both horizontally and vertically, occurred in the upper parts of the structure, so the failure surface was also mainly located in the crushed rock layer.
  - In structures with no slope, the failure surface ran through the lowest part of the crushed rock and rose higher immediately outside the loading area.
- The resilient moduli back-calculated for the gravel layer from the measurements were lower than those determined in laboratory tests, and the back-calculated moduli for the clay layer were higher. Correspondingly, it was observed that according to various measurements, less stresses are concentrated in the gravel layer and more in the upper part of the clay layer than was anticipated on the basis of the modelling.
- The speed of rutting decreased in each load step as the number of load repetitions increased.
- Rut deepness, slope steepness and load distances from the edge were used to deduce the equation for the GEOM factor representing the shape of a road cross section, which can be used for designing improved road structures. This factor allows estimation of the impact of the cross section on rutting speed.

10 REFERENCES

Kangas H. and Törnqvist J. *Tutkimusaltaan vaikutus rakenteiden muodonmuutoksiin HVS-kuormituksessa.* Draft 6.2.2001. 15 p.

Korkiala-Tanttu L., Rathmayer H. and Kangas H., *Performance evaluation of a Bi-component geotextile in accelerated pavement test.* Seventh International Conference on Geosynthetics 22.9.-27.9.2002 Nice. In print.

11 APPENDICES

Appendix 1. Levelling results for the upper surface of different layers
Appendix 2. Density measurements of structural layers
Appendix 3. Bearing capacity measurements of structural layers
Appendix 4. Map and cross sections of test site
Appendix 5. Falling weight deflectometer measurements before testing
Appendix 6. Radiometric density and moisture measurements before testing
Appendix 7. Pore pressure measurements
Appendix 8. Earth pressure measurements
Appendix 9. Accelerometer measurements
Appendix 10. Profilometer and straight edge measurements
Appendix 11. Loadman measurements
Appendix 12. Crushed rock deformations
Appendix 13. Gravel deformations
Appendix 14. Clay deformations
Appendix 15. Lateral displacements
Appendix 16. Cracking, steep slope
Appendix 17. Element grid, bulk moduli of the materials, level curves in the calculation model and the state of the elements in the load states, slope steepness 1:1.5, load 50 kN.

LEVELLING RESULTS FOR THE UPPER SURFACE OF DIFFERENT LAYERS

Clay top surface

Date:			27.10.2000	/ jue
	No slope	Slope 1:3	Slope 1:1,5	Planned
average	15.739	15.738	15.746	+15.75
deviation	0.012	0.011	0.010	
min	15.722	15.713	15.729	
max	15.762	15.754	15.767	

Gravel
central level control line

Date:			13.11.2000	/ jue
	No slope	Slope 1:3	Slope 1:1,5	Planned
average	15.951	15.950	15.959	+15.95
deviation	0.005	0.005	0.003	
min	15.939	15.934	15.954	
max	15.966	15.960	15.967	
thickness of the layer	0.212	0.212	0.213	

Crushed rock

Date:			15.11.2000	/ jue
	No slope	Slope 1:3	Slope 1:1,5	Planned
average	16.348	16.343	16.362	+16.35
deviation	0.007	0.007	0.004	
min	16.337	16.329	16.351	
max	16.359	16.356	16.368	
thickness of the layer	0.396	0.393	0.402	

AC

Date:			24.11.2000	/ jue
	No slope	Slope 1:3	Slope 1:1,5	Planned
average	16.395	16.380	16.403	+16.40
deviation	0.002	0.006	0.003	
min	16.391	16.369	16.397	
max	16.398	16.389	16.407	
thickness of layer	0.047	0.037	0.041	

Average thicknessess of the layers.

Layer	No slope	1:3 slope	1:1,5 slope
AC 40 mm	47	37	41
Crushed rock 400 mm	396	393	402
Gravel 200 mm	212	212	213

DENSITY MEASUREMENTS OF STRUCTURAL LAYERS

Troxler and volumeter test results for the gravel layer. The maximum dry bulk density according to laboratory tests is 21.3 kN/m^3. The comparison of degree of density was carried out between that and the volumeter tests considered more reliable.

Measurement 7.11.2000	**Water content w-% Troxler / volumeter**	**Bulk density, kN/m^3 Troxler / volumeter**	**Dry bulk density, kN/m^3 Troxler / volumeter**	**Degree of density % Sand cone volumeter / maximum dry bulk density**
No slope	7.70 / 9.07	21.56 / 21.27	20.02 / 19.49	91.5
Slope 1:3	8.37 / 8.05	21.77 / 22.31	20.08 / 20.65	96.9
Slope 1:1.5	7.27 / 7.83	21.53 / 21.22	20.07 / 19.69	92.4
Average	7.8 / 8.3	21.6 / 21.6	20.1 / 19.9	93.6

Troxler and sand cone volumeter test results for the crushed rock layer. The maximum dry bulk density according to laboratory tests is 21.9 kN/m^3. The comparison of degree of density was carried out between that and the volymeter tests considered more reliable.

Measurement 15.11.2000	**Water content w-% Troxler / sand cone volumeter**	**Bulk density, kN/m^3 Troxler / sand cone volumeter**	**Dry bulk density, kN/m^3 Troxler / sand cone volumeter**	**Degree of density % Sand cone volumeter / maximum dry bulk density**
No slope	3.26 / 3.3	21.34 / 20.15	20.67 / 19.49	89.0
Slope 1:3	4.95 / 4.5	19.47 / 21.85	18.58 / 20.91	95.5
Slope 1:1,5	4.78 / 4.6	20.58 / 21.28	19.65 / 21.28	97.2
Average	4.3 / 4.1	20.5 / 21.1	19.6 / 20.6	93.9

BEARING CAPACITY MEASUREMENTS OF STRUCTURAL LAYERS

Loadman measurements on gravel level

E_{300} (MPa)	No slope	1:3 slope	1:1,5 slope
Line 1, point 1	24	20	23
Line 1, point 2	24	19	25
Line 1, point 3	23	16	25
Line 1, point 4	23	17	24
Line 1, point 5	23	15	23
Line 2, point 1	21	20	30
Line 2, point 2	21	20	27
Line 2, point 3	20	20	28
Line 2, point 4	20	20	28
Line 2, point 5	20	20	28
Line 3, point 1	24,0	22,0	23,0
Line 3, point 2	23	24	24
Line 3, point 3	22	23	25
Line 3, point 4	22	23	24
Line 3, point 5	22	23	23
Average	22,13	20,13	25,33

Loadman measurements on crushed rock layer

E_{300} (MPa)	No slope	1:3 slope	1:1,5 slope
Line 1, point 1	35	38	29
Line 1, point 2	43	46	46
Line 1, point 3	51	46	48
Line 1, point 4	52	47	47
Line 1, point 5	51	46	51
Line 2, point 1	22	26	28
Line 2, point 2	34	40	40
Line 2, point 3	39	42	41
Line 2, point 4	40	44	42
Line 2, point 5	40	44	43
Line 3, point 1	29	36	25
Line 3, point 2	43	51	38
Line 3, point 3	48	54	41
Line 3, point 4	48	57	42
Line 3, point 5	48	56	44
Average	43,2	50,8	38

FALLING WEIGHT DEFLECTOMETER MEASUREMENTS

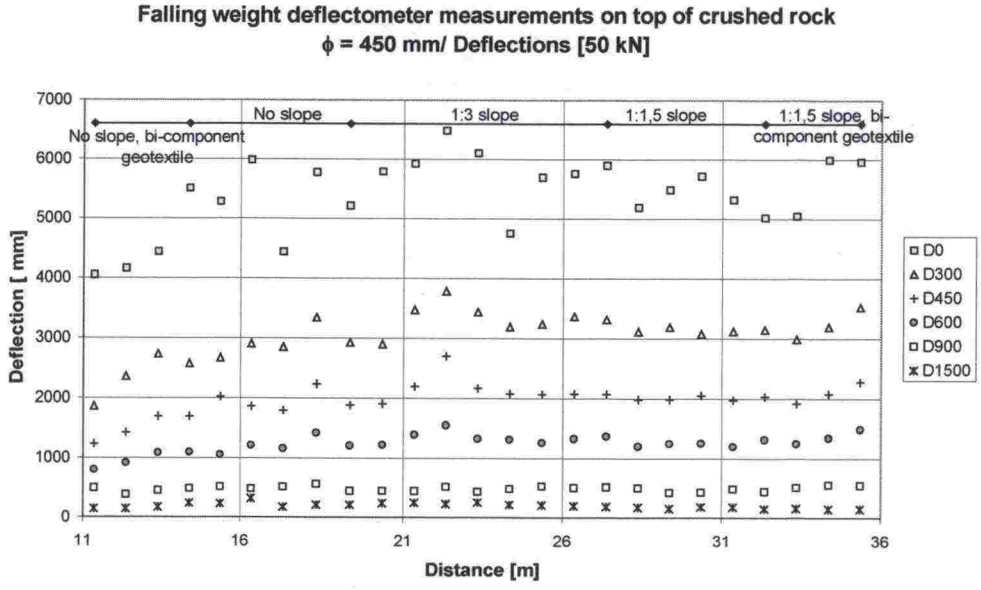

Falling weight deflectometer measurements on top of crushed rock. Deflections.

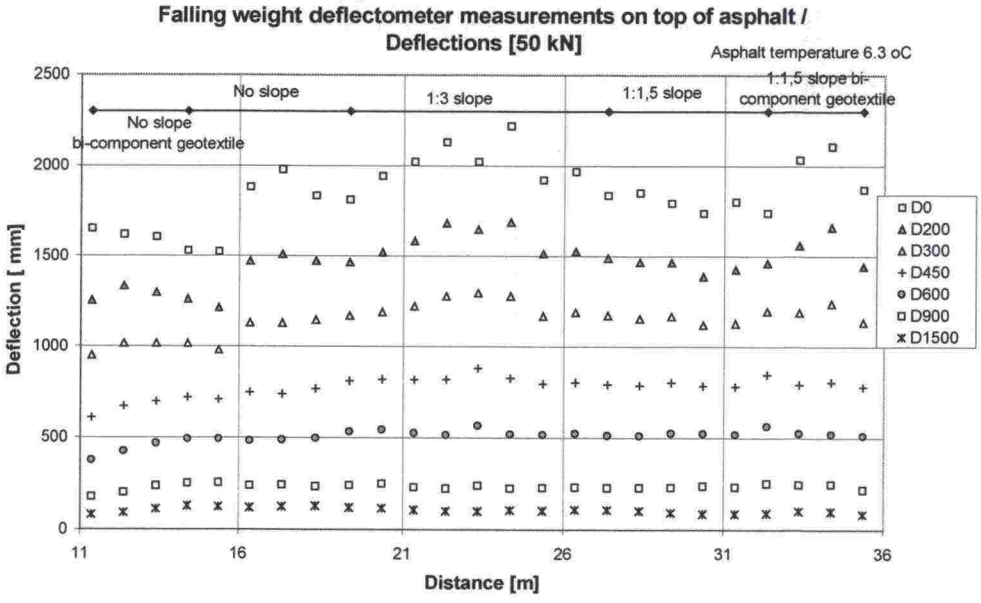

Falling weight deflectometer measurements on top of asphalt measured immediately after building. Deflections.

MAP AND CROSS SECTIONS OF TEST SITE

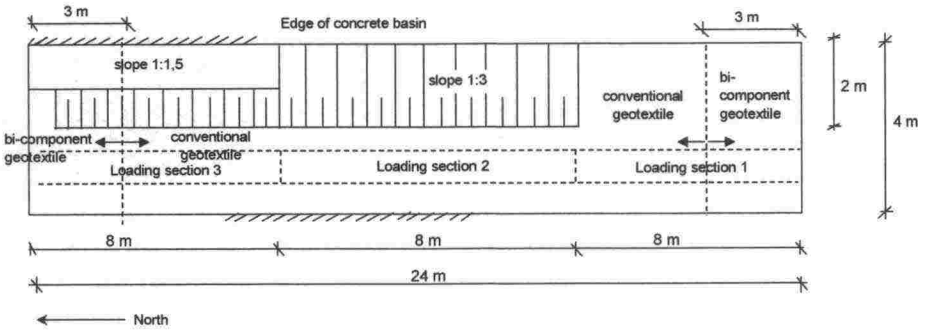

Map of test areas

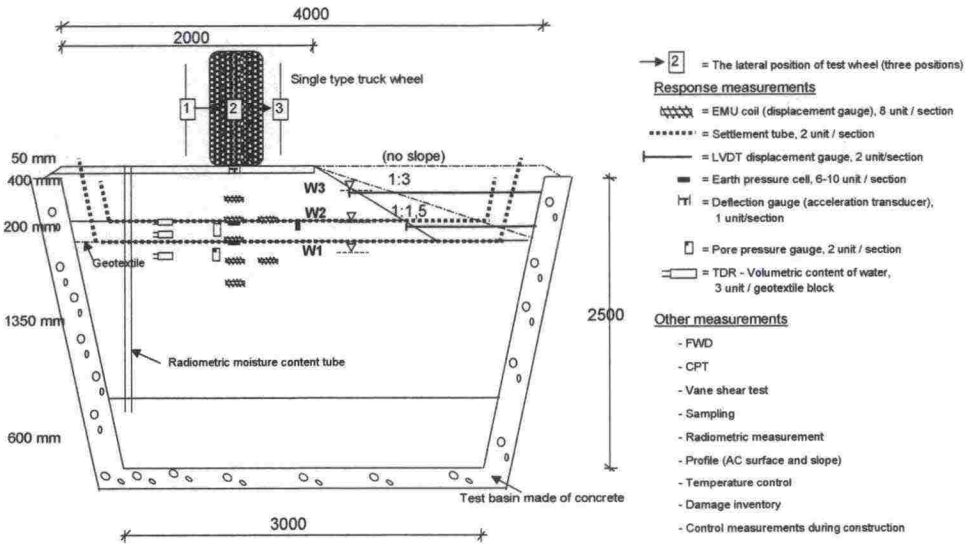

Cross sections

Structure with no slope, instrumentation, map and longitudinal profile

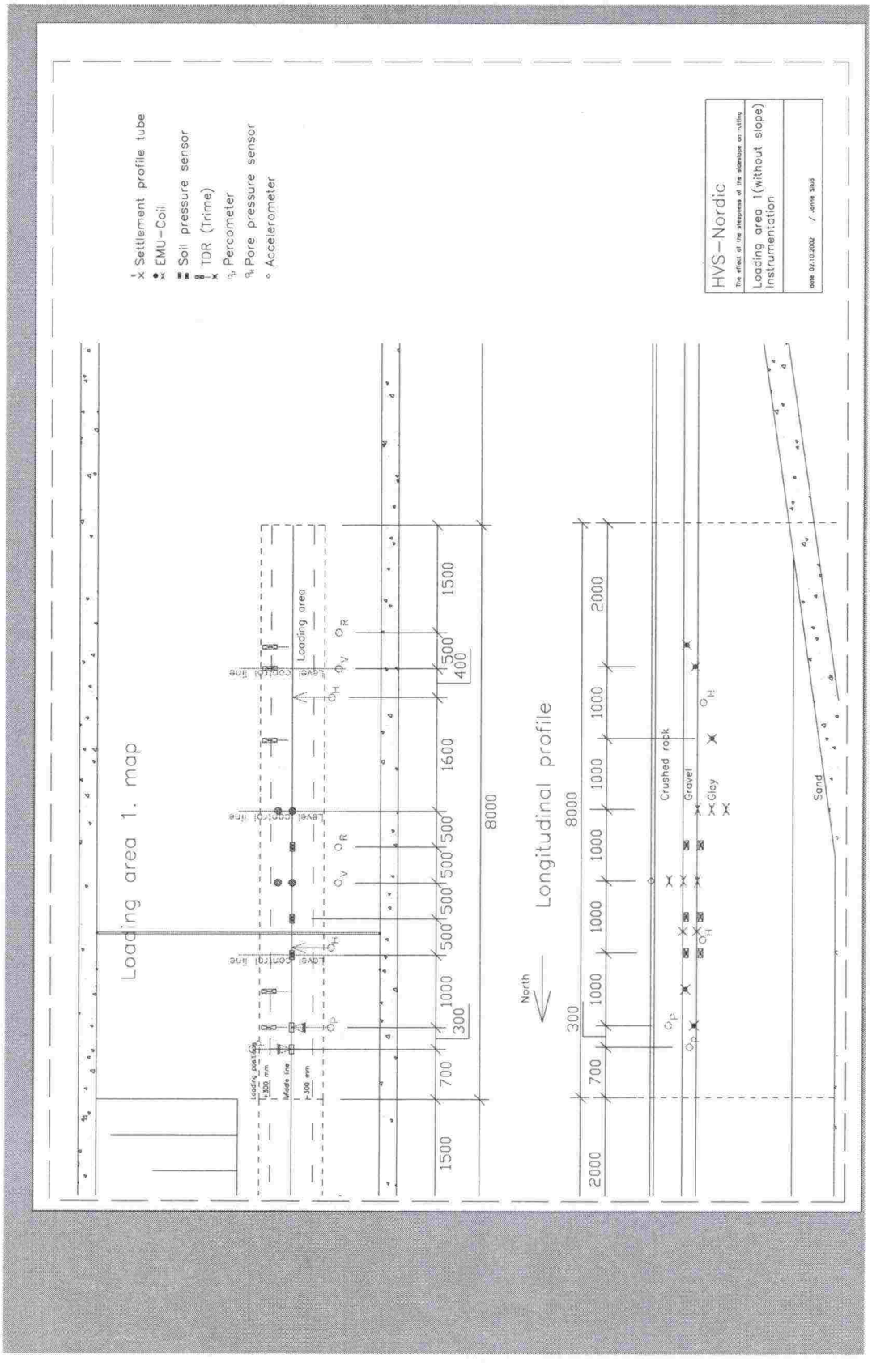

Structure with 1:3 slope, instrumentation, map and longitudinal profile

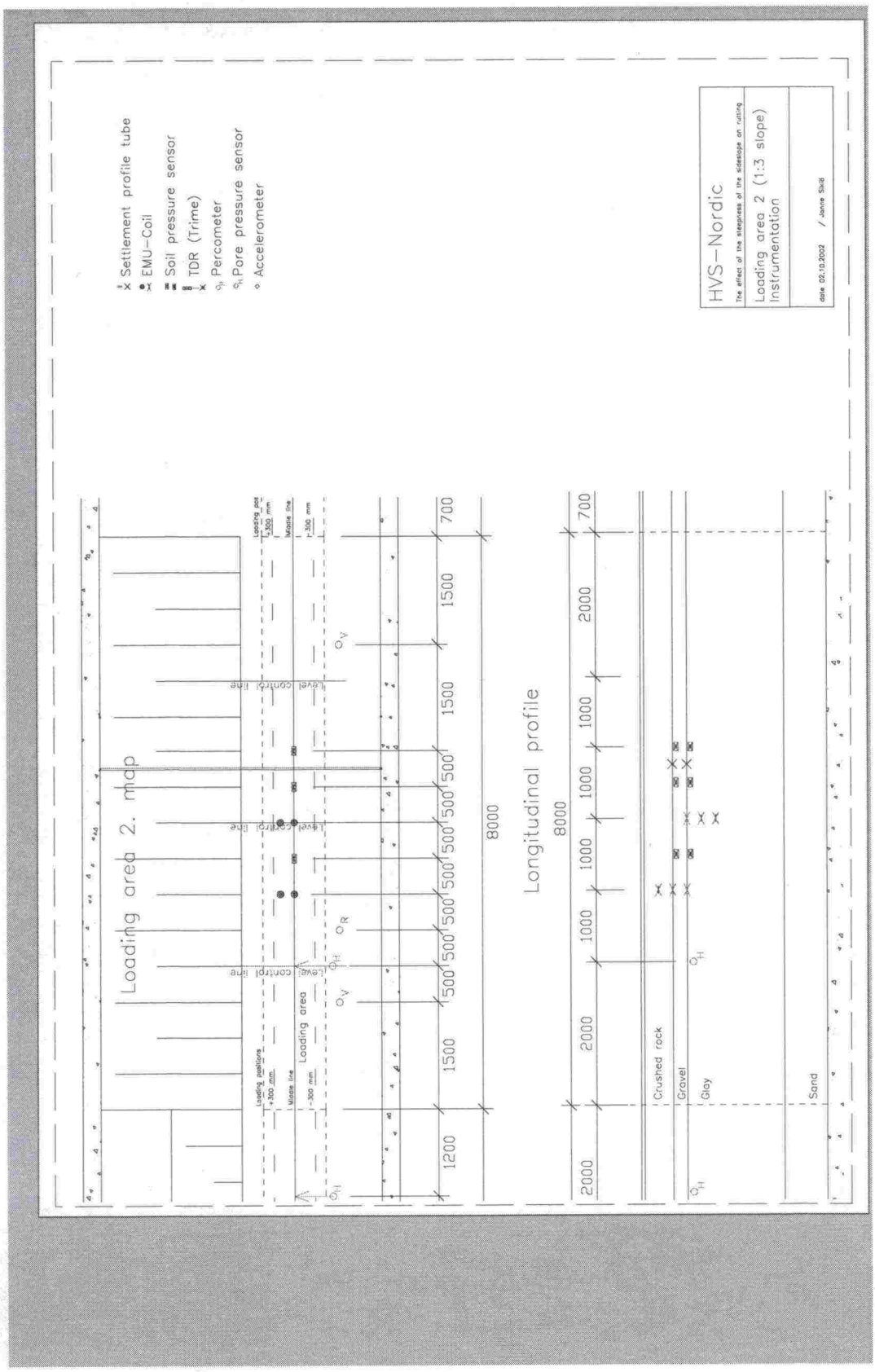

Structure with 1:1.5 slope, instrumentation, map and longitudinal profile

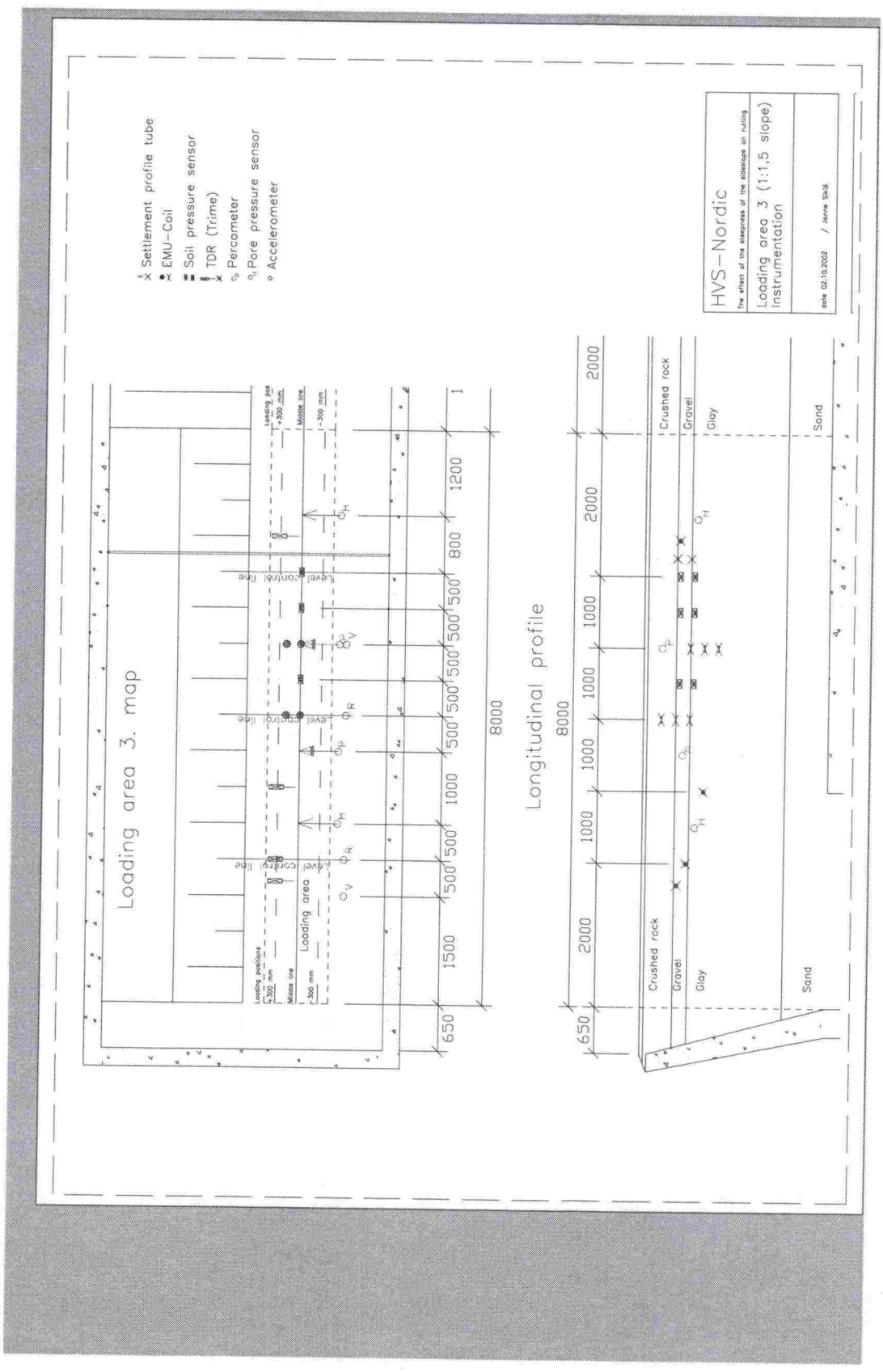

FALLING WEIGHT DEFLECTOMETER MEASUREMENTS BEFORE TESTING

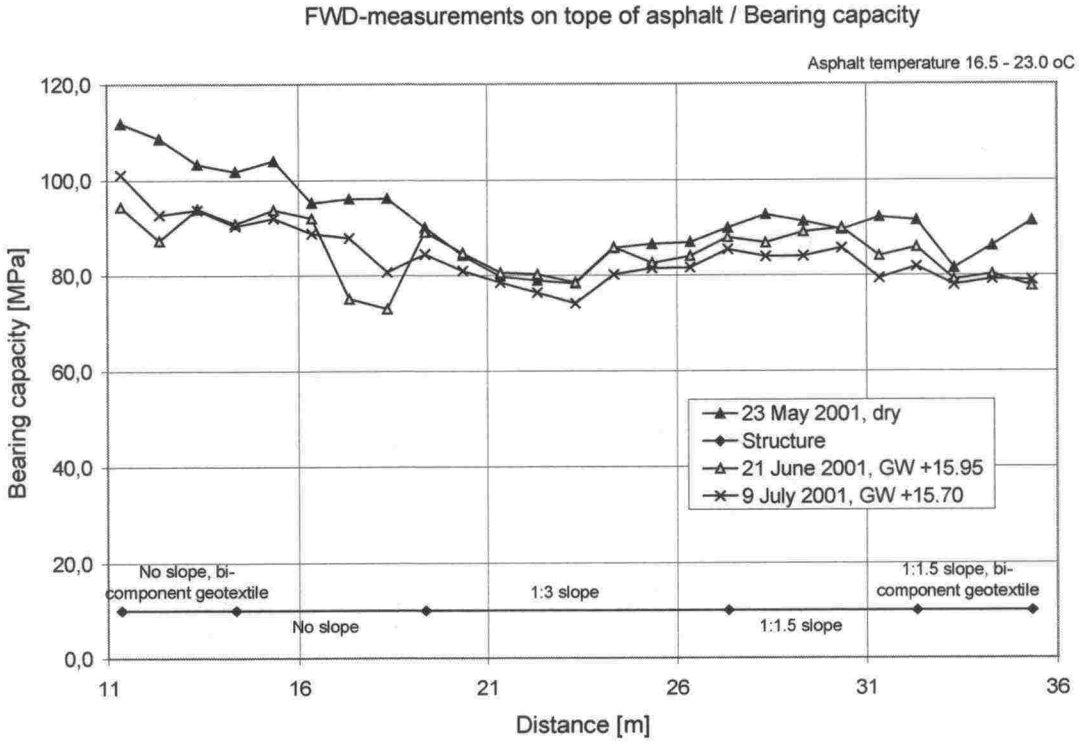

Figure 1. Results of bearing capacity measurements 23 May, 21 June and 9 July 2001

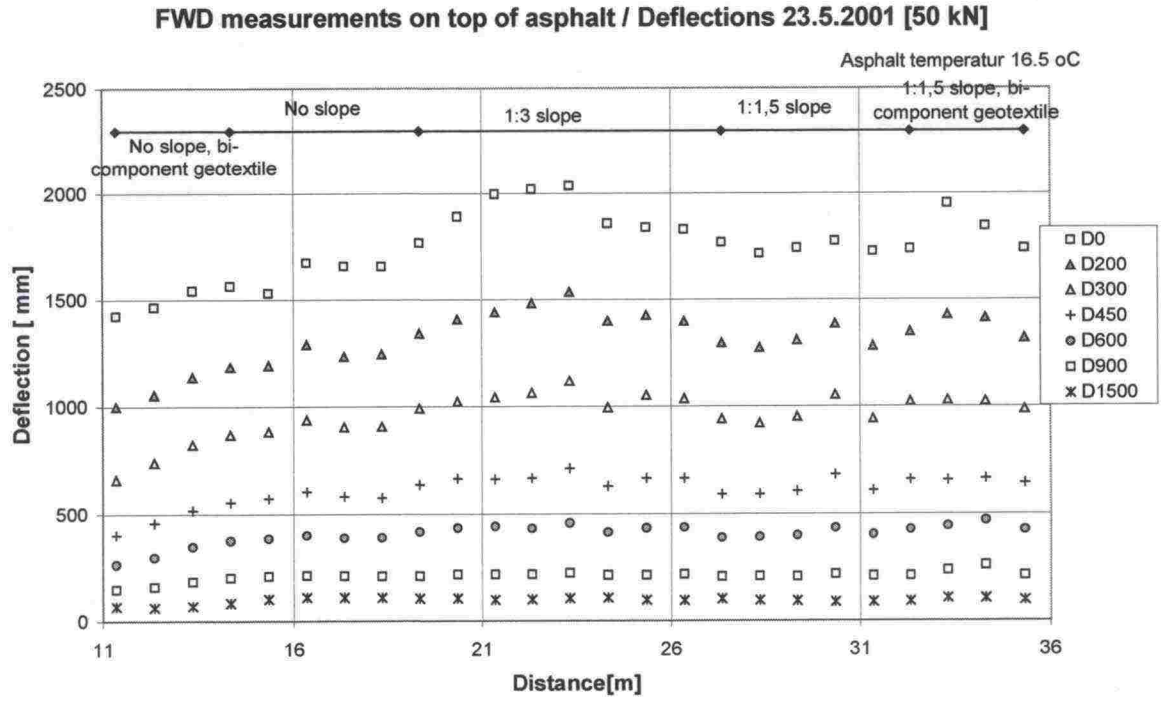

Figure 2. Bearing capacity measurements 23 May 2001

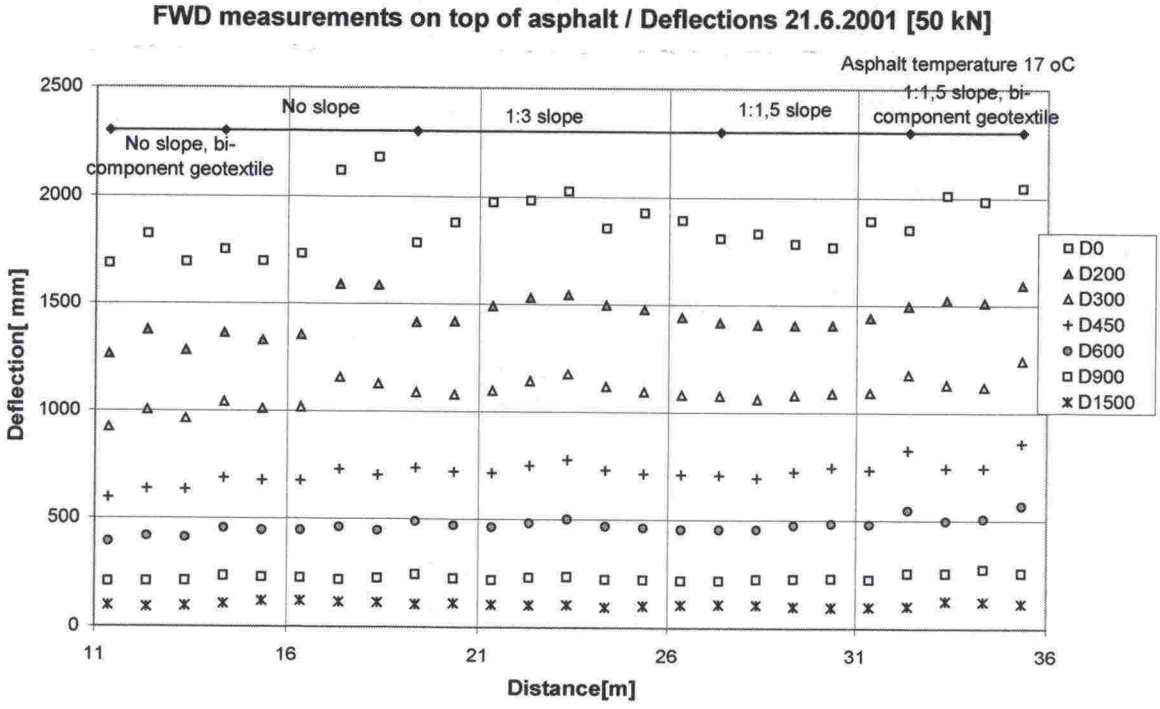

Figure 3. Bearing capacity measurements 21 June 2001

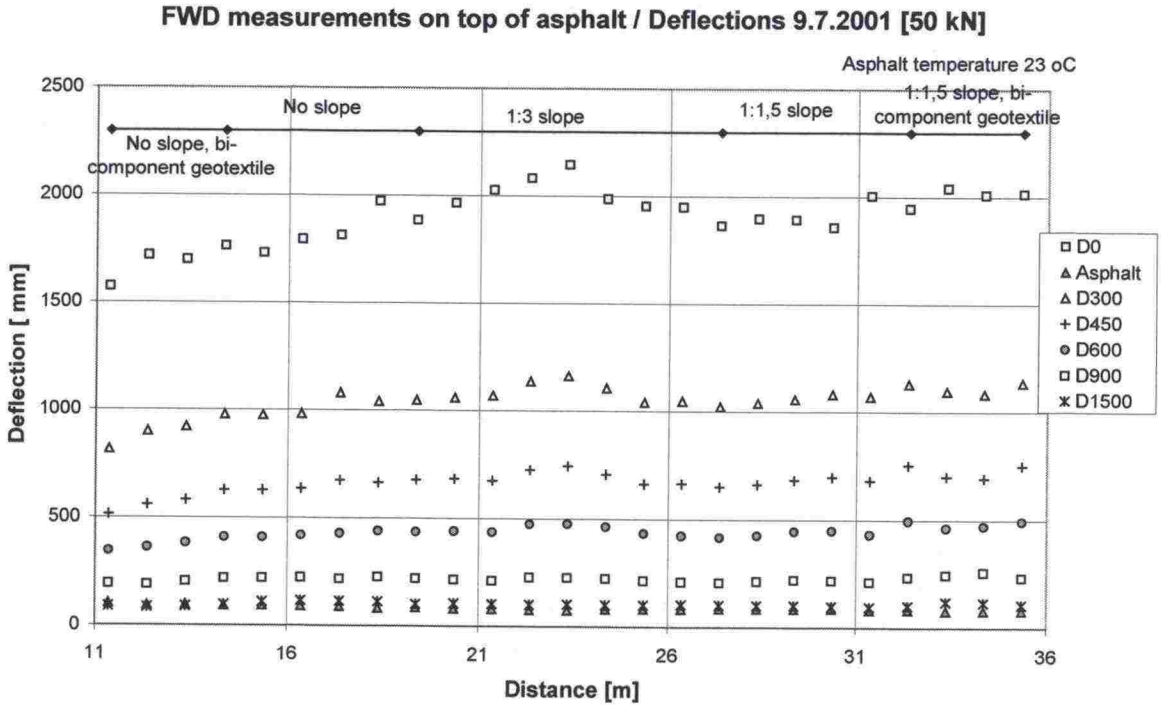

Figure 4. Bearing capacity measurements 9 July 2001

RADIOMETRIC DENSITY AND MOISTURE MEASUREMENTS BEFORE TESTING

25 June 2002 Ground water level W2 +15.95
29 June 2002 Ground water level lowered to W1 +15.70

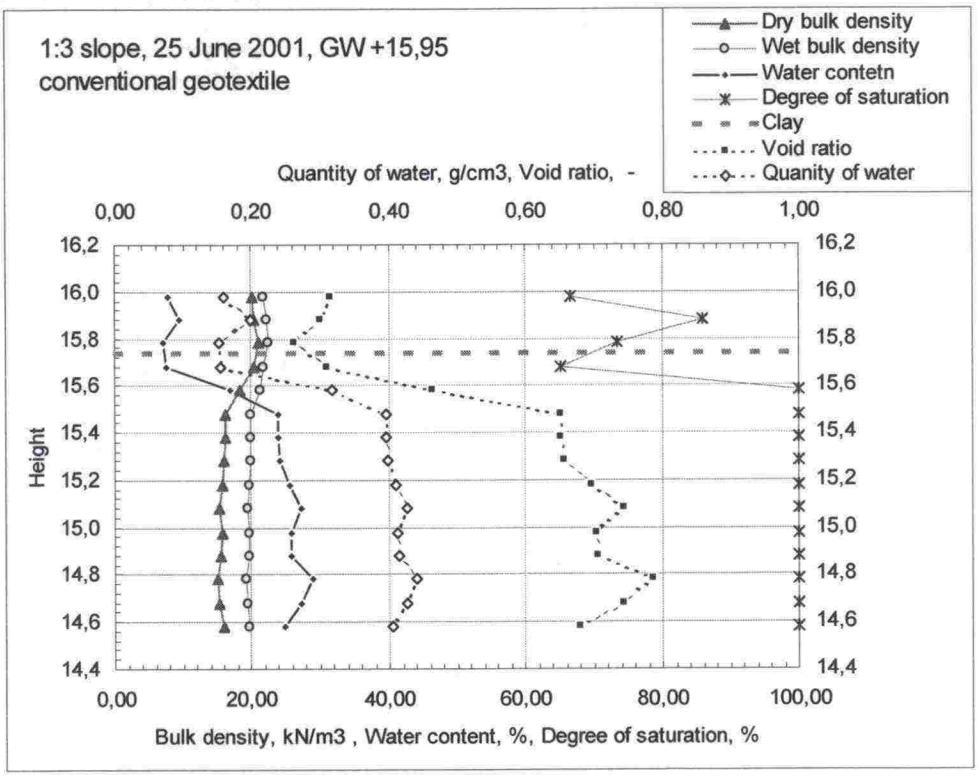

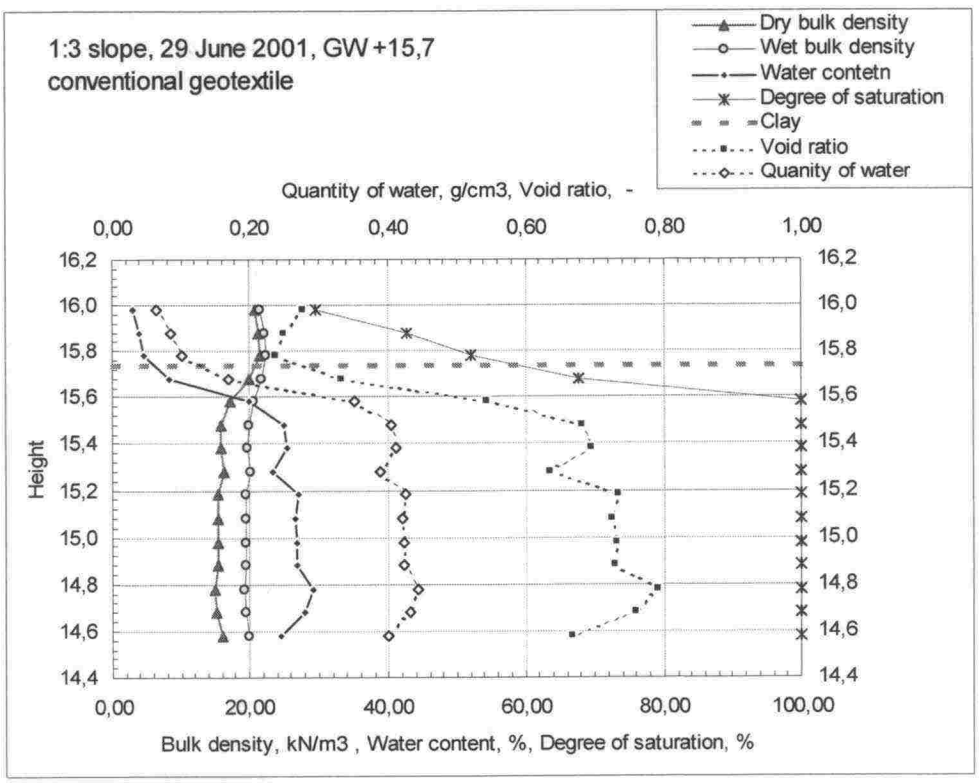

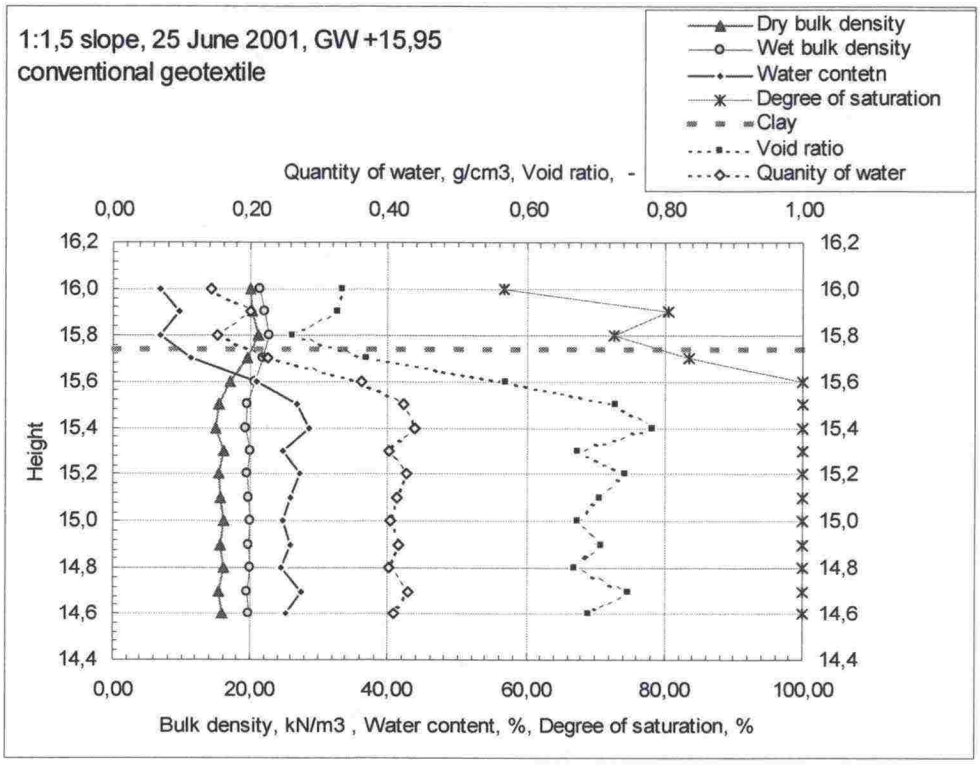
1:1,5 slope, 25 June 2001, GW +15,95
conventional geotextile
Dry bulk density
Wet bulk density
Water contetn
Degree of saturation
Clay
Void ratio
Quanity of water
Quantity of water, g/cm3, Void ratio, -
0,00 0,20 0,40 0,60 0,80 1,00
Height
16,2 16,0 15,8 15,6 15,4 15,2 15,0 14,8 14,6 14,4
0,00 20,00 40,00 60,00 80,00 100,00
Bulk density, kN/m3 , Water content, %, Degree of saturation, %

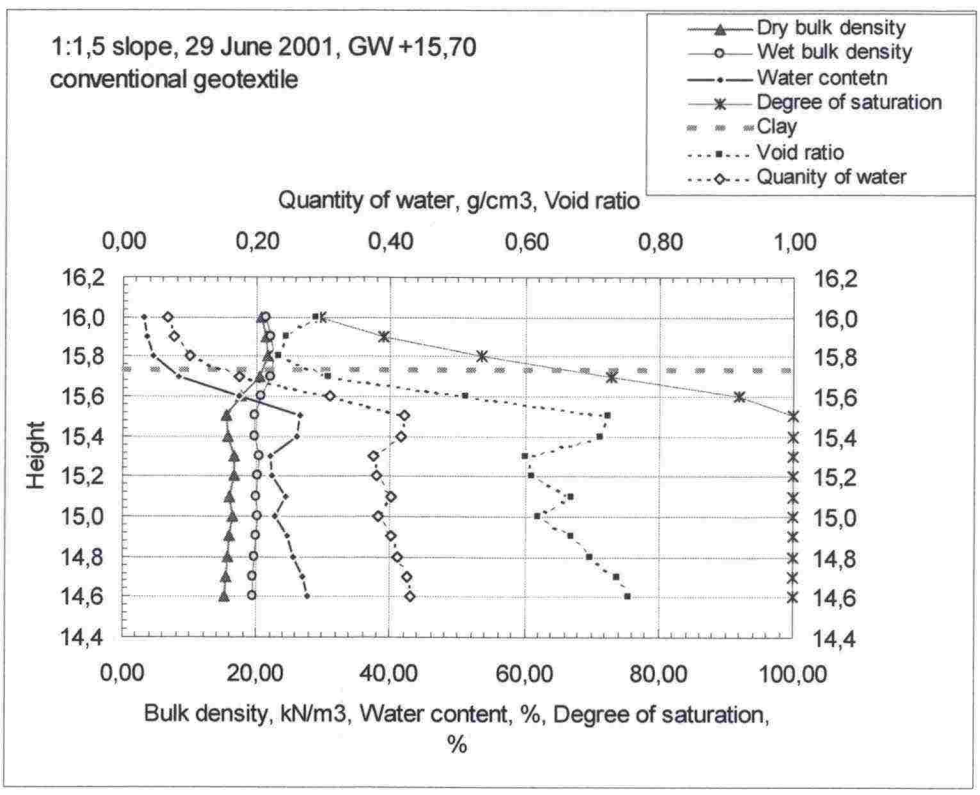
1:1,5 slope, 29 June 2001, GW +15,70
conventional geotextile
Dry bulk density
Wet bulk density
Water contetn
Degree of saturation
Clay
Void ratio
Quanity of water
Quantity of water, g/cm3, Void ratio
0,00 0,20 0,40 0,60 0,80 1,00
Height
16,2 16,0 15,8 15,6 15,4 15,2 15,0 14,8 14,6 14,4
0,00 20,00 40,00 60,00 80,00 100,00
Bulk density, kN/m3, Water content, %, Degree of saturation, %

PORE PRESSURE MEASUREMENTS

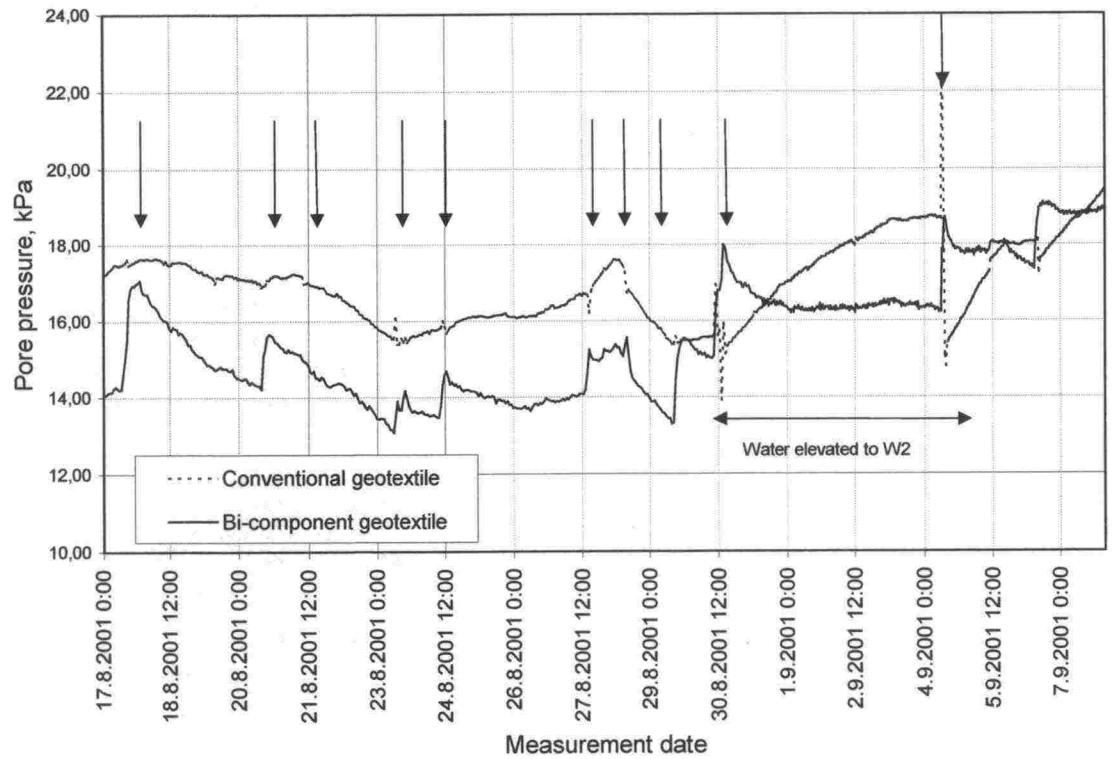

Figure 1. Structure with no slope. Pore pressure measurements. Arrows indicate testing dates.

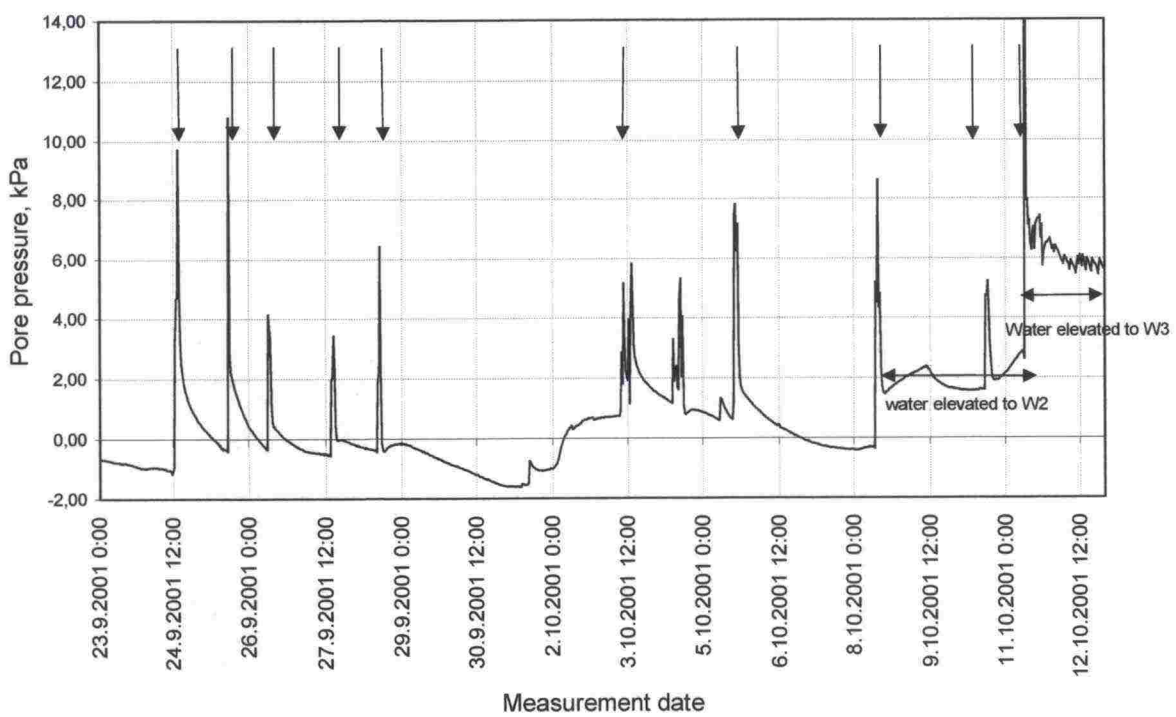

Figure 2. Slope 1:3. Pore pressure measurements. Arrows indicate testing dates.

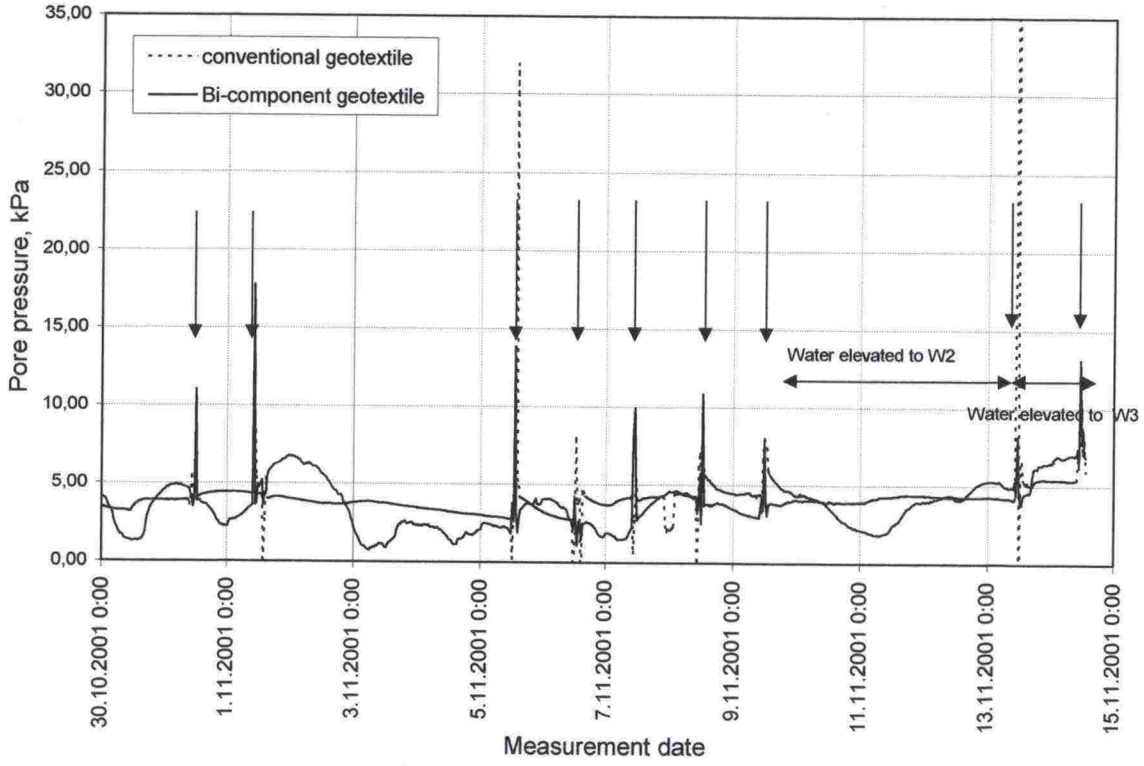

Figure 3. Slope 1:1.5. Pore pressure measurements. Arrows indicate testing dates.

EARTH PRESSURE MEASUREMENTS

Earth pressure on top of gravel, structute with no slope

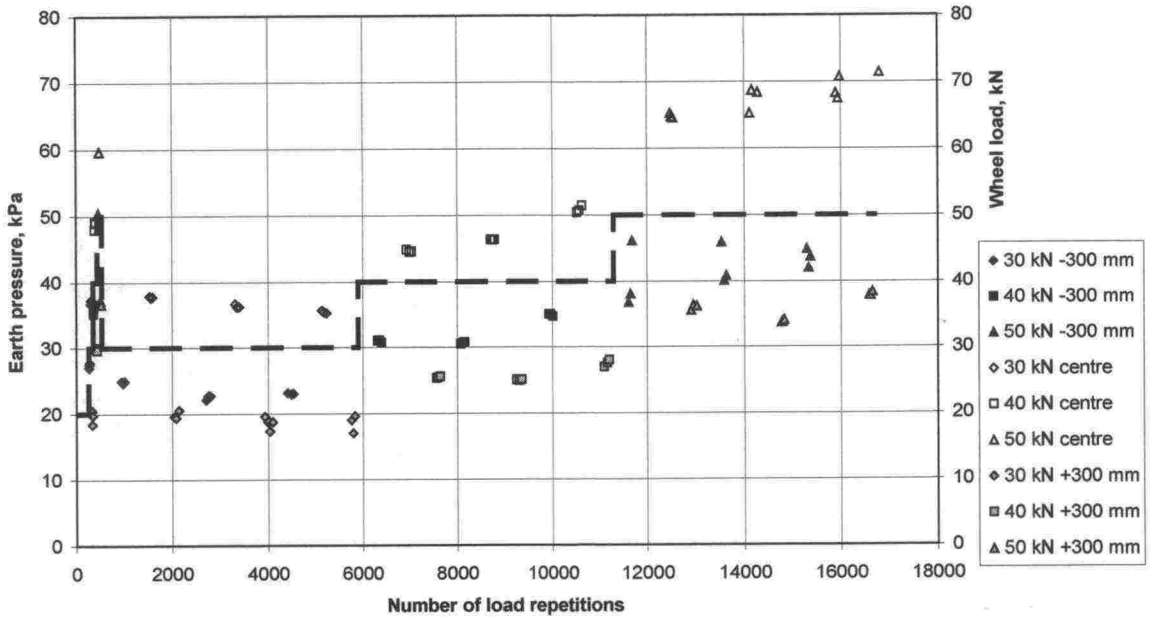

Earth pressure on top of clay, structure with no slope

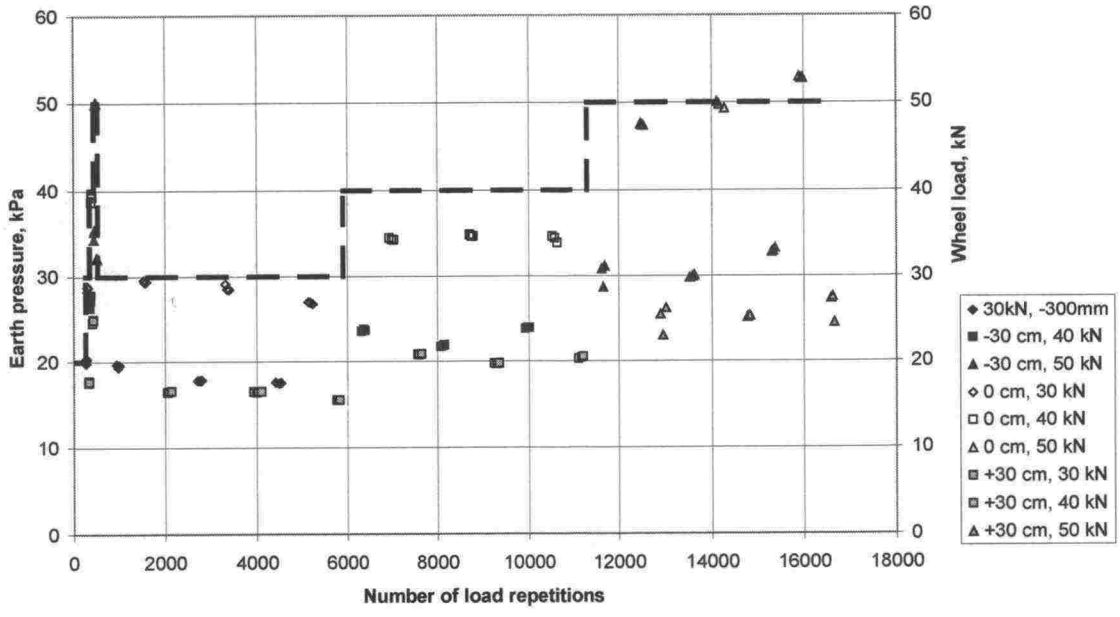

Earth pressure on top of gravel, 1:3 slope

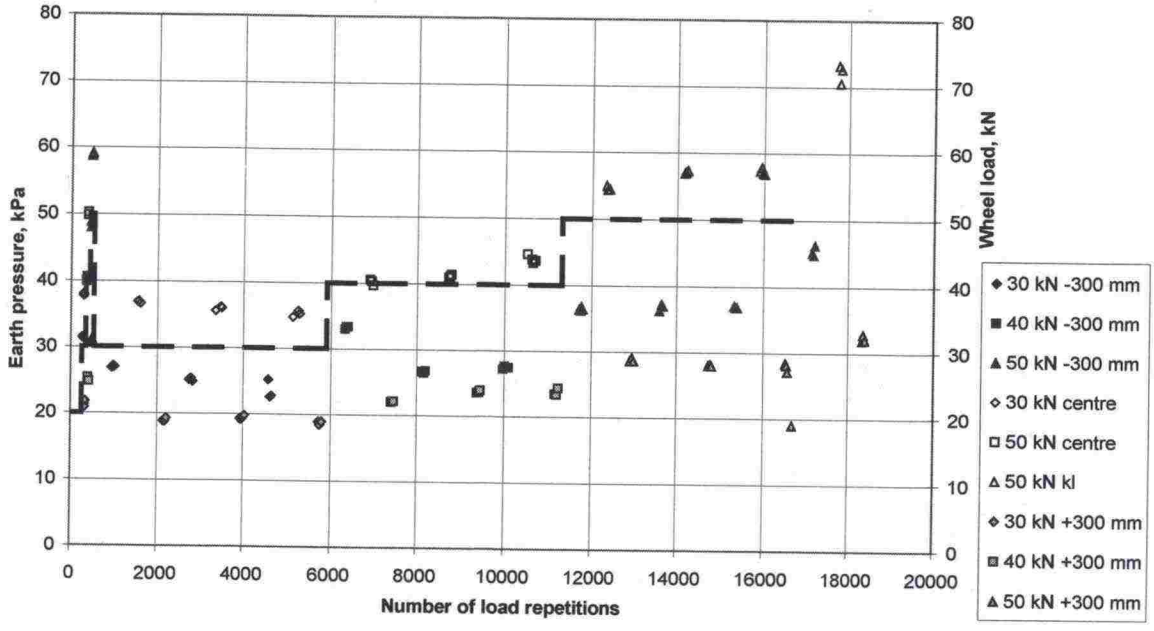

Earth pressure on top of clay, 1:3 slope

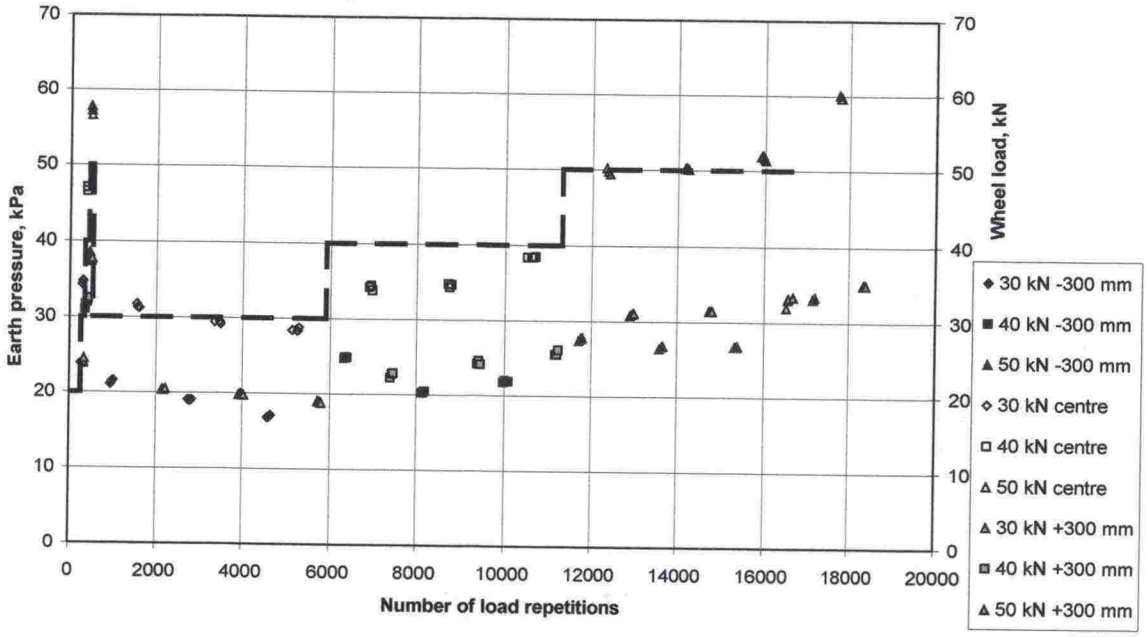

Earth pressure on top of cravel, 1:1.5 slope

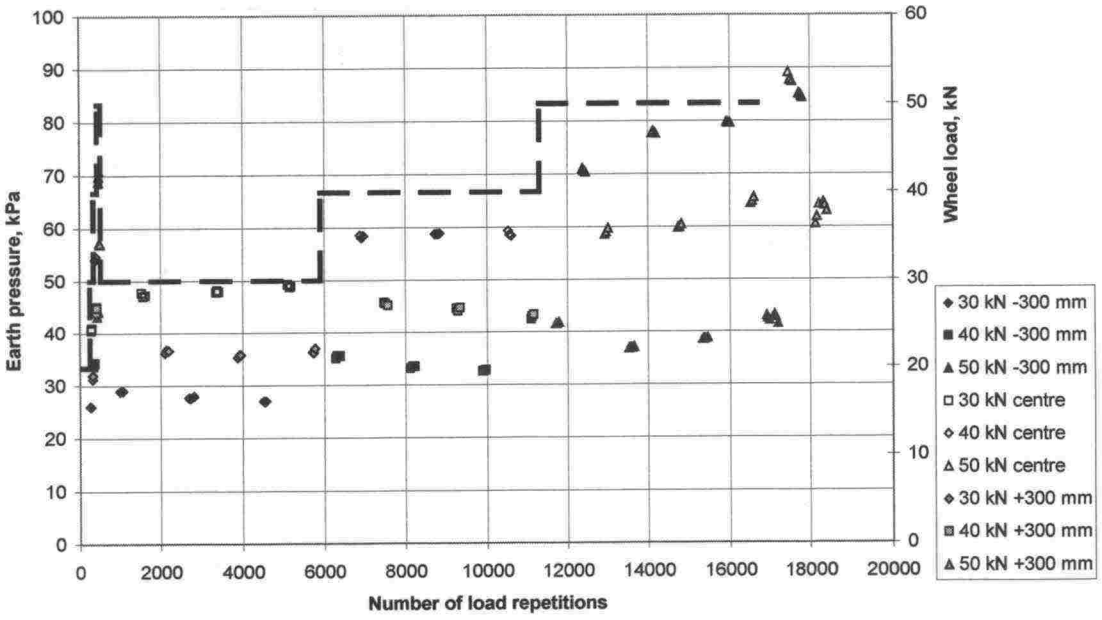

Earth pressure on top of clay, 1:1.5 slope

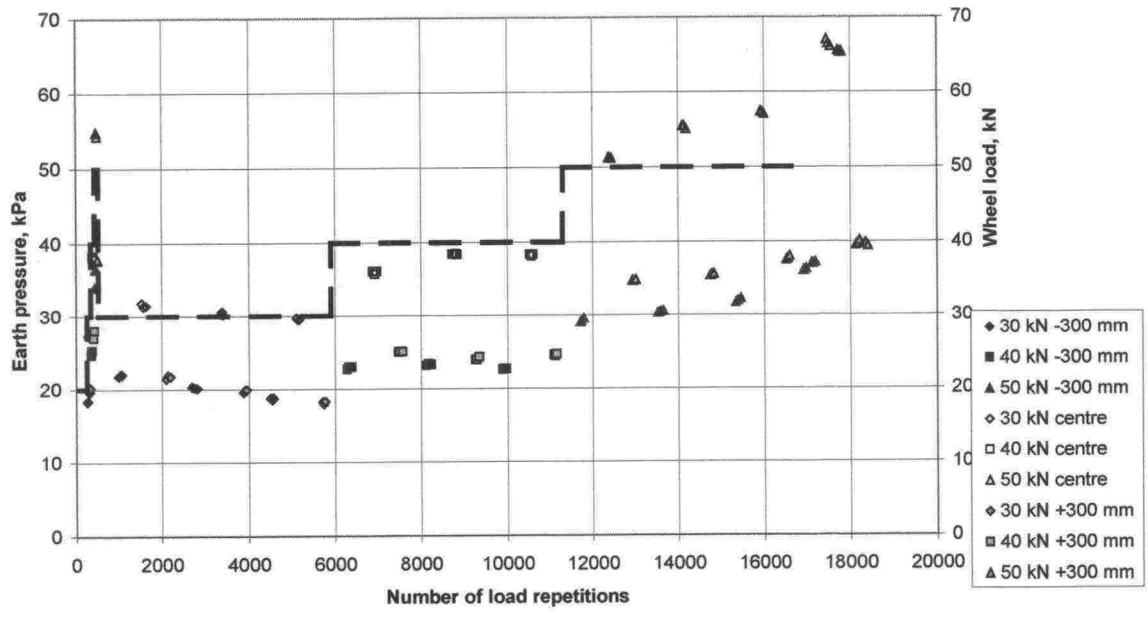

ACCELEROMETER MEASUREMENTS

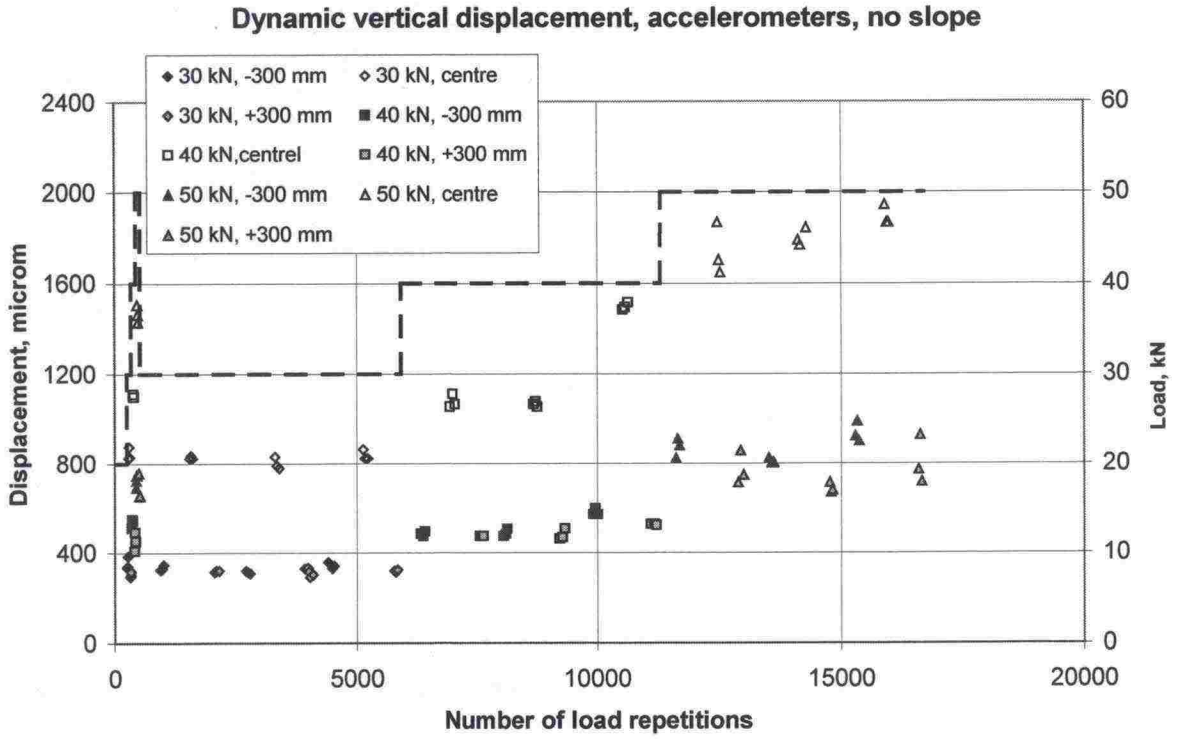

Figure 1. Resilient vertical displacement, accelerometer, test section with no slope

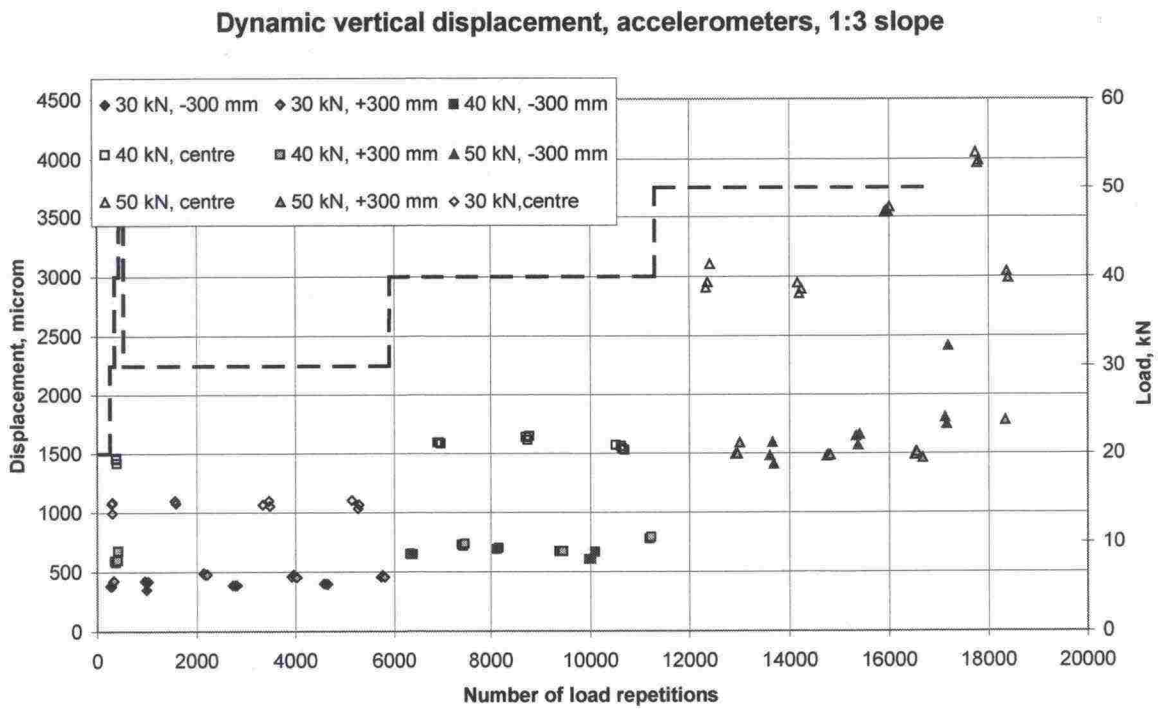

Figure 2. Resilient vertical displacement, accelerometer, test section with 1:3 slope

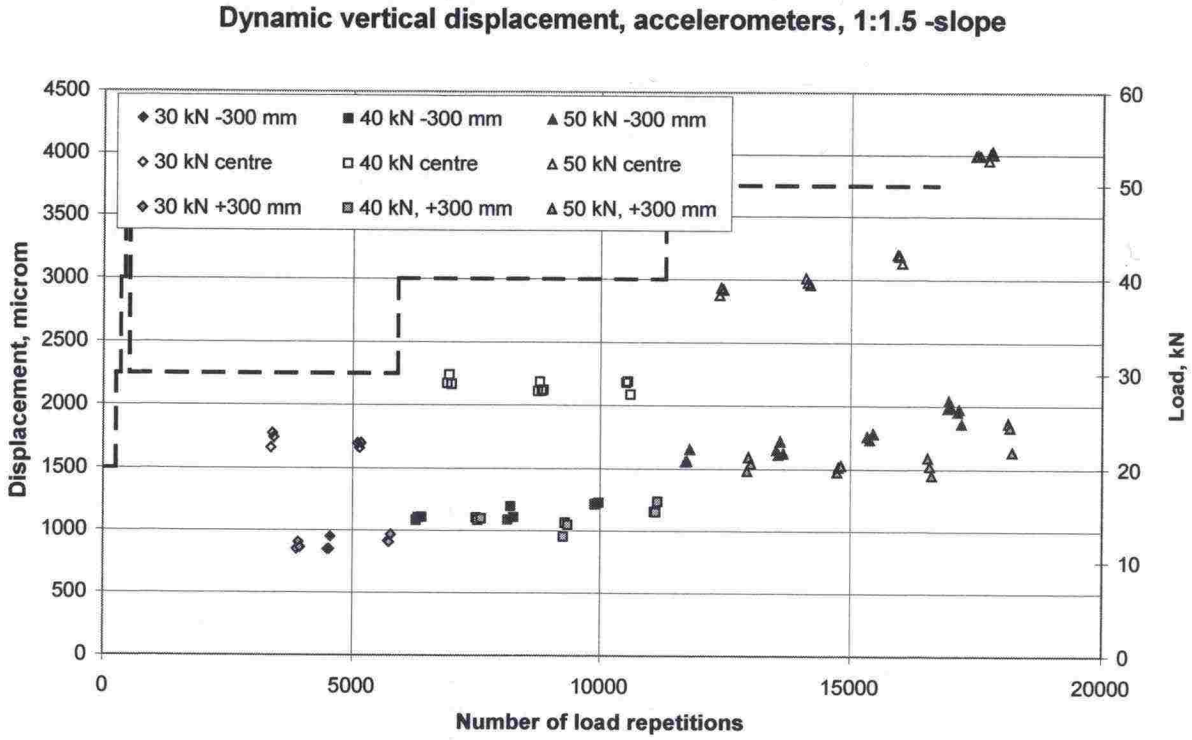

Figure 3. Resilient vertical displacement, accelerometer, test section with 1:1.5 slope

PROFILOMETER MEASUREMENTS

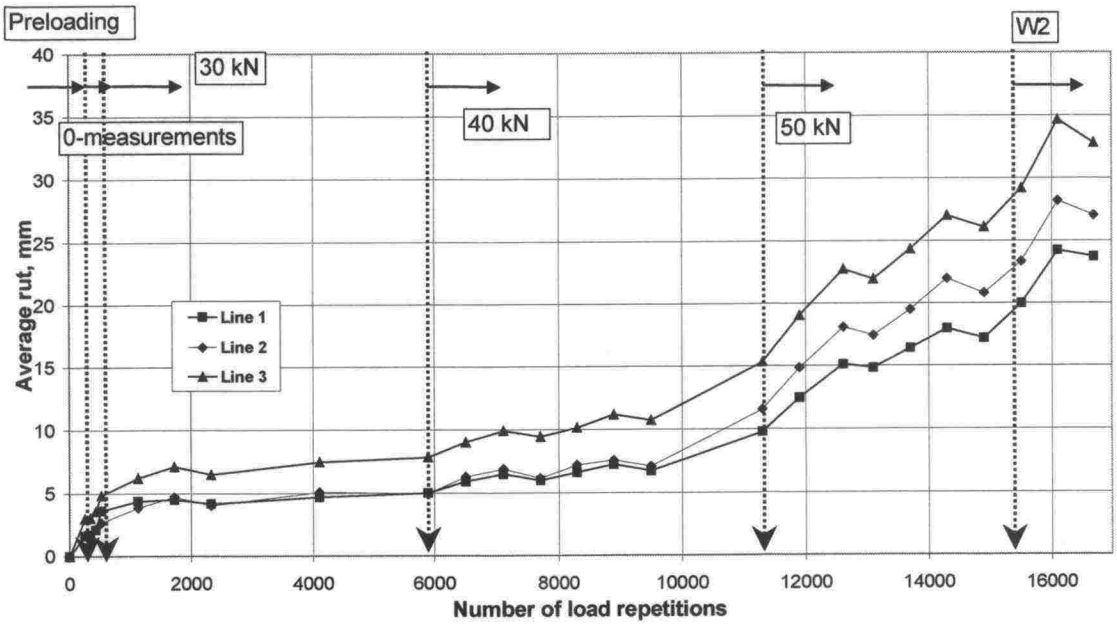

Profilometer measurements, section with no slope, Levelling line 1 = Line 1 etc.

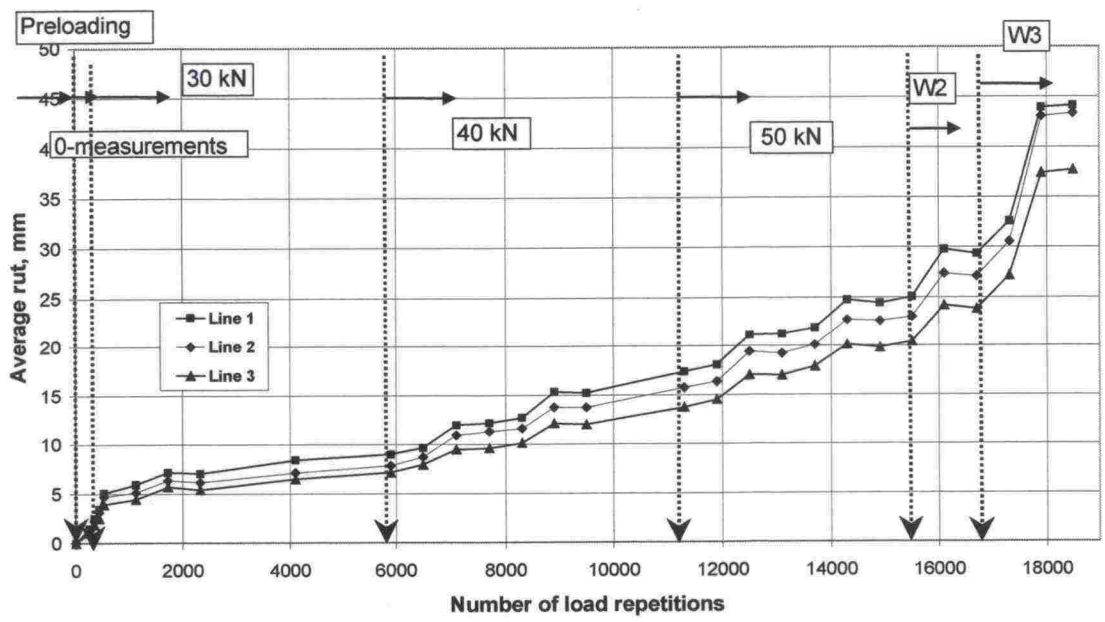

Profilometer measurements, section with 1:3 slope, Levelling line 1 = Line 1 etc.

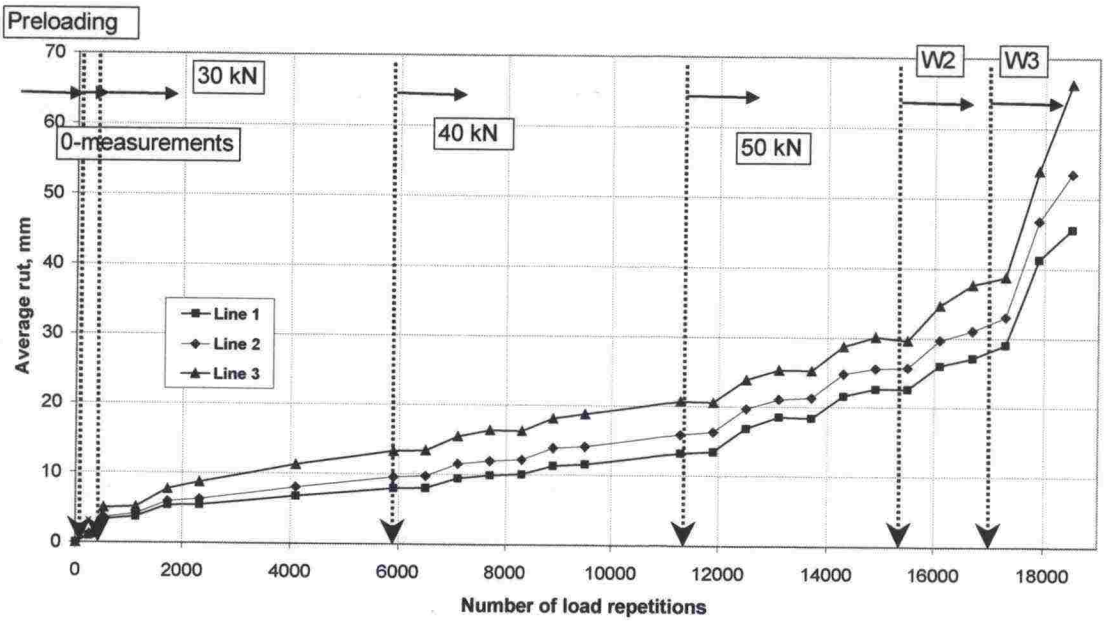

Profilometer measurements, section with 1:1.5 slope, Levelling line 1 = Line 1 etc.

LOADMAN

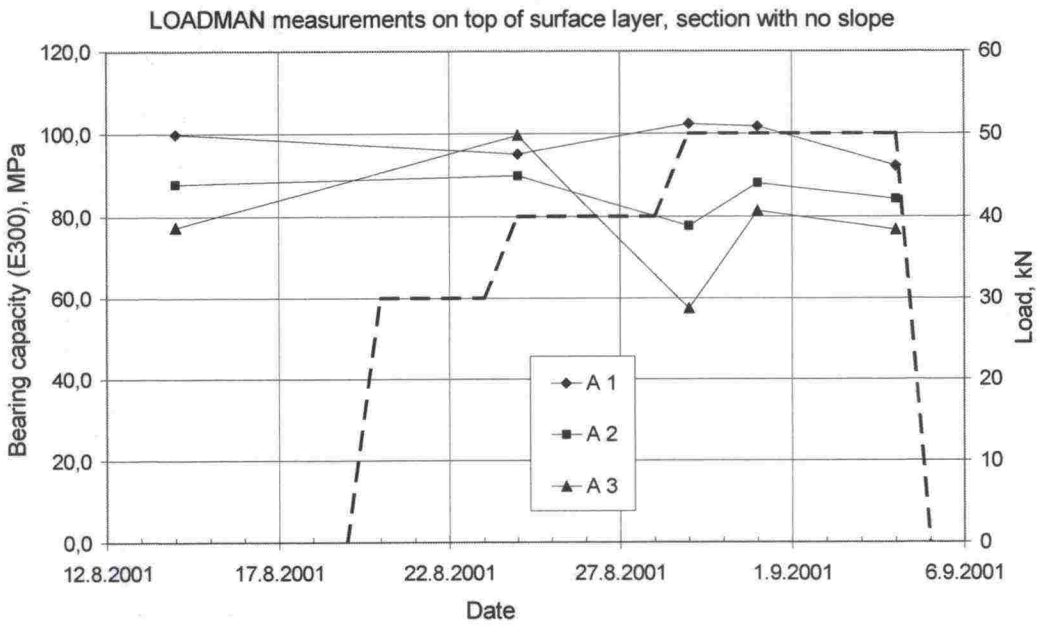

Figure 1. Loadman measurements on top of asphalt, section with no slope. Measurements on different levelling lines A1, A2 and A3. A1 is located in the bi-component geotextile area. Lines A2 and A3 are located over conventional geotextile. Heavy rain occurred on 28 August and the structure got wet.

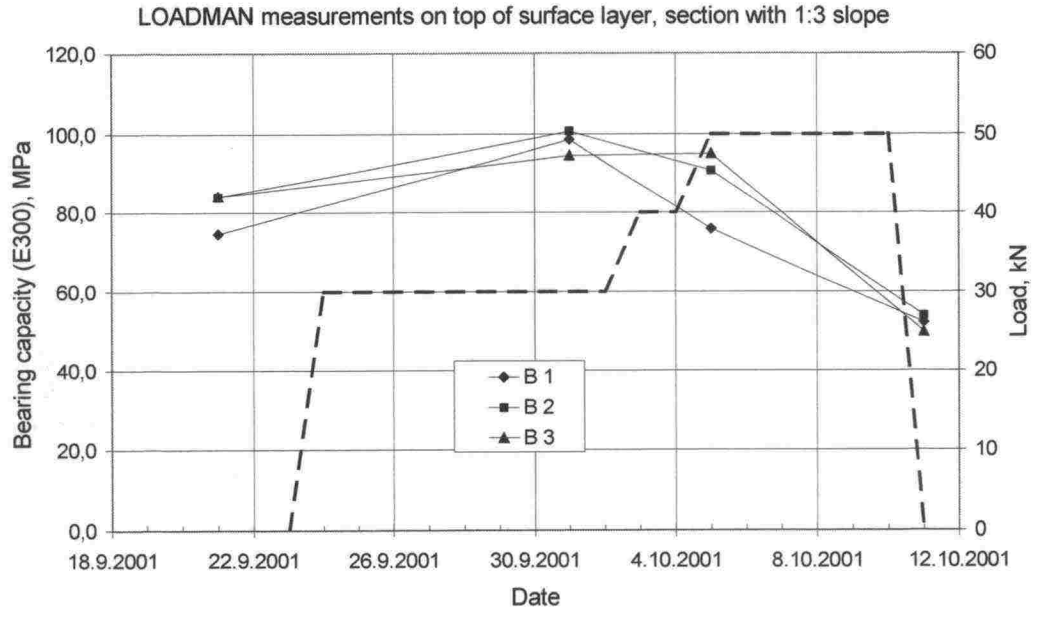

Figure 2. Loadman measurements on top of asphalt, section with 1:3 slope. Measurements on different levelling lines B1, B2 and B3.

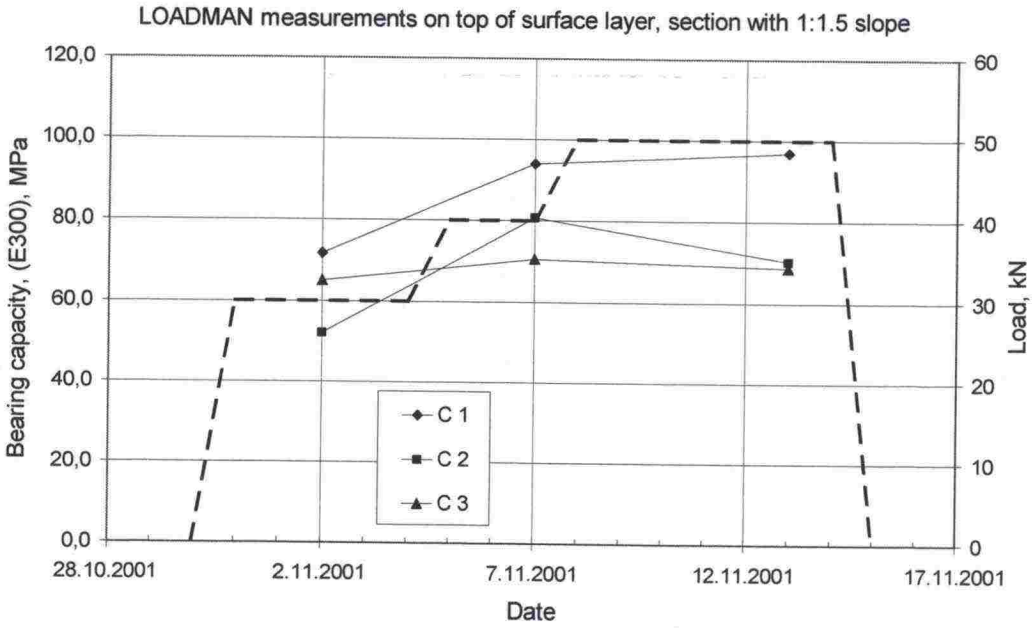

Figure 3. Loadman measurements on top of asphalt, section with 1:1.5 slope. Measurements on different levelling lines C1, C2 and C3. C3 is located in the bi-component geotextile area. Lines C1 and C2 are located over conventional geotextile.

CRUSHED ROCK DEFORMATIONS

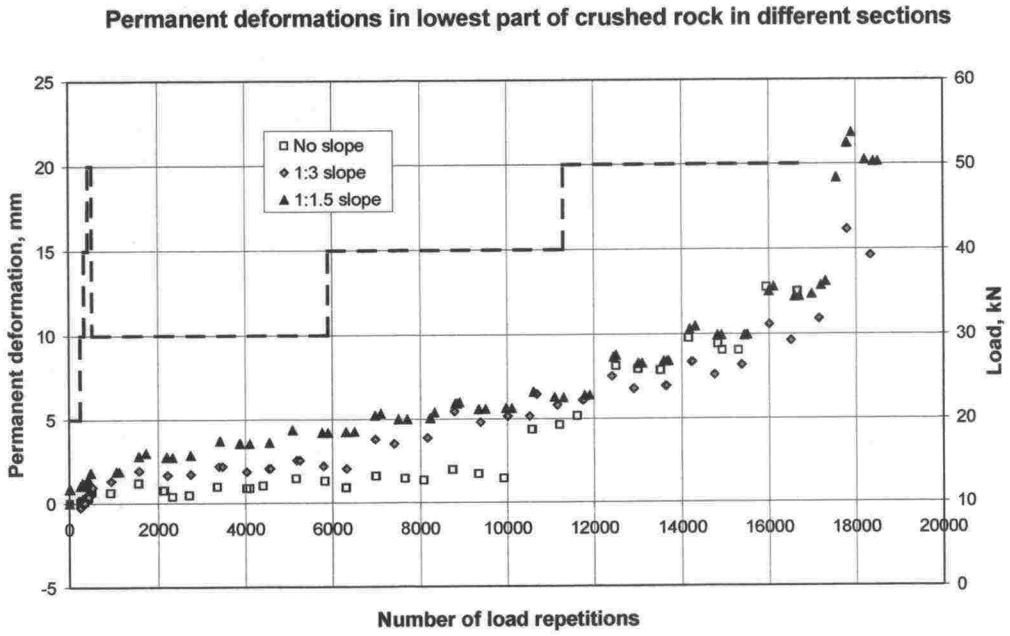

Figure 1. Permanent vertical deformations in the lowest 200 mm of crushed rock.

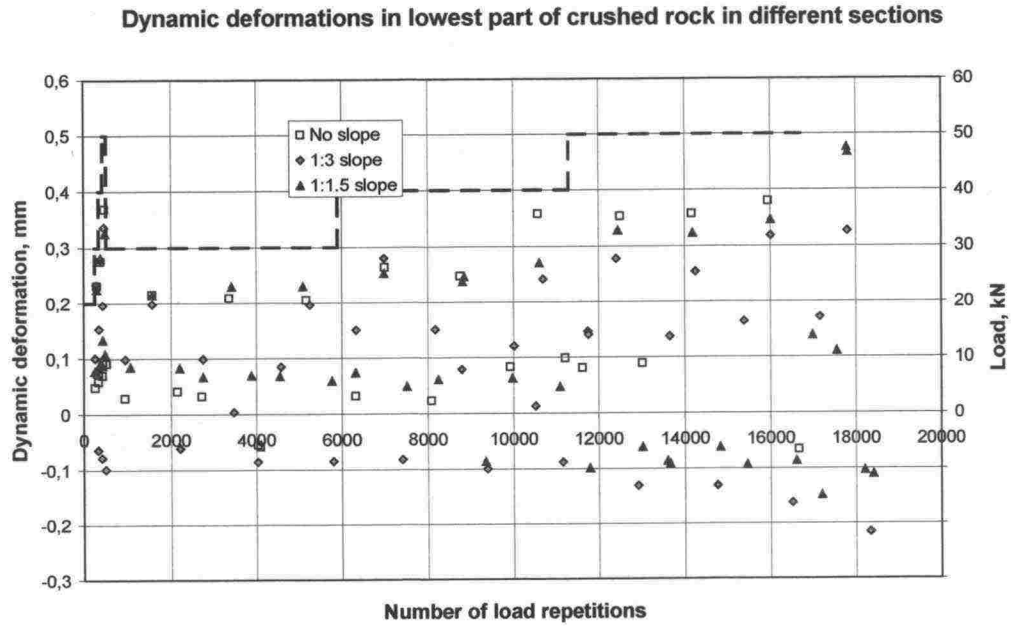

Figure 2. Resilient vertical deformations in the lowest 200 mm of crushed rock.

GRAVEL DEFORMATIONS

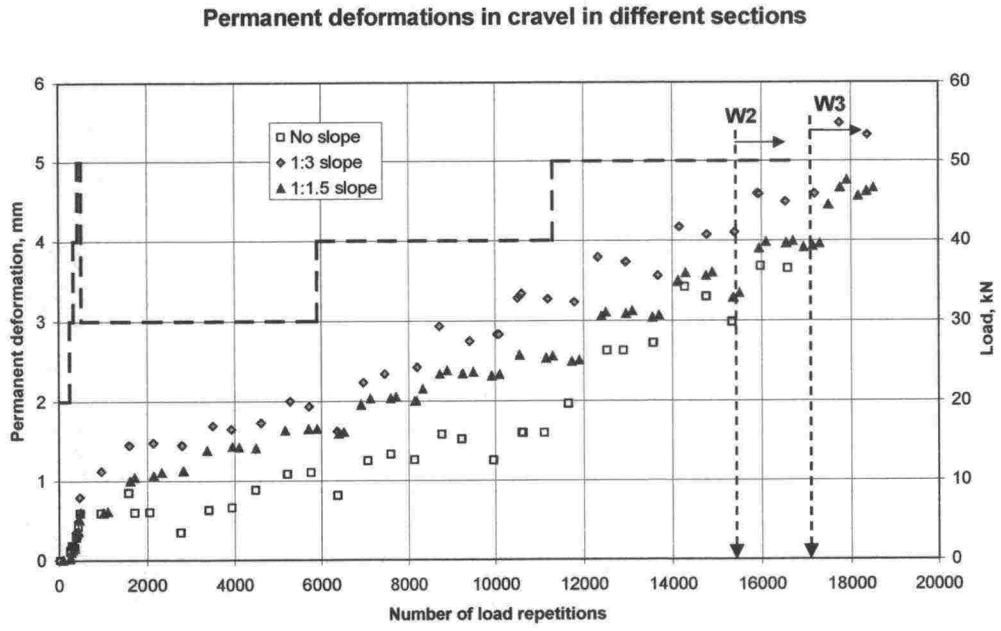

Figure 1. Permanent vertical deformations in the gravel (200 mm).

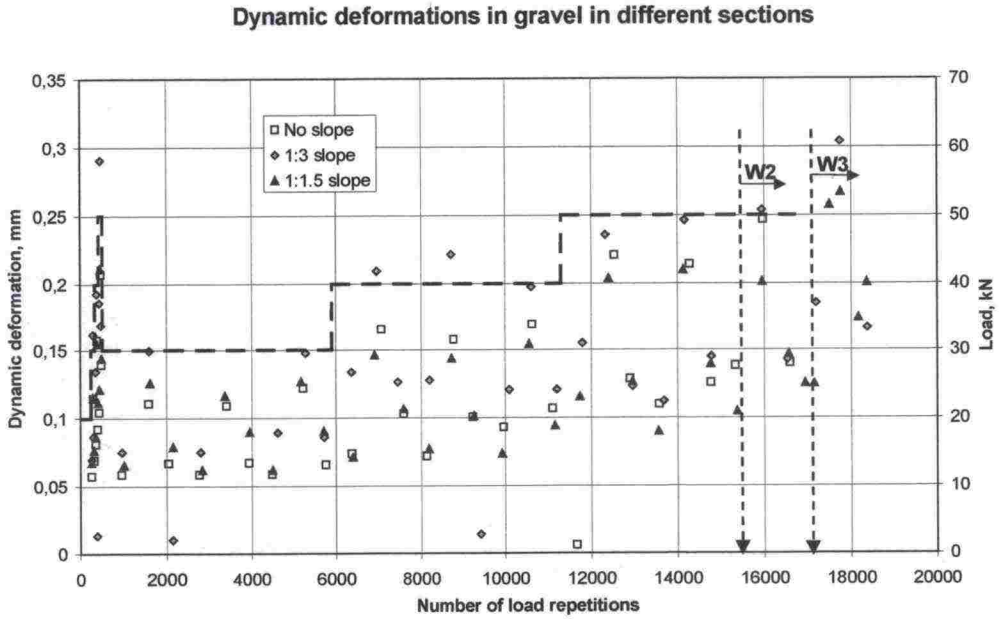

Figure 2. Resilient vertical deformations in the gravel (200 mm).

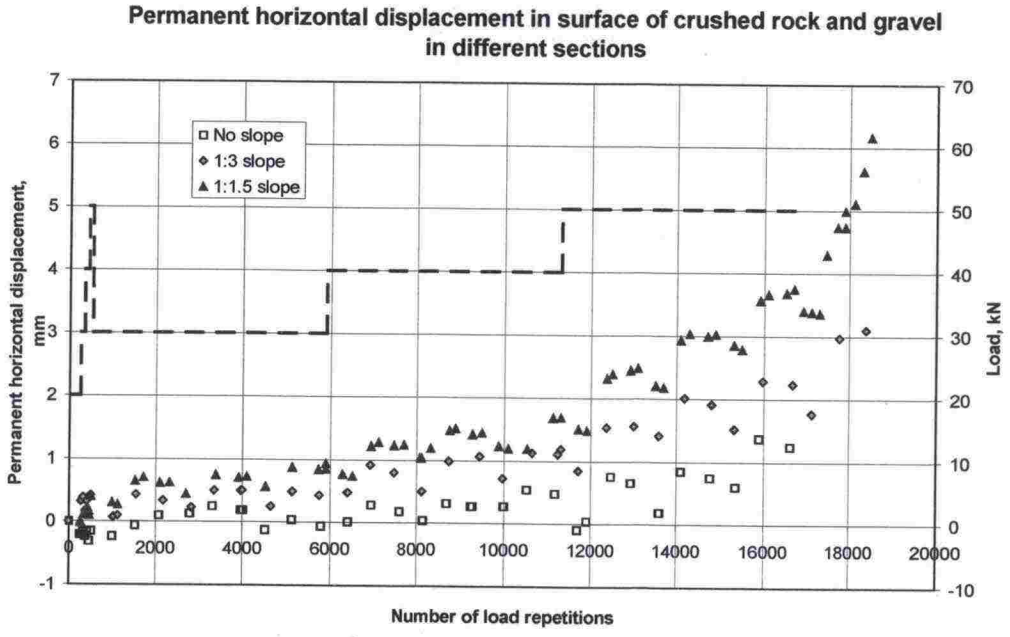

Figure 3. Permanent horizontal displacements in surface of crushed rock and gravel.

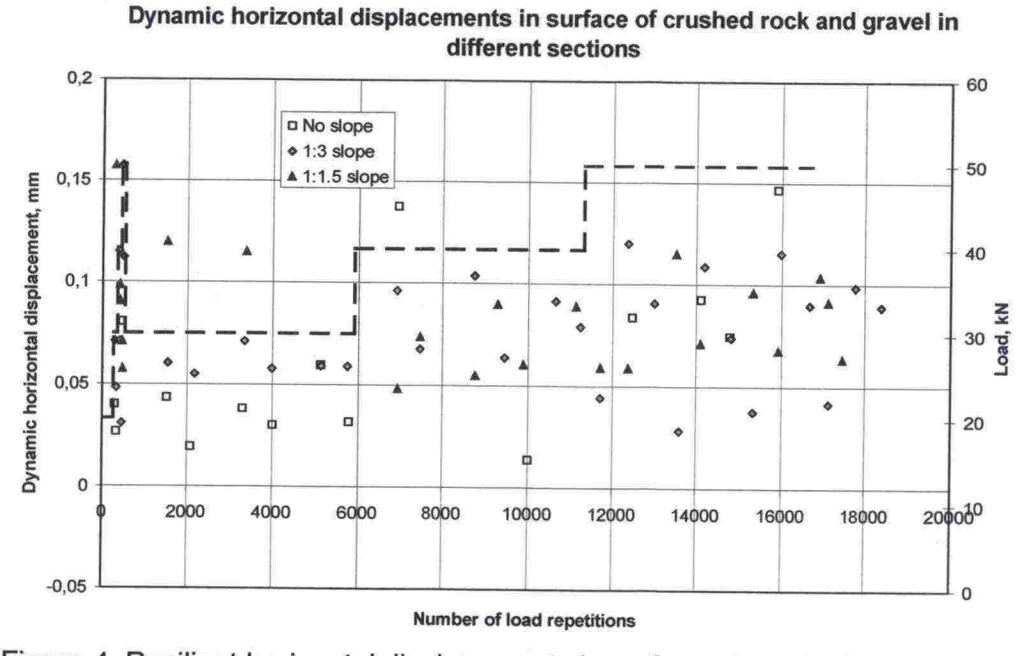

Figure 4. Resilient horizontal displacements in surface of crushed rock and gravel.

CLAY DEFORMATIONS

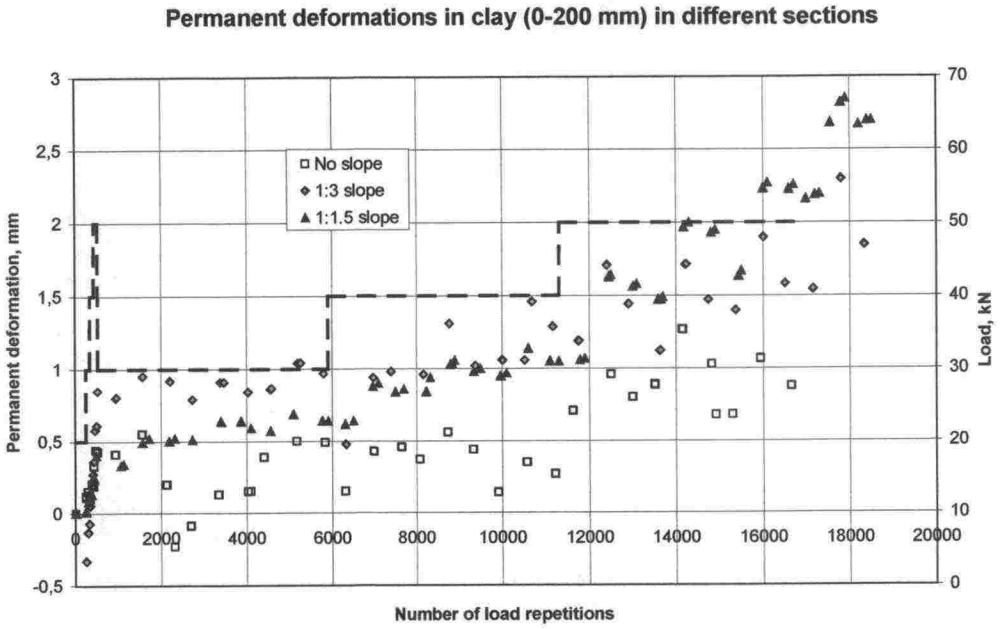

Figure 1. Permanent vertical deformations in clay (0-200 mm)

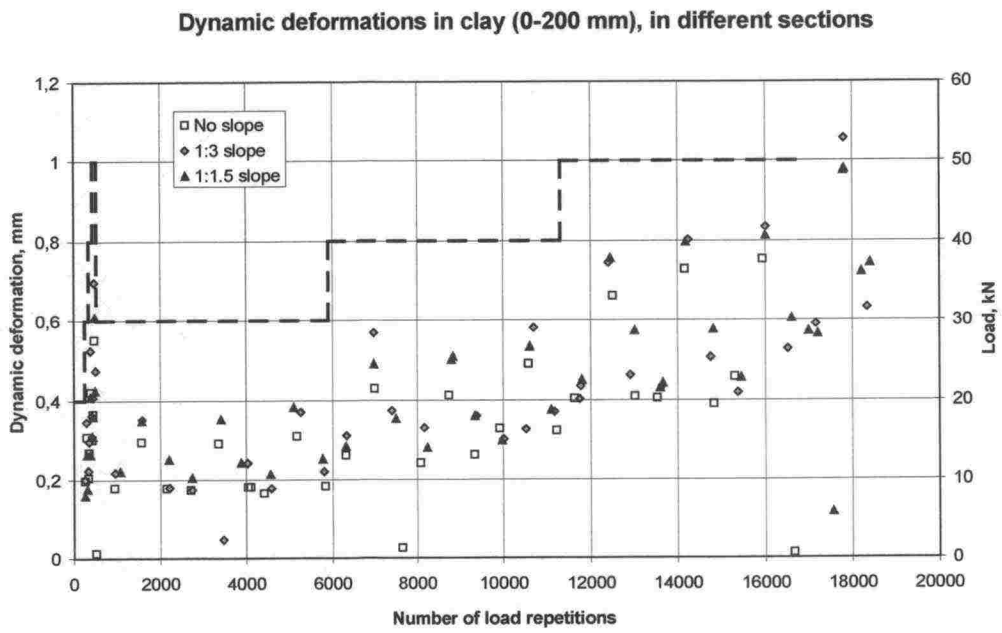

Figure 2. Resilient vertical deformations in clay (0-200 mm)

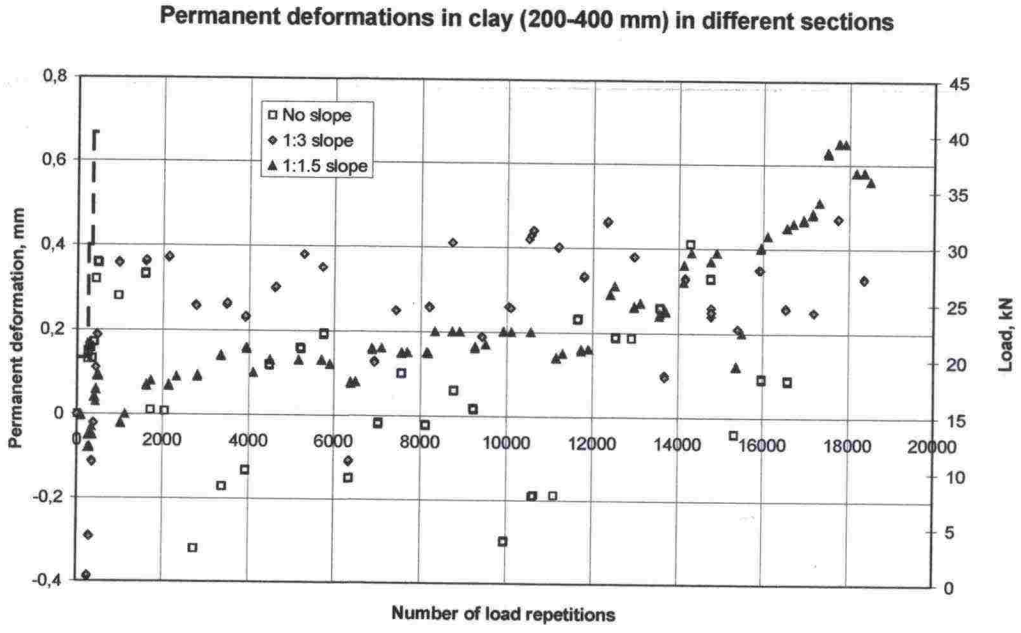

Figure 3. Permanent vertical deformations in clay (200- 400 mm)

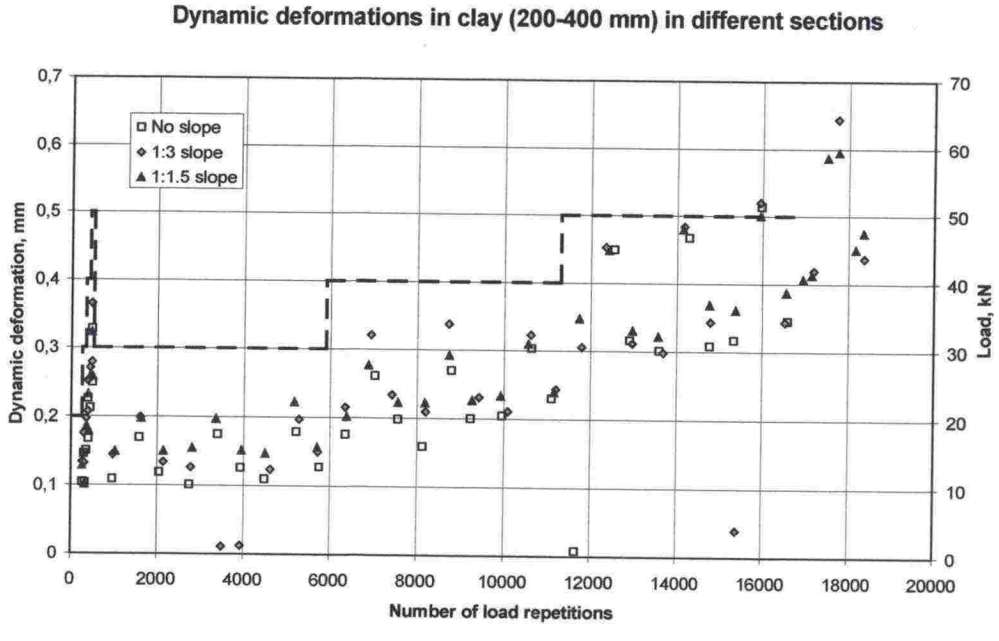

Figure 4. Resilient vertical deformations in clay (200-400 mm)

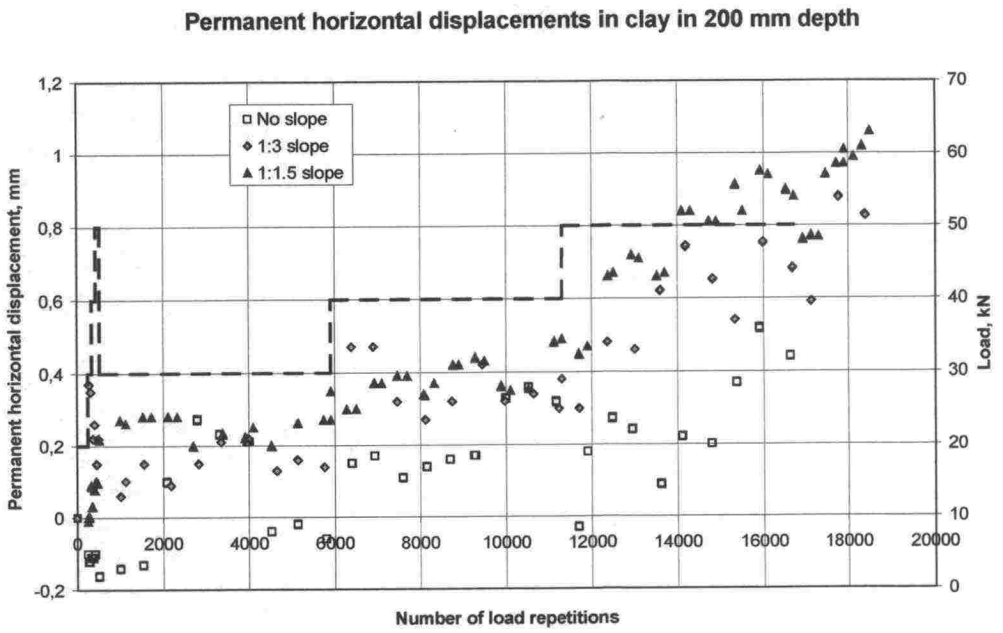

Figure 5. Permanent horizontal displacements in clay in 200 mm depth.

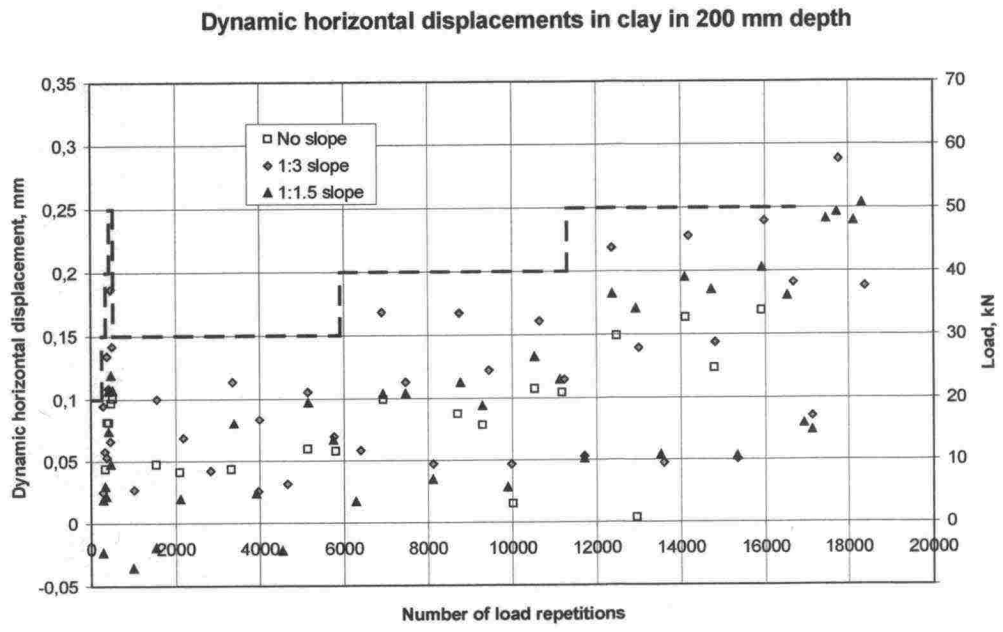

Figure 6. Resilient horizontal displacements clay in 200 mm depth.

LATERAL DISPLACEMENTS

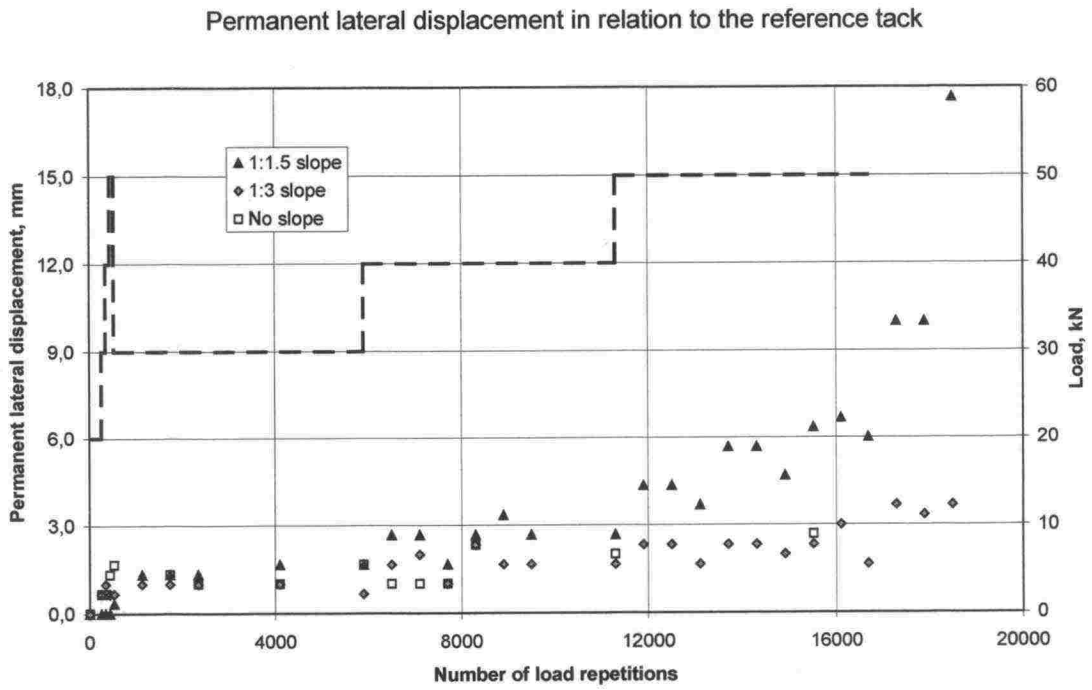

Figure 1. Permanent lateral displacements in reference to the reference tack, different sections with slopes.

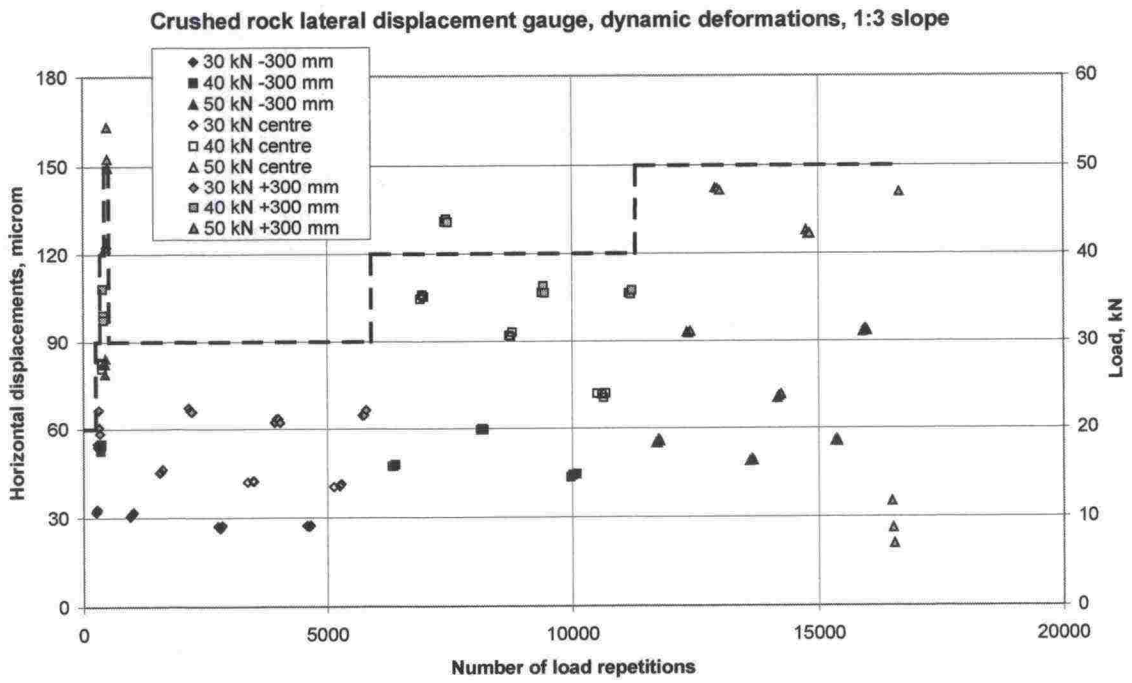

Figure 2. Resilient horizontal total deformations in the crushed rock, 1:3 slope.

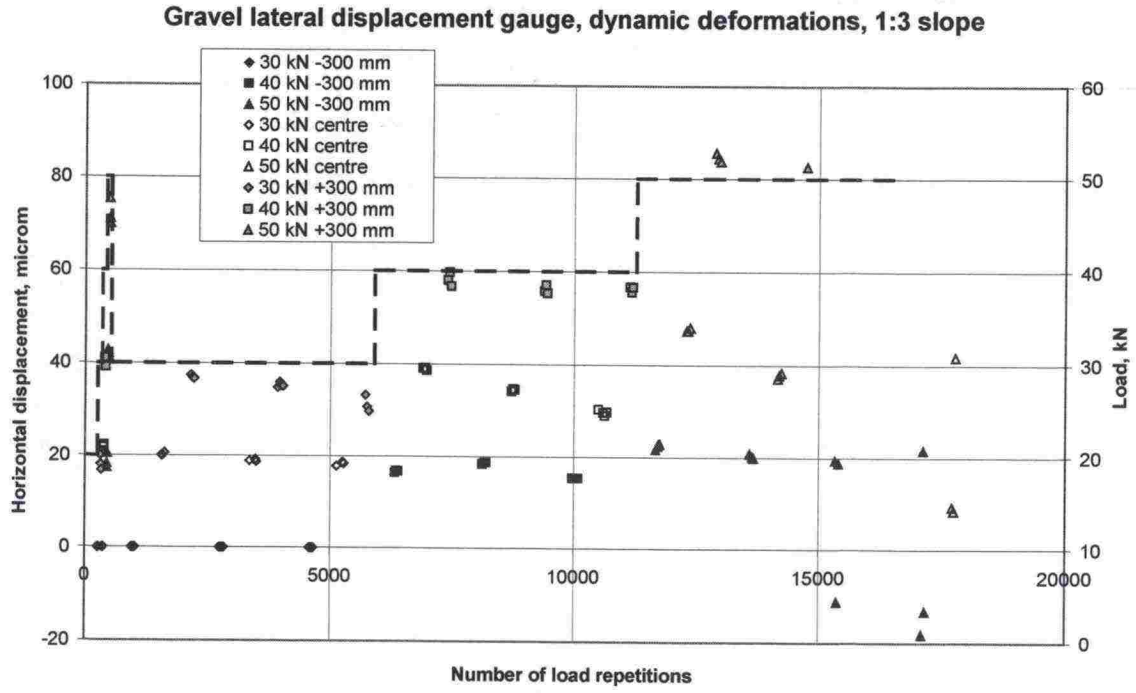

Figure 3. Resilient horizontal total deformations in the cravel, 1:3 slope.

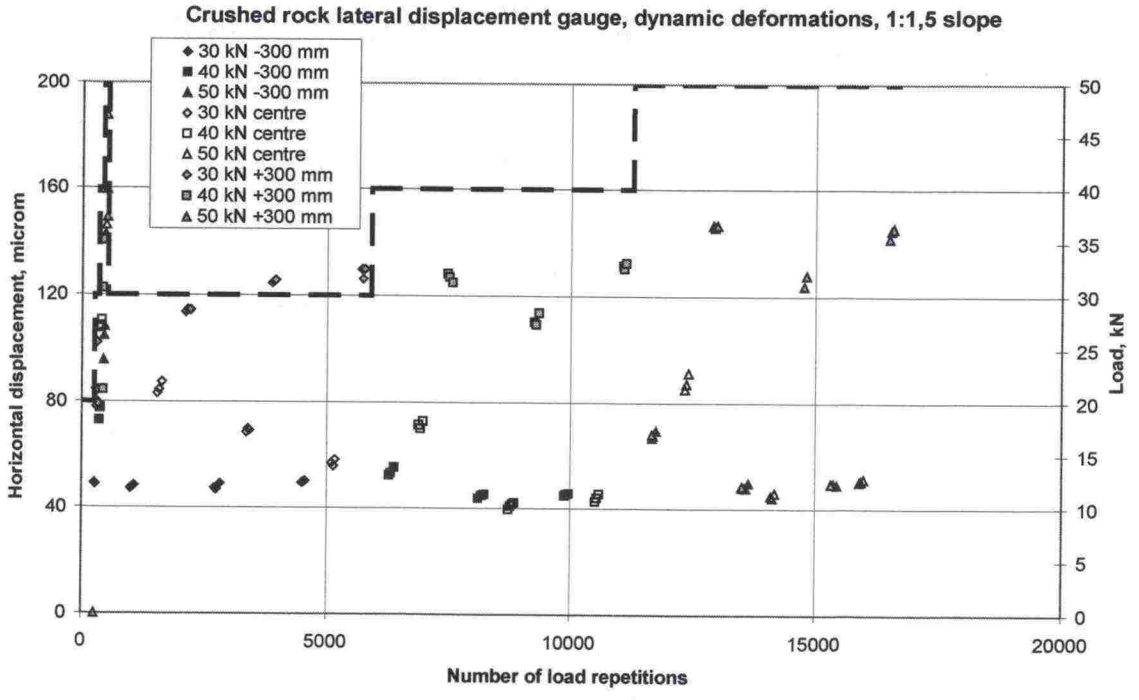

Figure 4. Resilient horizontal total deformations in the crushed rock, 1:1.5 slope.

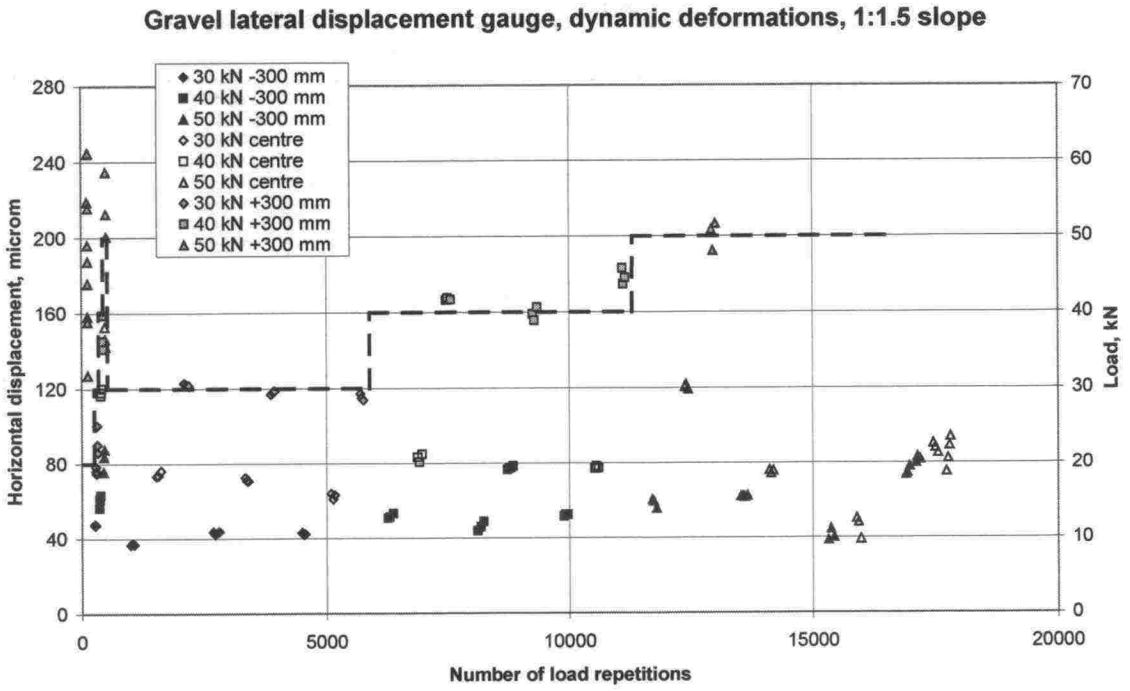

Figure 5. Resilient horizontal total deformations in the cravel, 1:1.5 slope.

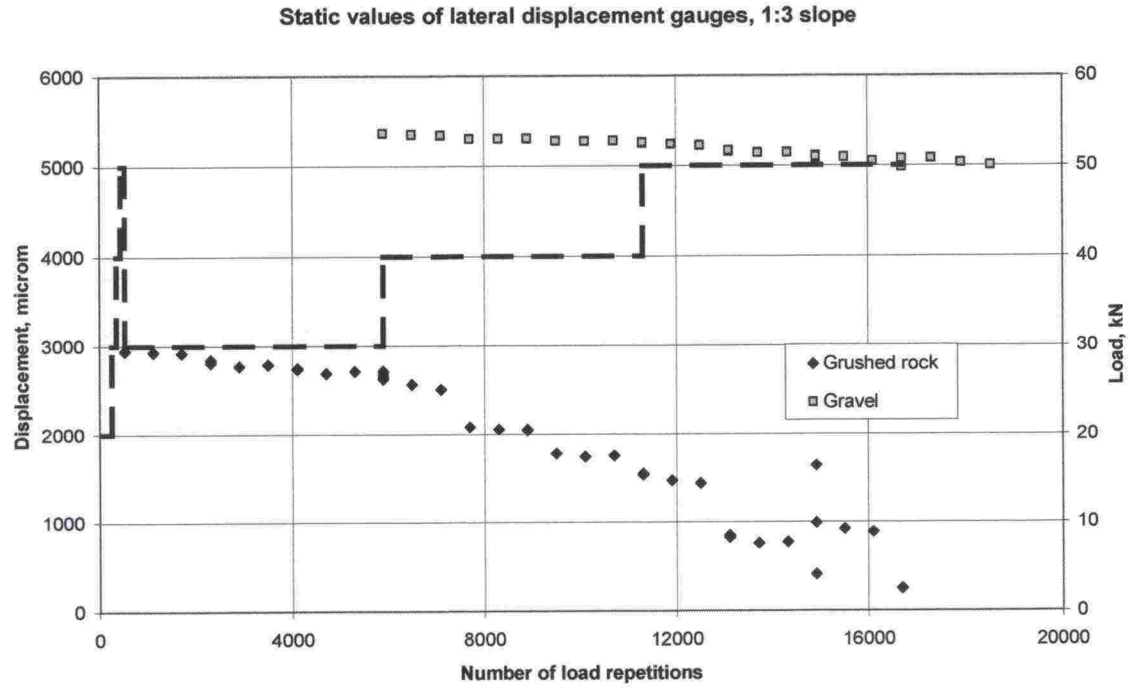

Figure 6. Permanent horizontal displacements in crushed rock and gravel, 1:3 slope.

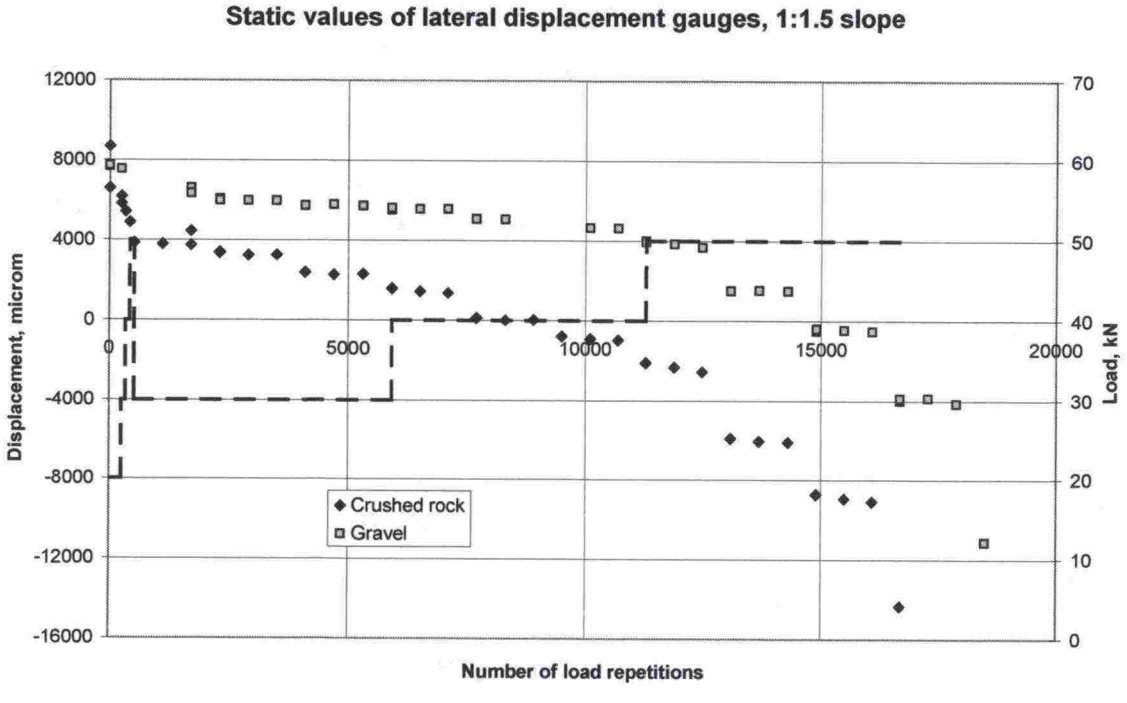

Figure 7. Permanent horizontal displacements in crushed rock and gravel, 1:1.5 slope.

CRACKING, STEEP SLOPE

Figure 1. Cracks of the entire structure. Slope on right.

Figure 2. Cracks of middle part of structure.

ELEMENT GRID, BULK MODULI OF THE MATERIALS, SLOPE STEEPNESS 1:1.5

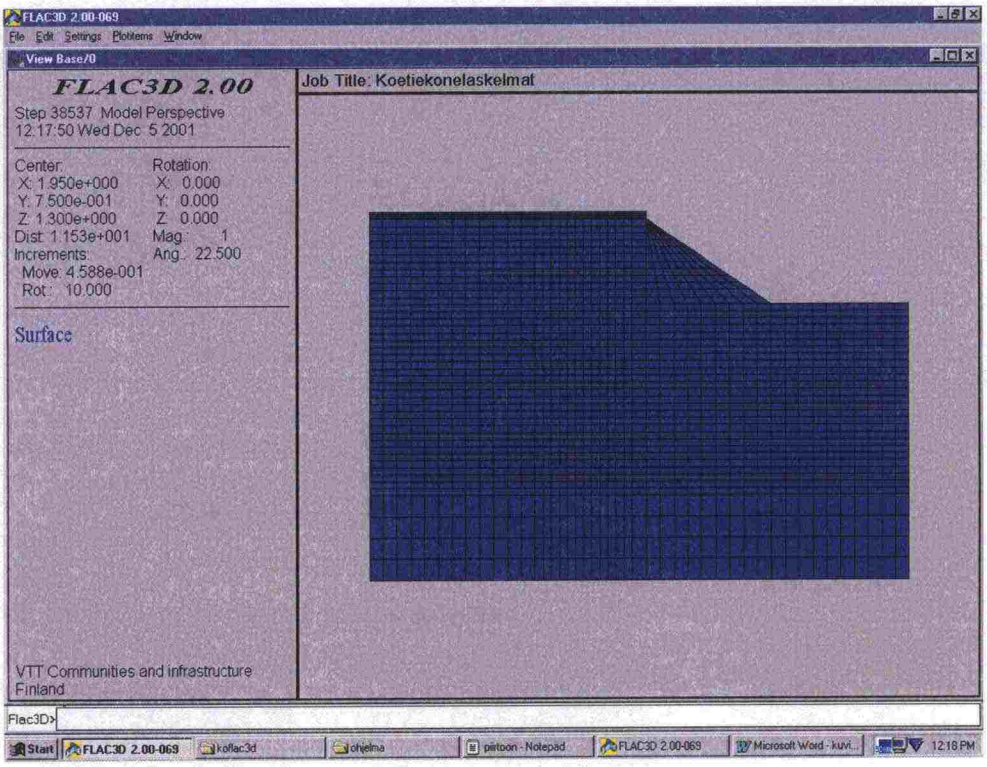

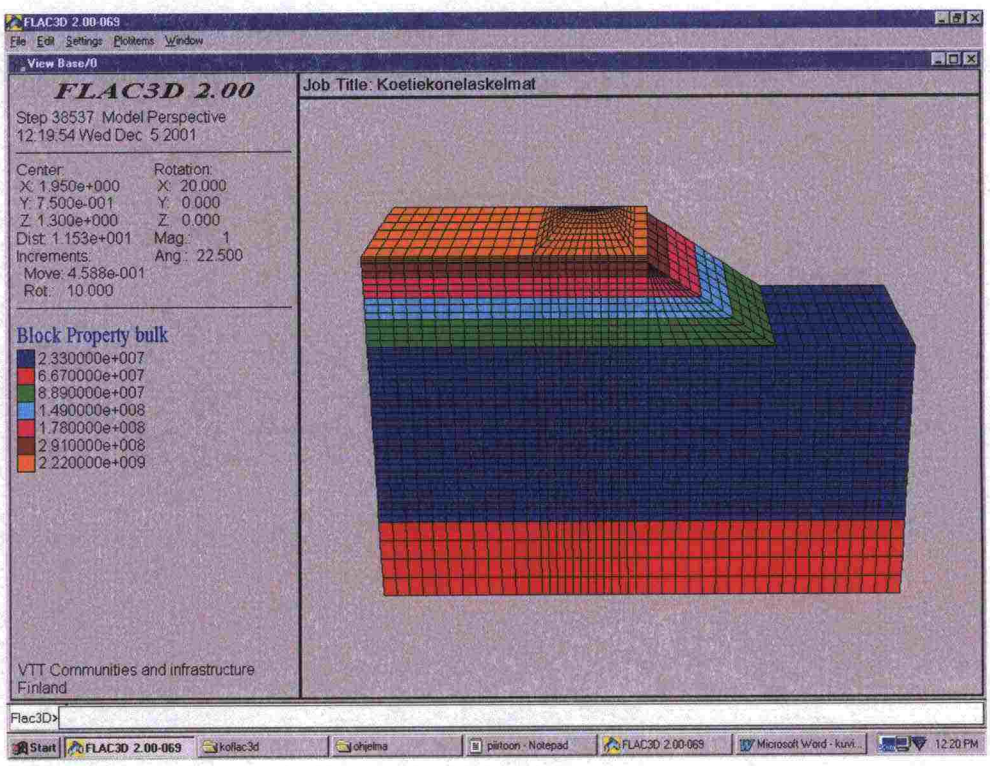

LEVEL CURVES IN THE CALCULATON MODEL AND THE STATE OF THE ELELEMENTS IN THE LOAD STATES, SLOPE STEEPNESS 1:1.5, LOAD 50 KN

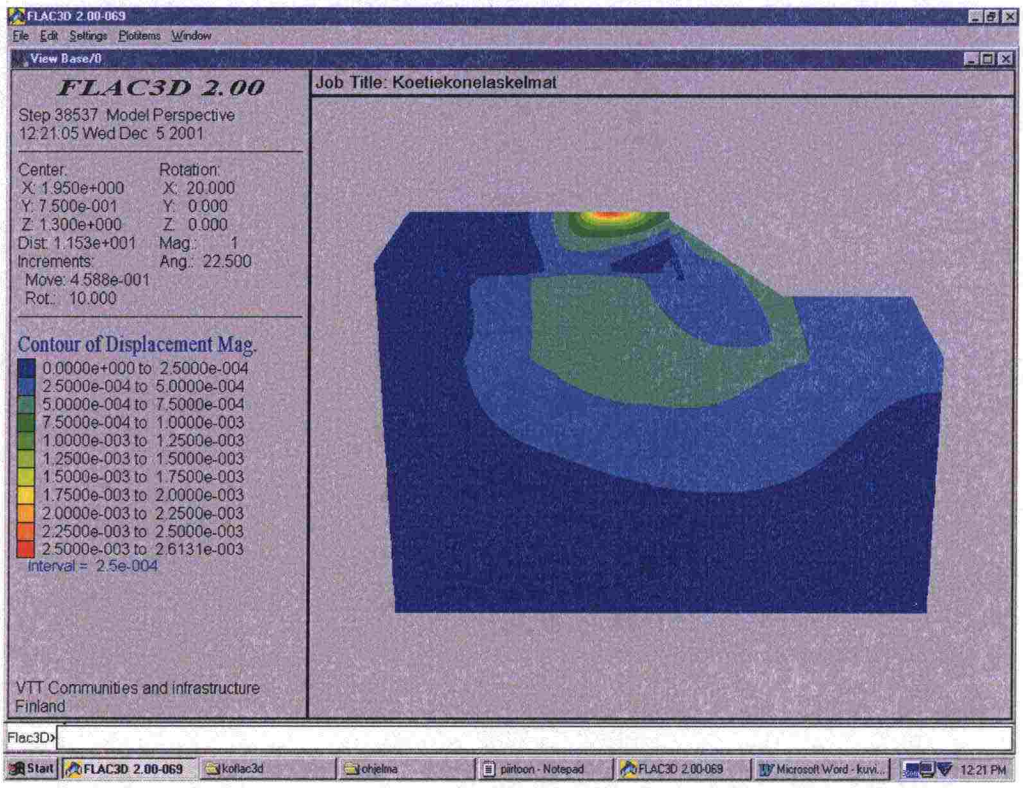

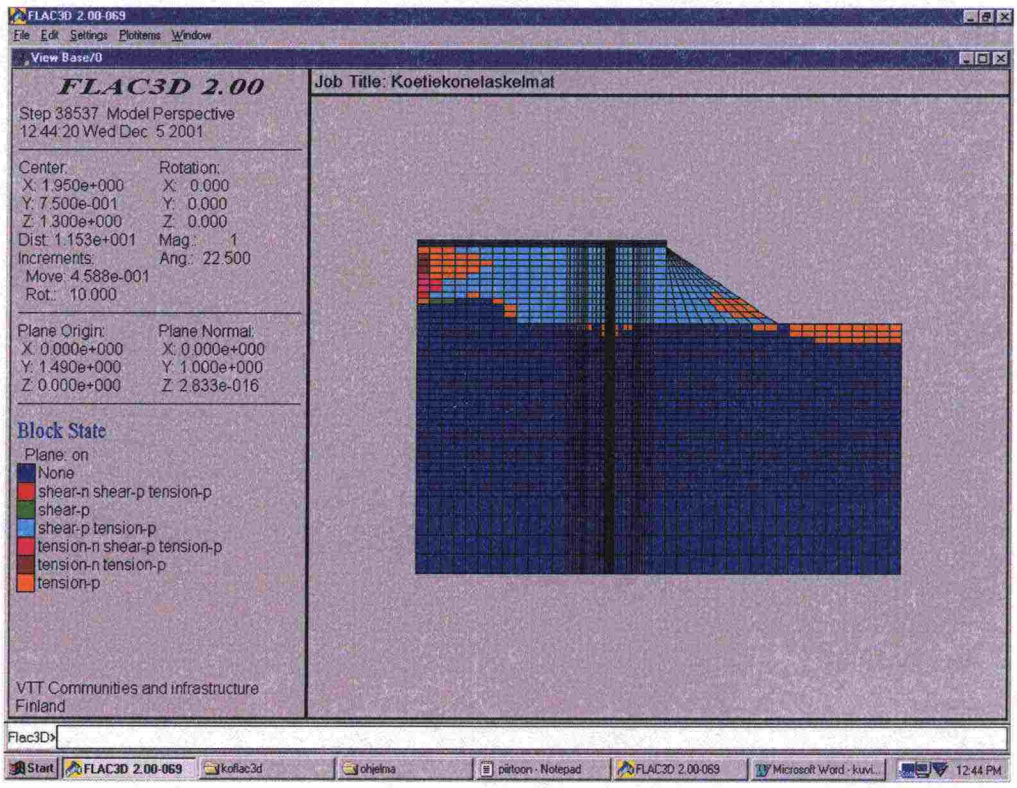

ISSN 1457-9871
ISBN 951-803-042-1
TIEH 3200765E